Author:
James, Jasper W

Title:
Soft Biomimetic Optical Tactile Sensors for Slip Detection and Grasp Recovery

Soft Biomimetic Optical Tactile Sensors for Slip Detection and Grasp Recovery

By

JASPER WOLLASTON JAMES

Bristol Robotics Laboratory
UNIVERSITY OF BRISTOL & UNIVERSITY OF THE WEST OF ENGLAND

A dissertation completed at the FARSCOPE Centre for Doctoral Training
in Robotics and Autonomous Systems.

JULY 2021

Abstract

Tactile sensing gives humans the ability to interact directly with the environment and has resulted in the world being shaped such that it is easy for us to interact with. Tactile sensing is useful in robotic grasping and provides information complementary to vision such as contact forces and surface texture. Bringing tactile sensing to robots is essential to provide human-level touch capabilities. One aspect of human touch is slip detection, which is the ability to detect when something is moving relative to the skin. Slip detection is utilised by humans in a variety of scenarios including determining ideal grasping strength and inferring object properties.

This thesis involves the study of new sensors and methods of slip detection, and an analysis of how slip detection can be used to improve robot touch. Additionally, this thesis explores how one can mimic human sense of touch to improve slip detection in robots. Work is conducted using different variations of the TacTip, a soft biomimetic optical tactile sensor. Experiments are performed with single sensors featuring different skin morphologies and a novel design of tactile robot hand with integrated miniaturised versions of the TacTip. It is demonstrated that the TacTip is effective at real-time slip detection and grasp recovery, and that mimicking structures in the human fingertip elicits incipient slip allowing for early detection of grasp instability.

This thesis seeks to convince the reader that slip detection is as useful a sense to robots as it is to humans and should be included in any future tactile robot system interacting with the cluttered environment around us. Several contributions to the field of tactile robotics are made by furthering knowledge relating to gross slip detection, tactile robot grasping and incipient slip.

Dedication and acknowledgements

This PhD has involved years of work and has been simultaneously an eye-opening intellectual endeavour and an extremely difficult personal challenge. As such, there have been many emotional highs and lows, and there are many people, too numerous to mention, who have helped me complete it. First, Nathan, thank you for your supervision throughout my PhD. I really cannot stress enough how much I appreciate all the help you've given me throughout the past four years. This thesis and all the work in it could not have existed without it.

Thank you to all the other members of the Tactile Robotics group for their help; particularly Nick, Luke, Ben, John and Kirsty. Everything from proof-reading to your valuable research insights helped get me across the line. Gareth and Andy, thank you for all of your technical assistance with my work; apologies for all the stupid questions. Also, to other great friends I have made at the BRL. Chanelle, thanks for all the laughs and excellent food which has contributed to my ever expanding waistline. Nick, thanks for all the tea and exercise to take it all off again! Matt, our climbing adventures have been the best way to take my mind off the PhD and I hope they continue for many years to come.

To Richard, no-one knows better than you how tough a PhD can be and the sort of strains it can put on you. Sharing our respective stories of PhD life has been an excellent source of solidarity and made me laugh a lot. Our years together at Oxford were the most incredible period of my life and I can't wait for the collaboration to restart. Also, thanks for the memes.

The only reason I was ever in a position to start this PhD was because of my family. To my parents, Sarah and Adrian, I can't thank you enough for the unwavering support you have given me all of my life. Thank you for teaching me to always ask questions, to push myself and for being incredible role models through the example you have set as professionals, parents and friends. To my sisters, Lucy and Alice, thank you for keeping me grounded and for always being there for me. You both do such amazing work in increasingly difficult circumstances and I can only aspire to contribute to the world in the way you do.

Finally, to my fiancée Flo, thank you everything you have done for me throughout my PhD, our relationship and especially this bizarre last year. There is no other person on Earth who I would rather have had alongside me throughout the tricky ride that this PhD has been. I know that our adventures are only just beginning and the fact that wherever we go next you'll be alongside me for all the tea and takeaways brings me indescribable comfort.

AUTHOR'S DECLARATION

I declare that the work in this dissertation was carried out in accordance with the requirements of the University's Regulations and Code of Practice for Research Degree Programmes and that it has not been submitted for any other academic award. Except where indicated by specific reference in the text, the work is the candidate's own work. Work done in collaboration with, or with the assistance of, others, is indicated as such. Any views expressed in the dissertation are those of the author.

SIGNED: ..... DATE: .....

Table of Contents

List of Tables

List of Figures

Figure **Page**

CHAPTER 1

INTRODUCTION

Tactile sensing gives humans the ability to interact directly with the environment and has resulted in the world being shaped such that it is easy for us to interact with. Bringing tactile sensing to robots is essential to provide human-level touch capabilities [1]. In this thesis, steps are made towards this goal by developing several enhancements and modifications to an existing optical tactile sensor, the TacTip (TACtile fingerTIP) originally presented by Chorley et al. (2009) [2]. The TacTip is a 3D-printed optical tactile sensor which provides several advantages including being low-cost (<£100), easy to modify, robust and highly versatile when applied to a variety of applications [3].

The focus of this thesis is slip detection and its uses in various aspects of robot grasping. Using both a single sensor and multiple sensors integrated onto a robot hand the TacTip's ability to detect slip using simple methods capable of operating in real-time is investigated. Futhermore, capability at slip detection in several functional grasping tasks is demonstrated. The results presented here have led to multiple publications in peer reviewed journals and conferences in the field of robotics.

The remainder of this introductory chapter is organised as follows. First, in Section 1.1 I will provide the motivation for the work conducted in this thesis. Section 1.3 presents the research questions addressed throughout the thesis. Section 1.4 summarises the contributions made by this work. Section 1.5 contains a list of publications which have been obtained during my postgraduate study. In Section 1.6 I provide a glossary of key terms which appear frequently in this thesis for the convenience of the reader. Finally, Section 1.7 sets out the structure for the remainder of the thesis.

1.1 Motivation

Tactile afferents provide information about the state of a grasp and, crucially, whether the grasp is failing. It is well known that tactile sensing is useful in robotic grasping and provides information complementary to vision [4, 5], such as contact forces and surface texture. To paraphrase Bajcsy et al. (1987): vision hypothesises, touch verifies [6]. Studies have shown that the ability to grasping and manipulation tasks such as fastening a button or holding a cup can be seriously impaired with reduced tactile sensation [7, 8]. However, when vision is impaired tasks may take significantly longer and manipulating objects carries a greater risk of damage due to the increased difficulty of localising the object and potential hazards. As such both senses are extremely valuable when performing effective grasping.

One aspect of human touch is slip detection, which is the ability to detect when something is moving relative to the skin. Slip detection is utilised by humans in a variety of scenarios including determining ideal grasping strength [9] and inferring object properties [10, 11] and it has been shown to lead to disastrous consequences when impaired [8].

Attempting to replicate slip detection in robots has been an area of interest for decades with software and hardware solutions utilising everything from accelerometers by Howe et al. (1989) [12] to deep neural networks in recent years [13, 14, 15]. What is fascinating about slip detection is that the idea is so simple and the benefits crystal clear; if you're holding something you don't want to accidentally drop it and if you feel it slipping you want to take an action to prevent grasp failure. However, slip detection and particularly incipient slip - where only part of the contact surface slips and the rest remains static - are far from solved problems with a wide variety of sensors and methods used to this day [16].

This thesis involves the study of new sensors and methods of slip detection, and an analysis of how slip detection can be used to improve robot touch. Additionally, this thesis explores how one can mimic human sense of touch to improve slip detection in robots, as has been done in many areas of robotics such as localisation [17] and flight [18]. By observing phenomena present in human touch and studying the physical structures which help facilitate them we can reap the benefits of billions of years of evolution and simultaneously push the boundaries of what is possible with robots [19].

A specific niche within slip detection that has interested me is the development of low-cost systems which utilise simple classifiers for inference. The benefit of low cost systems is that they make adoption of the technology easier for a larger group of researchers and end-users which can lead to faster progress through collaborative effort. Focusing on simple methods of detection means that this functionality will not take up a large amount of the processing capacity of the robot and can therefore be easily included on systems. Slip detection and response could even be devolved to smaller computers distributed throughout a machine analogously to how reflexes such as pain response is rapidly rooted through the spinal cord and not the brain [20].

Therefore, slip detection coupled with low computational load can form an integral part of a

robotic system's sensory smorgasbord. This thesis seeks to convince the reader that slip detection is as useful a sense to robots as it is to humans and should be included in any future tactile robot system interacting with the cluttered environment around us.

1.2 Hypothesis

Before breaking down this thesis into specific research questions I will lay out my hypothesis which was spawned from the research motivation discussed above. The fundamental hypothesis which this thesis addresses is:

Slip detection capability, defined as the ability to detect when the contact surface of a sensor is moving relative to object, can be implemented using the TacTip and utilised to improve performance in multiple of the stages which comprise a robot grasp.

This hypothesis has three key parts. First, it defines slip which is necessary to be clear about exactly what phenomenon we are trying to detect. Secondly, as it is the sensor used throughout this research, it is important to clarify that it is the TacTip's suitability to detect slip which is being investigated. Going further, we can investigate how modifying the sensor in shape and size whilst retaining the operating principle as a soft optical sensor can make it suitable to being used on robotic hands, detect slip in various scenarios and be used to detect some early signals of slip - incipient slip.

Finally, it was my belief when starting this research that slip detection can be applied to several stages of a grasp. This includes when making initial contact with an object and when the grasp needs to be altered, for example if weight is added to an object. As we seek to find a detection method which looks at the fundamentals of what slip is - the contact surface of a sensor moving relative to an object - it would be beneficial if the same method can be applied to these different scenarios.

To approach this hypothesis it is useful to break it down into several research questions. These are outlined in the next section.

1.3 Research Questions

The overall goal of this thesis is to explore the various aspects of slip detection and determine its usefulness to robot grasping. This goal has been broken down into several smaller research questions tackling different areas relating to slip detection which will be unified at the end of the thesis and discussed in relation to the overall research aim and the hypothesis given above. The questions which will be answered are as follows:

- Can a simple method be used with the TacTip biomimetic optical tactile sensor to detect slip and prevent total loss of contact with an object?
- Does the addition of tactile sensing to a robotic manipulator enhance effectiveness of the system?
- Can a low-cost multi-fingered manipulator be used to reliably detect slip?
- Can slip detection be used as a metric to evaluate the stability of a grasp and improve grasping efficiency?
- Does mimicking the human fingerprint result in detectable incipient slip in a tactile sensor?

1.4 Contributions

The research conducted in the development of this thesis has resulted in the following contributions:

- Developed a slip detection method using the TacTip which was able to prevent a slipping object from being dropped.
- Miniaturised the TacTip such that it is suitable for integration into robotic hands.
- Developed a modified 3D-printed three-fingered hand containing three miniature TacTips.
- Developed a slip correction strategy for when a grasped object is about to be dropped.
- Designed a fingerprint-inspired TacTip for inducing and detecting incipient slip.

1.5 Publications

Below is a list of the published works in peer-reviewed journals and conferences achieved over the course of my postgraduate work and included in this thesis.

- J. W. James and N. F. Lepora, "Slip Detection for Grasp Stabilization With a Multifingered Tactile Robot Hand," in IEEE Transactions on Robotics, early access. doi.org/10.1109/TRO.2020.3031245.
- J. W. James*, A. Church*, L. Cramphorn & N. F. Lepora. (2020). Tactile Model O: Fabrication and testing of a 3D-printed, three-fingered tactile robot hand. Soft Robotics, ahead of print. doi.org/10.1089/soro.2020.0019.
- J. W. James, S. J. Redmond & N. F. Lepora. (2020). A Biomimetic Tactile Fingerprint Induces Incipient Slip. 2020 IEEE/RSJ International Conference on Intelligent Robots and Systems (IROS), pp 9833-9839.

- J. W. James, N. Pestell & N. F. Lepora. (2018). Slip detection with a biomimetic tactile sensor. IEEE Robotics and Automation Letters, 3(4), 3340-3346.
- J. W. James & N. F. Lepora (2018). Slip Detection on Natural Objects with a Biomimetic Tactile Sensor. In Conference on Biomimetic and Biohybrid Systems (pp. 232-235). Springer, Cham.

The asterisk is to indicate that A. Church and myself contributed equally to this paper.

1.6 Key Terms

For the convenience of the reader I have provided a short glossary of key terms which appear frequently throughout this thesis.

- Gross Slip - Slip characterised by the motion of the **entire** contact surface of a tactile sensor relative to the object or surface with which it is in contact.
- Incipient Slip - Slip characterised by the motion of **any part** of the contact surface of a tactile sensor relative to the object or surface with which it is in contact. The remainder of the contact surface remains static.
- Offline Testing - The validation of a classifier using data which has been previously been collected.
- Online Testing - The validation of a classifier and hardware by performing an experiment in real time using data collected on-the-fly.

1.7 Thesis Structure

This thesis contains six further chapters as follows:

- **Chapter 2** contains an overview of literature relevant to the fields of human tactile sensing, slip detection and tactile-enabled robot hands. This provides the foundation upon which the remainder of the thesis builds.
- **Chapter 3** focuses on gross slip detection with the TacTip. The camera system is updated to allow for higher frame rate sensing and a simple method is used to detect slip in real time. It is demonstrated that the TacTip is robust to changes in the object being contacted and can reliably prevent a slipping object from being dropped.
- **Chapter 4** introduces the Tactile Model O (T-MO) a three-fingered tactile robot hand which is a modification of the GRAB Lab Model O. Small camera modules are added to the hand

allowing for onboard processing of tactile data coming from three miniaturised TacTips. The grasping capabilities of the T-MO are also assessed in this chapter.

- **Chapter 5** investigates the slip detection capabilities of the Tactile Model O. The smaller TacTips are first compared to the larger 'traditional' TacTip before all three are used to detect slip with the whole hand. Slip detection as a metric to determine grasp stability is also explored in the context of real-world grasping experiments.
- **Chapter 6** involves the evolution of the TacTip design such that it facilitates incipient slip. Two fingerprint-inspired design iterations are presented which work towards the goal of having detectable incipient slip using the TacTip.
- **Chapter 7** summarises the work presented in the preceding four chapters and presents the main conclusion of the thesis. The limitations and future avenues of the research are also discussed.

CHAPTER 2

LITERATURE REVIEW

The field of tactile robotics stretches over multiple domains and includes everything from the design of sensors to perform a specific function to the development of hands and feet. This provides robots with some of the tactile sense possessed by humans and therefore allows them to interact with objects around them and gain information with which to perform tasks.

This thesis aims to develop a sensor suited to detecting slip and integrate it onto a robotic hand to demonstrate its effectiveness at improving grasping performance. This literature review will therefore be split into four sections. First, I will briefly discuss the tactile sensing in the human hand. Secondly, I will discuss the various tactile sensor technologies. Thirdly, I will discuss relevant work in the field of slip detection. Finally, I will discuss the integration of tactile sensors onto grippers and multi-fingered robotic hands.

2.1 The Human Sense of Touch

The benefit of working in tactile robotics is that every day you are reminded of what is possible with the combination of a complex manipulator, sophisticated tactile sensors and a remarkable computer. Replicating the capability of human hands and the brain that controls it is the long term goal of tactile robotics and provides the principal motivation for the entire field.

2.1.1 Human Hand Structure

The human hand consists of 27 bones which fall into five categories [22] (Fig. 2.1). At the base are eight carpal bones forming the wrist which connects the hand to the forearm. There are then five metacarpals which are the intemediate bones separating the wrist from the fingers.

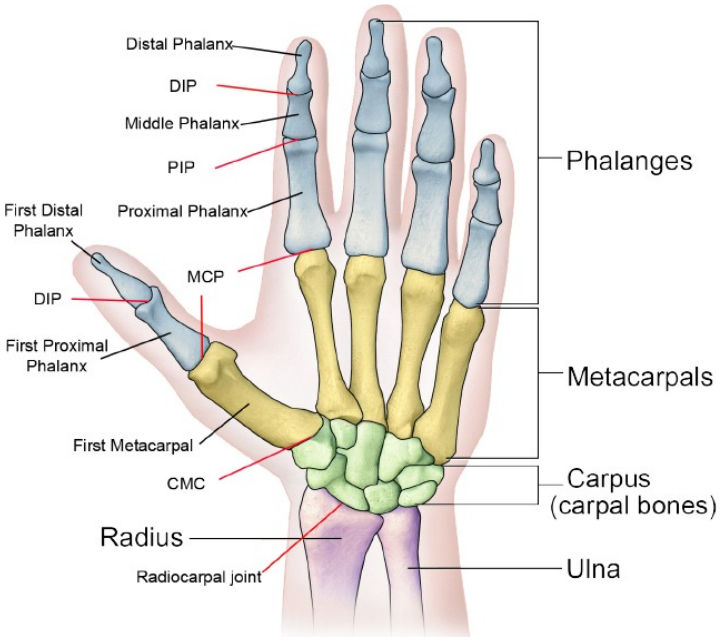

Figure 2.1: The bones in the human hand [21]. ©Wiley [2015].

The remaining fourteen bones are all phalanges. The four outer fingers contain three phalanges each: proximal, intermediate and distal. The thumb contains only two: the proximal and distal phalanges.

The hand is moved by the activation of muscles which are connected to tendons which are in turn attached to bones in the hand. Flexor muscles allow the fingers to close and extensor muscles allow them to open. Each finger has two flexor muscles; one is attached to the distal phalanx and one to the intermediate phalanx. There is one extensor tendon per finger, except for the index and little finger which have an extra tendon each. The thumb is more complicated having muscles and tendons for flexion, extension and opposition.

The structure of the hand allows for movement in four locations [23]:

- At the hinges between phalanges in the fingers
- At the joint between metacarpals and the fingers (metacarpophalangeal joints)
- At the joint between palm and wrist
- At the wrist

These hinges combined with the thumb's ability to be opposed to the fingers makes the human hand highly effective at grasping and dexterous manipulation.

2.1.2 Tactile Sensing in the Hand

Whilst the structure of the hand helps to facilitate our high level of skill at manipulation tasks it is the sense of touch that provides crucial information which allows this to happen [24]. In fact, our tactile sense extends beyond the hands, covering our entire body and provides information relating to heat, pressure, pain and proprioception [25]. Touch can even be used to communicate emotions [26] and plays a role in developing social relationships in humans and primates [27].

As this thesis focuses on touch associated with robot fingertips greater detail of the touch receptors in the glabrous (non-hairy) skin in the human fingers and palms will be provided. The hand contains many tactile mechanoreceptors [1] (Fig. 2.2) and the fingertip has the highest level of spatial acuity for touch [28]. This, not only allows for manipulation but also allows humans to detect the orientation of edges [29], interpret braille [30] and identify objects by touch alone [31].

There are four principal mechanoreceptors in the glabrous (non-hairy) skin that provide this tactile sense (list adapted from Johansson et al. (2009) [1]):

1. **Meissner Corpuscle**
    - Rapidly adapting type one (RA-I)
    - Sensitive to dynamic skin deformation at frequencies between 5-50 Hz
    - Cannot sense static force
    - Detects edges and braille-like features
2. **Pacinian Corpuscle**
    - Rapidly adapting type two (RA-II)
    - Sensitive to high frequency vibrations 40-400 Hz
    - Cannot sense static force
    - Detects vibration [32]
3. **Merkel Corpuscle**
    - Slowly adapting type one (SA-I)
    - Sensitive to skin deformation at low frequencies < 5 Hz
    - Sensitive to static force
    - Provides information about object surface features [33]
4. **Ruffini Endings**
    - Slowing adapting type two (SA-II)
    - Low sensitivity to dynamic skin movement

- Sensitive to static force
- Detect when skin is stretched [34]

When a stimulus is introduced to a mechanoreceptor they will 'fire' at an elevated rate. Adaptation (rapid or slow) refers to how long before the rate returns to the resting level. Rapidly adapting mechanoreceptors will only provide a signal for a short period which explains why they are insensitive to static force. Slowly adapting mechanoreceptors will continue to fire whilst the static stimulus remains.

Another facet of mechanoreceptors is the frequencies to which they are sensitive. RA-I and RA-II mechanoreceptors are sensitive to high frequency deformation of the skin. This is different from rate of adaption as this refers to the frequency of the stimulus which will initiate a response from the mechanoreceptors. For example RA-I and RA-II are sensitive to dynamic events such as high frequency vibrations whereas SA-I and SA-II are more suited to detecting static events such as skin indentation and stretching [35, 36, 37].

RA-I and SA-I mechanoreceptors have a small receptive field which provides accurate information about the location of the stimulus.This explains their high density in the fingertips where high acuity is desirable [38]. RA-II and SA-II have large receptive fields which allows for stimuli to be detected from up to several centimeters away [39].

The distribution of mechanoreceptors varies across the skin. RA-I receptors are densely packed in the fingertips and much less dense throughout the rest of the hand which demonstrates how important collecting information about dynamic events is to effective grasping [1]. RA-II afferents are more uniformly spread across the hand and given their large receptive field this means many hundreds of can be excited when contact is made, or broken, with an object during grasping [40]. The slowly adapting afferents follow a similar pattern. SA-I afferents are dense in the fingertips (albeit less so than RA-I), less dense in the rest of the finger and sparse in the palm of the hand. SA-II afferents are uniformly distributed at low density across the entire hand.

The four mechanoreceptors above combine to give the human hand a very sophisticated sense of touch. The ability to detect two stimuli as distinct is best at the fingertips where two indentations approximately 2mm apart can be distinguished [42] whereas on the belly it is approximately 30mm [43]. Other sensations that can be detected by the fingertips include vibrations (up to 700 Hz [25]), low contact force (down to 0.055 gram-force (gf) for men and 0.019gf for women [44]) and small temperature changes (approximately 0.16 °C [45]) to name but a few.

2.1.3 Slip Detection in Humans

Tactile slip detection, the ability to tell when something is moving relative to the skin, is another useful sense that can be performed. This is useful in many situations including finding the minimum grasping force when handling items [46], detecting roughness [10] and determining the object's shape [47, 48].

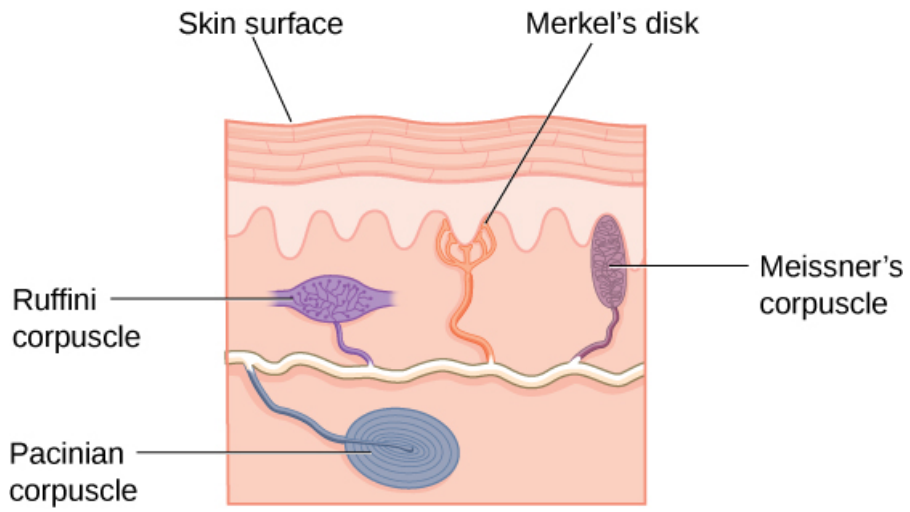

Figure 2.2: Location of tactile afferents in the skin [41].

To determine that slip detection is being performed by the mechanoreceptors in the skin, and not by another means such as proprioception, a simple test can be performed. Johansson and Westling (1984) anaesthetised the fingertips of subjects who then attempted to lift objects using a two finger grip and it was shown that where initial grasping force was insufficient to lift the object the fingers slid over the object without the subject noticing [8]. They determined that humans can make adjustments to the onset of slip after only 0.06s which they argue, due to the small latency, is executed automatically [49]. When reacting to a slip it was shown that humans will grasp with more force than is necessary to stop the slip by a margin of 10-40% [46]. In other words, humans overreact to slip with a noticeable safety margin to ensure the cessation of slip.

On a mechanoreceptor level Srinivasan et al. (1990) demonstrated that slip is detectable due to the firing of rapidly adapting mechanoreceptors (Meissner or Pacinian corpuscles) depending on the surface [9]. When a smooth plate with a single raised dot (4 µm high, 550 µm diameter) was moved over a finger pad the firing of Meissner corpuscles (which have small receptive fields) provided a spatio-temporal code in the direction of sliding.

When the stimulus was instead a matrix of dots (1 µm high, 50 µm diameter, spaced at 100 pm center-to-center) and was stroked the resulting vibrations in the skin activated the Pacinian corpuscles sufficiently to provide a code which could be interpreted as slip. Interestingly, without the stroking this matrix would be undetectable by humans [50].

Additionally, Srinivasan et al. (1990) discovered that humans are unable to detect slip on a glass plate. They were able to detect in which direction the skin was being stretched (and therefore infer the direction that slip occurs) but could not identify relative motion between the finger pad and glass. Therefore, through a combination of vibratory and spatio-temporal signals from mechanoreceptors humans are able to reliably detect slip on structures that cannot be detected through static touch.

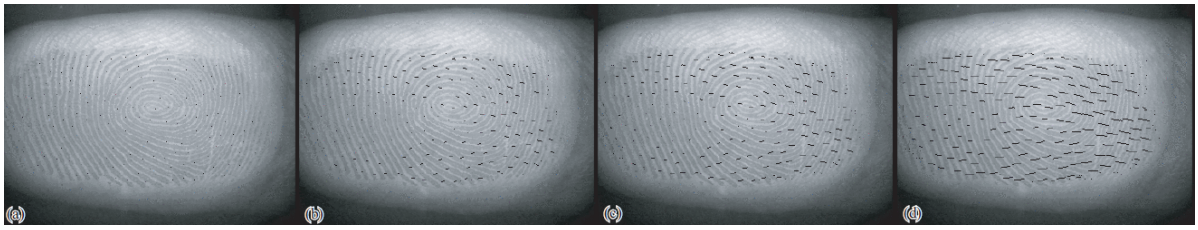

Figure 2.3: Incipient slip in the human fingertip. From left to right, motion of the fingertip (shown by arrows) starts from the periphery and moves inward as the slip progresses [52] ©IEEE [2004].

Due to the distribution of normal force across the fingertip certain regions of the finger may slip before others [51]. As the normal force (and therefore frictional force) is lower on the outside of the contact area these regions are seen to slip first (Fig.2.3 [52]). This is known as *incipient* slip and on the mechanoreceptor level this provides significant stimulation to the FA-1 and SA-1 afferents [53]. These incipient slips were observed to trigger an increase in grip force in a similar fashion to when the entire fingertip slip, although less marked. Although it is important to note that these incipient slips were inferred from an accelerometer signal and not directly observed as in Tada and Kanade (2004) [52].

To summarise; humans have a sophisticated sense of touch which allows them to manipulate the objects in the environment around them. Humans can detect the slippage of all but the smoothest objects by sensing both when localised areas of the skin begins to move and when the entire contact surface moves. A rapid response is then initiated which stops the slipping and secures the object. I will now discuss the development of artificial tactile sensors which have sought to replicate the success of the human tactile sensory system.

2.2 Artificial Tactile Sensors

Nicholls and Lee (1989) [54] define a tactile sensor as "a device which measures parameters of a contact interaction between the device and some physical stimuli" the ultimate goal of which is to replicate and better the human sense of touch. To put into context the state of the art, I will briefly describe the early state of the field of tactile robotics before discussing more contemporary work germane to this thesis.

The 1970's produced several primitive tactile sensors [55, 56], including a sensor using a conductive elastomer where the change in conductivity due to pressure allowed for the identification of different surfaces [57]. These early sensors resulted in industrial interest in tactile robotics which led to a list of design criteria which needed to be satisfied to be useful in an industrial setting [58] (Table 2.1).

In the 1980's research output grew rapidly [59] and with it, more complex sensors (many of which utilised sensing technologies that are still in use today) were developed. Such technologies include conductive sensors such as that developed by Christ & Sanderson (1982) which had

Description	Criteria
Sensing Surface	Compliant & Durable
Taxel Resolution	1-2 mm
Number of Taxels	50-200
Pressure Sensitivity	1g
Dynamic Range	~1000:1
Output Response	Monotonic
Frequency	>100 Hz
Stability & Repeatability	Good
Hysteresis	Low

Table 2.1: Harmon Criteria for tactile sensors. Adapted from [59].

two 16x16 arrays of conductors filled with a conductive foam. When compressed the resistance changes and contact location can be inferred with a resolution of 1/4 inch [60]. Other popular sensing methods included piezoelectric [61, 62], capacitive [63, 64], magnetic [65, 66] and optical [67, 68].

The diversity of sensing technologies continues to this day with no particular sensing method proving to be the standard. In a recent review Kappassov et al. (2015) identify the following technologies as the dominant areas of research within tactile robotics: Piezoresistive, piezoelectric, barometric, capacitive, quantum tunnel effect and optical [69]. The remainder of this section will focus on recent advances in each sensing mode with particular focus on optical tactile sensors.

2.2.1 Piezoresistive & Piezoelectric Sensors

The piezoresistive effect is when the resistance of a material changes due to an applied stress [70]. Similarly, the piezoelectric effect is when an electric charge is generated when a stress is applied to a material [71]. Piezoresistive sensors have the advantage of being able to detect dynamic and static loads and work well when detecting very low frequency loads [72]. One method of constructing piezoresistive sensors is to use a conductive rubber or foam above two separate electrodes. The resistance of the material changes under load and is detected by measuring the resistance between the two electrodes [73]. This method was used by Koiva et al. (2013) to develop a small fingertip sensor containing 12 taxels. By printing the electrodes on flexible PCB the resulting sensor was able to conform to the shape of a human fingertip and had a data collection frequency of >1 kHz [74]. This flexibility also allows for tactile fabrics to be created which would be beneficial for a tactile skin [75]. However, piezoresistive sensors are sensitive to changes in temperature and suffer from high hysteresis [76].

Piezoelectric sensors have numerous advantages including: high frequency range (>500 kHz), high repeatability and insensitivity to electromagnetic fields and radiation [77]. The significant disadvantage is that they can only be used for dynamic tactile sensing. Materials such as polyvinylidene fluoride (PVDF) have been used to develop tactile sensors for applications such as

endoscopy [78] robot grasping [79]. Goger et al. (2009) combined piezoelectric and piezoresistive technologies to develop a tactile sensor which could detect both static and dynamic loads [80].

2.2.2 Barometric Sensors

At its heart, the majority of barometric sensors can be thought of as a subset of piezoresistive sensors as many of them use microelectromechanical systems (MEMS) barometers embedded in a material such as liquid, rubber or foam. Zillich & Feiten (2012) use a piezoresistive MEMS barometer surrounded by foam to create small (25x25mm) sensors which are suitable for covering a curved surface and therefore acting as a skin [81]. The TakkTile [82], has mutliple MEMS barometers cast in rubber to create a tactile array. Such barometric sensors are cheap to produce and have a reasonably high data output frequency (~100 Hz) but do usually suffer from poor localisation accuracy (~1mm) [83] and spatial resolution due to the size of the barometer chip.

Sensors using MEMS barometers embedded in liquid do not suffer from the low frequency response of rubber and can therefore detect much higher frequency signals. The BioTac (SynTouch LLC) [84, 85, 86] has the ability to detect frequencies up to 1 kHz and is also multi-modal; containing temperature and impedance sensors as well as the barometer. This combination has proved successful with the BioTac being deployed in multiple scenarios such as texture detection [87] and medical examination [88].

2.2.3 Capacitive Sensors

Capacitive sensors operate by having a dielectric material sandwiched between two conductive plates. When the sensor is compressed under load the capacitance changes. Capacitive sensors are, perhaps, the most encountered due to their prevalence in mobile phone touch screens. They are not solely restricted to normal forces; Lee et al. (2009) embedded multiple capacitors in polydimethylsiloxane (PDMS) to detect both normal force and shear force [89]. Many well known robotic hands and platforms have utilised capacitive technology as their tactile sensor [69] including the iCub fingertip [90], the Allegro hand [91], the PR2 grippers [92] and the Robotiq Adaptive Gripper [93]. Capacitive sensors can suffer from *creep* where the reading slowly changes over time despite a constant load.

2.2.4 Quantum Tunnel Effect Sensors

Quantum tunnelling is a quantum mechanical phenomenon where a particle can pass through a potential barrier with higher energy than the kinetic energy of the particle; thus making it forbidden by the laws of classical dynamics [94]. This effect, which is important in maintaining fusion in stars [95] has been applied to robotics through Quantum Tunnel Composites (QTC). QTCs are electrical insulators which, under load, become conductors when metal particles in the material are close enough for electrons to *tunnel* through the material, thus generating a

potential difference. QTC sensors are highly sensitive and have been made into a flexible arrays [96] and integrated onto robotic hands [97, 98].

2.3 Optical Tactile Sensors

As the work presented in this thesis uses an optical tactile sensor, the TacTip (and variants thereof), it is beneficial to look at other optical tactile sensors and draw comparisons with the TacTip. The fundamental working principle behind optical tactile sensors is to use an electronic sensor - usually a CMOS/CCD camera - to 'see' features on the sensor surface. These features can be anything that is visable by a camera for example embedding markers or pins in the surface (as with the TacTip) or using multiple small rubber pyramids and LEDs to generate shadows [99]. Each pixel in the image becomes a taxel which, depending on the resolution of the camera, can give the sensor very high dimensionality.

A major benefit of this approach is that the delicate and potentially expensive part of the sensor, the camera, is kept away from the contact surface so that in the event of damage to the sensor the camera is unaffected. If the surface of the sensor is easy to manufacture and replace this minimises down-time. Additionally, advances in camera technology and computer vision are able to be leveraged by optical tactile sensors. The remainder of this section will focus primarily on the TacTip but also discuss other optical tactile sensors. For further reading see recent reviews by Shimonomura [100] and Abad et al. [101].

2.3.1 The TacTip

The TacTip was originally presented by Chorley et al. (2009) and the fundamental operating principle has not altered greatly since [2]. The sensor consists of a 3D printed rubber-like hemisphere with white protrusions on the inside which mimic the intermediate ridges in the human fingertip. The sensor is filled with transparent silicone gel and sealed with an acrylic lens. A CMOS camera mounted above the lens views the protrusions, hereafter referred to as 'pins' as they contact objects and surfaces. Originally, the TacTip used a CCD camera but more recent iterations use a CMOS sensor. Using super-resolution methods the TacTip has achieve a resolution of 0.1mm when localising the TacTip on the surface of an object [102]. The TacTip has also been used for a wide variety of tasks such as contour following, edge detection and manipulation with many different software methodologies including Bayesian sequential analysis [103], maximum likelihood estimation [104], Principal Component Analysis [105] and Deep learning [106].

The surface of the TacTip is generally smooth, however Cramphorn et al. (2017) [107] added small nodules which mimic the human fingertip to the surface. The nodules are comparable to the epidermal ridges of the human fingertip and the pins are comparable to the Merkel cells. The localisation perception of the sensor with a fingerprint provided a 140-170% improvement

over a sensor without a fingerprint. Work has also been performed on using the TacTip as a force sensor. Giannaccini et al. (2016) [108] pressed the TacTip vertically against a load cell at various compression depths as a calibration procedure. They found that a 7mm compression of the TacTip is possible before irreversible damage occurs and could differentiate between depths differing by 0.5mm. Other work has included texture analysis [109] and lump detection in soft tissue [110].

Other camera technologies have been used in the TacTip. Pestell et al. (2018) [111] integrated a 30x30 pixel optical mouse sensor (ADNS-3080 [112]) into the TacTip. The sensor can be operated in two modes: high frequency (2 kHz) which returns various statistics of the image such as movement of features in the image, maximum pixel value and image quality (a measure of the number of features present in the image); and low frequency mode (3 Hz) which returns the 30x30 image. These modes were used to detect sensor orientation and modulate sensor contact depth when performing a 3D contour following task. Ward-Cherrier et al. (2020) have used neuromorphic camera technology with the TacTip to perform texture classification using various spike train encoding methods [113]. Neuromorphic cameras provide an efficient way to transmit information by only providing information about changes in the image from one frame to the next. Up to 12 million events can be detected per second and by detecting events instead of the entire image the power consumption of the camera is reduced [114].

2.3.2 Other Marker Based Solutions

Many other optical tactile sensors work on the principle of having markers embedded in the sensor skin within a gel. For example, the GelForce has two layers of markers embedded in an elastic substance whose positions are read by a camera; a design very similar to the TacTip [115]. In the original paper the GelForce was able to determine the force applied to an accuracy of 0.3N and the angle of the force (with respect to the normal) within 5 degrees. Originally, the camera was not integrated into the sensor; however, later work involved the development a GelForce finger sensor with a 60fps VGA camera [116].

Lin et al. (2020) presented an optical tactile sensor where magenta and yellow markers are embedded in different layers of a clear elastomer and then folded into a hemispherical shape before being imaged by a camera with a fisheye lens [117]. The relative movement of the different coloured markers allows for an estimate of the 3D motion of the sensor which was used to determine the curvature of stimuli with only a 1mm contact depth. This sensor is an evolution of the earlier ChromaTouch sensor by Lin & Wiertlewski (2019) which had a similar working principle but had a planar surface rather than curved [118]. The justification for curving the sensor was that it allows the sensor to contact a wider variety of surfaces - for example a flat sensor cannot be deformed by a concave object.

The sensors presented in this section so far all involve using large images of 640x480 pixels or similar and are all single-mode. Knoop et al. (2013) [119] developed a dual-mode optical tactile sensor that uses a CMOS sensor with only 18x18 pixels. A transparent resin sits inside a black

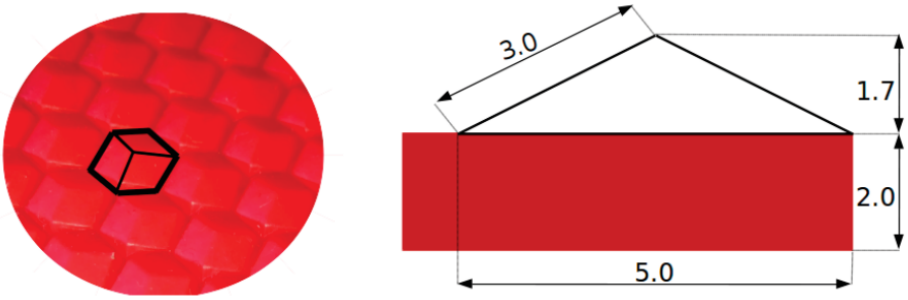

Figure 2.4: The pyramidal tactile elements developed by [99]. The left hand image highlights a single pyramid within the deformable rubber surface and the right hand image gives the dimensions of each pyramid in mm. ©IEEE [2016]

rubber hemisphere with painted white dots. The dots are approximately 1mm in diameter and spaced 2mm apart. The imaging system is a tracking image sensor with onboard Digital Signal Processing which allows for a frame rate of 1500Hz. This outputs the movement of objects in x and y as well as raw pixel values. Extracting the entire image slows the frame rate down to 4.6Hz. The authors used both modes of operation with the higher frame rate being used to quickly estimate the normal force applied to the sensor and the lower frame rate mode to gain a more accurate force estimate. They compare the use of two modes to humans who will make quick decisions or more calculated ones depending on the situation. The high speed mode would certainly be useful for slip detection as it is a situation that requires a very fast response.

2.3.3 Skin Reflection

Corradi et al. (2015) [120] presented a low cost optical tactile sensor, the Bath Tip, which is very similar to the TacTip. It consists of a 40mm radius hemisphere illuminated by LEDs and an eSecure USB webcam. Unlike the TacTip it doesn't contain pins or gel. When the tip is in contact with an object the surface deforms changing the pattern of shade on the inside of the hemisphere. The camera records this shading pattern to determine the properties of the object. The Bath Tip was able to recognise and distinguish between ten common household objects with 95% accuracy. The camera in the Bath Tip runs at 30 frames per second which is common for USB webcam devices.

Kolker et al. (2016) [99] developed an optical tactile sensor where the tactile elements are rubber pyramids whose centres are 5mm apart (Fig.2.4). These pyramids are viewed by a VGA USB camera. When illuminated the elements show up as triangles but contact with objects deforms the rubber hence the areas and locations of the triangles are altered. This can be thought of as a combination of the TacTip and the Bath Tip. There are distinct tactile elements, as with the TacTip, but they are the same material as the rest of the exterior of the sensor, as with the Bath Tip. The experiment presented in the paper focusses on using the sensor as a 3D force

sensor. The authors claim it has 'high sensitivity' however do not give specific values or tolerances to substantiate this claim. They do provide computational timings with the image processing taking 27ms and the frame capture running at approximately 18 frames per second which is significantly lower than the TacTip.

Another optical tactile sensor is the GelSight, first presented by Johnson el al. (2009) [121]. The original iteration consisted of a reflecting elastomeric gel whose surface topography is measured when the sensor deforms due to contact with an object. Initially the camera system wasn't integrated into the sensor and instead captured the gel from 40cm away but subsequent work resulted in a GelSight soft fingertip with an integrated webcam running at 30fps [122]. The GelSight has been since used for many purposes such as detection of lumps [123], texture classification [124] and slip detection [125].

2.3.4 Other Optical Solutions

Optic Fibres: This method means that expensive and often bulky imaging equipment can be moved away from the tactile surface yet keep the large amount of data available by using optical systems. Baimukashev et al. (2020) [126] presented a novel sensor where a multicoloured circular silicone surface is imaged using plastic optical fibres and as the sensor deforms shear and torsion are calculable.

Total Internal Reflection: (TIR) is a phenomenon where all light incident on a surface of different refractive index is reflected and none is refracted. Interestingly, one of the first optical tactile sensors utilising TIR was by Chodera (1957) for the purpose of pedobarography - the measuring of the pressure distribution caused by feet [127]. In this case the feet indent an elastic foil surface and the pattern of light caused by TIR allows for a reconstruction of the pressure across the feet. More recently Saga et al. (2014) utilised TIR for the reconstruction of objects indenting a silicone sensor surface. A camera measures the distortion of a square chessboard pattern due to TIR from which the shape of the indenter can be determined [128].

2.4 Tactile Dexterous Robotic Manipulators

The previous section discussed the variety of tactile sensors in existence. In this section we will give a brief overview of dexterous manipulators with an emphasis on under-actuated hands before discussing the integration of tactile sensing to robotic hands and grippers.

2.4.1 Dexterous Manipulators

The world of robotic hands is incredibly diverse with solutions ranging from two finger pinch grippers [129, 130, 131] to under-actuated hands with multiple joints but only a single actuator [132] to highly anthropomorphic hands with ten [133] or twenty degrees of freedom [134]. The choice of design depends on the desired use-case and control system at one's disposal. The

ultimate goal is to exceed the human level of grasping capability in a similar manner as has been achieved in strategy games such as Chess [135] and more recently Starcraft II [136] and Go [137]. To briefly cover the landscape of manipulators we will segment the discussion into visual design (gripper, anthropomorphic, non-anthropomorphic) and actuation capability (fully-actuated, coupled and under-actuated) [138, 139].

Anthropomorphic hands take a biomimetic approach in their construction; using the structures of the human hand as a blueprint to make design decisions. Key features include an opposable thumb, parallel fingers and a palm. The number of digits varies with many having all five [140, 141, 142] but others having fewer [143, 144].

The justification for an anthropomorphic approach is clear; the human hand is used to great effect to manipulate objects over a wide range of sizes with a skill level which far exceeds any existing robotic system [145]. Other benefits include prosthesis [146] and tele-operation [147] where a controllers hand movements must be precisely copied. The disadvantage is that the human hand is extremely complex. Not only do actuators need to be small to ensure the unit remains compact, powerful enough to lift a variety of objects and precise to allow for delicate manipulation but a control system is required to perform tasks.

Non-anthropomorphic hands seek to remove some of the complexity of anthropomorphic hands whilst maintaining strong grasping capabilities. Mathematical and engineering principles such as kinematic modelling of the fingers [148] are used to inform the manipulator design instead of mimicking nature. This results in a variety of different styles often including multiple opposable finger configurations (for different types of grasp) and identical fingers [149, 150]. Non-anthropomorphic hands are, perhaps, limited in versatility when compared to their highly complex anthropomorphic cousins and with continued advancements in manufacture and control may eventually struggle to compete.

Grippers consist of two parallel fingers facing each other whose operation is limited to performing pinch grasps and simple rolling maneuvers. There is variety, albeit small, within the world of grippers with single DoF parallel grippers [151] to four-bar linkage mechanisms which allow for simple planar manipulation [131]. This simplicity does, clearly, limit their operating capacity but - as discussed in the next section - when combined with tactile sensing they can be highly effecting grasping platforms.

Actuation design is another area where the complexity of robot hands can be segmented. First, it is helpful to distinguish between the degrees of freedom (DoF) and the degrees of actuation (DoA). DoF describes the number of modes of motion the mechanical system can make whereas degrees of actuation is the number of controllable actuators the system contains. Fully actuated hands have an equal number of DoF and DoA thereby providing a single actuator for each joint. Examples include the DLR Hand II which contains thirteen DoF and has been used for manipulating and catching objects and even playing the piano [152].

Coupled actuation is used to lower the number of actuators in a system by having the motion

of some joints dependent on others. DLR/HIT Hand II, which contains five identical fingers with four joints where the last two joints are coupled to reduce the degrees of freedom [153]. Historically fully actuated and coupled mechanisms were the most commonly seen solutions [139] but in recent years under-actuation has become increasingly popular.

Under-actuated mechanisms allow for passive movement of joints in a robot hand through the use of springs and mechanical limits resulting in fewer actuators than DoF [154]. For example, when closing on an irregularly shaped object, when one joint contacts the object and can move no further the force transfers to the subsequent joint which actuates until contact is established. This greatly simplifies the control systems required to grasp objects and by removing motors space and weight is saved. For example the IIT-Pisa SoftHand contains five fingers and nineteen joints yet uses only a single actuator to close the hand into a grasping configuration [132]. The hand was able to grasp over 100 objects because its morphology could adapt to each object. Further work has involved development of a tactile human-SoftHand interface for teleoperation [155] and performing safe human-to-robot handover tasks [156] which demonstrates the versatility of the underactuated system.

The OpenHand project develops open-source under-actuated robotic hands where many of the parts in the hand can be 3D-printed to ease in rapid prototyping and distribution to end-users [157]. Their first offering was the Model-T, which contains four identical fingers on a hand with a single actuator [158]. Despite the seemingly limiting factor of having a single actuator the Model T, with its underactuated design, is able to grasp a wide variety of objects.

Another OpenHand offerring, the Model O, is an open-source version of the three fingered i-HY hand [159] which won the ARM-H track of the DARPA manipulation challenge [160]. In fact, such is the increasing popularity of underactuated hands that in DARPA Robotics Challenge none of the entries were fully actuated anthropomorphic hands [139, 161]. The Model O is also 3D-printed and underactuated but has three fingers which are individually controllable by a single actuator. Two fingers have a coupled rotation at their base allowing for adduction and abduction thus providing a fourth degree-of-freedom. The Model O used this increased functionality to successfully grasp objects as small as a key and as large as a drill.

Actuation Method describes how the fingers in a hand are actually moved. Many of the hands described so far are tendon driven; this includes the Model O [159], the Xu & Todorov hand [133] and of course the human hand. The operating principle is that the motors are connected to the joints via a cable and when force is applied by the motor the joints actuate. This allows for motors (which are often heavy) to be kept away from the joints and stored in areas with more space such as the wrist.

Other systems use solid linkages to transfer the force between motor and joint. This is common in pinch grippers such as the GR2 [131]. Some robotic hands have the motor integrated into the joint so that when the motor is moving the joint is directly actuated - albeit often with a series of gears. The Allegro hand [91], for example, has a small unit at the joint containing a DC

motor, gears - to lower the gear ratio - and a joint angle sensor.

Another actuation method used is pneumatics, such as by the RBO Hand 2 [142] which uses seven inflatable PneuFlex actuators [162]. This design gives a highly dexterous hand, performing all but one of the poses in the Kapandji test [163] for evaluating human hand dexterity.

2.4.2 Integration of Tactile Sensors to Dexterous Manipulators

The fundamental motivating question behind tactile dexterous manipulators is: do tactile sensors improve the grasping and manipulation performance of robotic hands? Despite the undeniable usefulness to human grasping many robotic manipulators omit tactile sensors and use solely vision based grasping [164, 165, 166] or force and impedance sensing [167]. This may be a case of demonstrating the advances of data-driven methods such as Deep Learning in relatively controlled environments [168] as a comparison to tactile-enabled systems is not performed. Unfortunately, very few comparisons have been performed but in cases where it has been tactile sensing provides a marked performance increase [169, 170].

The TacTip has been mounted on robotic grippers and used to perform manipulation tasks. Ward Cherrier et al. (2016) used a variation of the TacTip, the TacThumb, to locate the position of a small cylinder that was being rolled along the surface of the thumb [171]. The TacThumb was mounted on a gripper based on the M2 gripper [172] which is itself an extension of the Yale OpenHand project [158]. More recently Ward-Cherrier et al. integrated the TacTip onto a GR2 two-fingered gripper [131] (Fig. 2.5) and performed manipulation of cyclinders held in a pinch grip [173].

Pestell et al. (2019) [174] integrated the TacTip onto the three fingered shadow modular grasper (Shadow Robot Company [175]). They extracted contact location and pressure information which enabled them to securely grasp objects from the YCB object set [176]. Having the TacTip technology already integrated on a hand will allow for a future research involving the integration of slip detection into the existing hands to be undertaken. Cramphorn (2019) [138] developed a fully actuated seven DoF hand with a modified TacTip on each of the six finger linkages (two per finger).

Looking beyond the TacTip, two GelSight optical tactile sensors were integrated onto a two finger parallel gripper and used for slip detection [15]. A slimmer version of the GelSight, the GelSlim, reflects the light signal down the finger to a camera module at its base [129]. This allows for the camera to be mounted in the base of the finger facing along its axis, thereby reducing the size of the sensor. More recent papers have continued using the GelSight for tactile object recognition [177] and surface-normal estimation [178].

Another bespoke tactile gripper is the FingerVision first presented by Yamaguchie and Atkeson (2018) [179]. It consists of a two layers of transparent silicone skin, one hard and one soft, with embedded black markers and was integrated onto a Baxter 1 DoF pinch gripper. The transparent skin allows for objects to be viewed directly and the markers provide further tactile

Figure 2.5: The TacTip integrated onto a GR2 gripper [131]. Image taken from [173]

information about the contact and has been used for such tasks as cutting vegetables and object manipulation [180].

Other widely-used platforms include the anthropomorphic iCub hand with integrated capacitive sensors [181], the Shadow hand with BioTac sensors placed at the fingertips [182] and with fabric and capacitive tactile sensors [74], the 4-fingered Allegro hand with PPS capacitive sensors [91] and with BioTac sensors [183] and the TWENDY-ONE hand with embedded force-torque sensors and a tactile skin [184]; this last hand was the first to use deep learning for object recognition. In addition, the i-HY hand used in this study has been integrated with MEMS barometric TakkTile sensors, to give a basic array of 4 pressure-sensitive taxels on each fingertip [159].

Testing of tactile enabled hands has largely taken the form of collecting a dataset of grasps on various objects and using various machine learning methods to try to distinguish between them. Spiers et al. (2016) use 11 objects from the Yale-CMU-Berkeley (YCB) object set [176] using data from an array of barometric pressure sensors attached to a two-fingered hand and classify them using random forests [185]. They obtained a validation accuracy of 94% when the objects' orientations were unconstrained.

Flintoff et al. (2018) also use random forests on a two-fingered hand containing barometric sensors and the Google Soli radar sensor [186] to classify 26 objects, obtaining 99% validation accuracy [187]. Schmitz et al. (2014) [184] identify a set of 20 objects with an accuracy of 88%

using a deep neural network on the four-fingered TWENDY-ONE hand [188]. Watkins-Valls et al. (2019) grasp 8 objects from the YCB dataset using visuo-tactile data. Using a tactile enabled Barrett hand they achieve 87.5% lifting success [189]. Li et al. (2014) use BioTac sensors attached to a four-fingered Allegro hand [190] to predict when a grasp is failing and deploy two strategies to find a stable grasp [191]. Cockburn et al. (2017) use a 4x7 tactile pressure array to predict grasp failure with 83.7% accuracy on a dataset of 54 object [192].

Another important area of manipulation is haptic exploration for determining object features such as shape, stiffness and texture. Humans are highly skilled at identifying objects from touch alone [31]. Okamura et al. (1997) use a two-fingered manipulator with strain gauges and an 8x8 tactile array for haptic exploration. The geometry of a sphere with a small ridge was determined using a controller by sliding one finger over the surface and rolling the object [193]. Yang et al. (2013) developed a controller which is able to determine the stiffness and shape of an object [194]. This controller operates without a contact force sensor which reduces the cost of the overall system. Falco et al. (2019) use a combination of vision and an opto-electronic deformation sensor to classify objects by exploring their surface and determining their shape [195].

2.5 Slip Detection Using Tactile Sensors

Tactile slip detection is the ability of a tactile sensor to determine when the contact area of an object being touched is moving relative to sensor surface. Reliably detecting slip is beneficial as it can be used as a sensory signal of when a grasped object is insecurely held and a physical response can be activated to prevent an object being dropped. Slip detection research can be broadly split into three categories [16]:

1. Slip prediction, where tactile signals can be used to predict when slip is about to occur.
2. Incipient slip, where *part* of the contact surface slip but the remainder is static.
3. Gross slip, where the entire contact surface area is slipping relative to the object.

When an object slips it will undergo these three stages in the above order; however, it is often helpful to describe them in reverse order to aid in providing intuition about the physical processes occurring. Gross slip is the final stage of slip where the object is completely slipping and an action must be swiftly taken to prevent it falling from one's grasp. This is the most prominent stage and is characterised by clear movement of the sensor surface and of the object as frictional forces are insufficient to keep it in place.

Incipient slip, the preceding stage, is characterised by slippage of parts of the surface whilst other areas remain static. In principle, this means that certain areas of contact will be moving relative to others which should be detectable. Incipient slip allows one to use physical movement of the sensor surface to determine that an object is insecurely held and take an action with minimal movement of the object.

Finally, it may be possible to predict that slip is likely to occur by modelling the interaction between sensor and object [196] or using a data-driven machine learning method to learn tactile features which precede slip [197, 198, 199]. Either way, to be robust to changes in object morphology, weight and texture one would need a very high fidelity model or a large dataset. I will now discuss relevant literature on slip detection focussing chiefly on gross and incipient slip as the work in this thesis involves the development of sensors and methods for the detection of those two phenomena.

Slip detection is an ever expanding field of interest with publication output expanding ten-fold since the early 2000s [200]. To cover it in detail this section will separate slip detection research into three categories. First, we will address slip detection research using single sensors and pinch grippers. Next, we will examine solutions using three or more fingers on a robotic hand before finally moving on to incipient slip research. There is, naturally, some overlap between these section but where incipient slip is the main area of interest in a paper it will be discussed in the third section.

2.5.1 Single Sensor & Grippers

Slip detection has been an area of study from the late 1980s. Early papers include those by Howe et al. (1989) [12] and Tremblay et al. (1993) [201] who used accelerometers embedded behind a 'skin' to detect when the surface of the sensor was slipping. More recently Hirai et al. (2010) developed a model of a compliant tactile sensor consisting of many 'virtual' cantilevers connected by springs [202]. The compression of the cantilevers models the normal force and the movement of the springs models shear and torque. This allowed for a mathematical model of slip to be created and tested. To test the model the authors placed a series of ridges on a semi-cylindrical surface and by using a load cell and force/torque sensor were able to extract information from the ridges. The sensor was slid across a horizontal surface at low speed (3-4mm/s) and slip was detected offline. They also investigate incipient slip and their results suggest that the centre of contact - the area subject to the highest normal force - is not the last to start slipping as one would intuitively suggest. The authors did not perform any experiments with an object falling under gravity which would lead to much greater slipping speeds.

Kondo et al. (2011) developed a fabric of electroconductive yarns whose electrical resistance depends on how stretched the fabric is [203]. At the moment directly prior to slip the extension of the yarns is at a maximum, leading to a minimum in resistance. It is the sharp increase in resistance when slip starts to occur that the authors used to detect slip. By performing a discrete wavelet transform to the resistance a threshold for slip was set. However, the authors mention that this isn't a very robust method and would require a more sophisticated classification method to work on varying loads and surfaces.

Yuan et al. (2015) used a GelSight tactile sensor to detect slip. They plotted the deviation of the markers in the sensor from their rest positions as a vector field and calculated the entropy

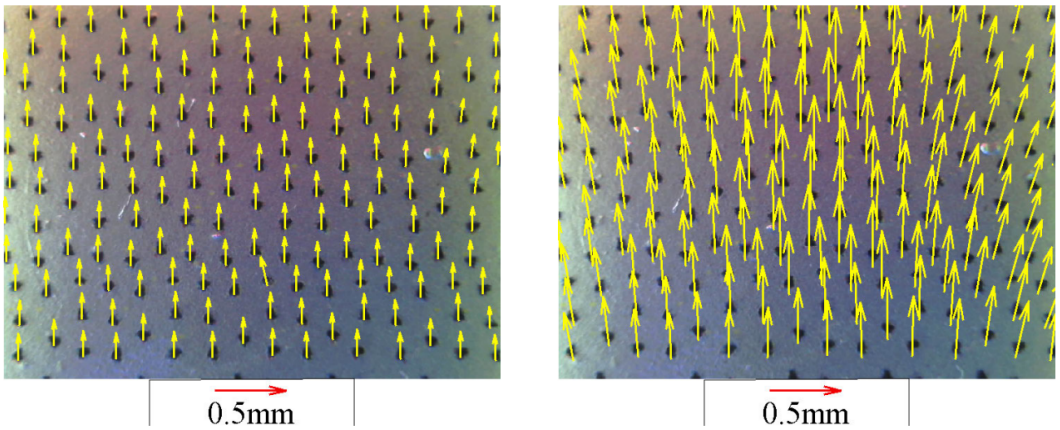

Figure 2.6: The Gelsight sensor with overlayed displacement arrows. The left hand image shows the effects on marker location due to a small load and the right hand image shows the effect of a large load [125]. ©IEEE [2015].

[125] (Fig. 2.6). It was noticed that slip was occurring at higher entropy and they were able to use a threshold to both detect slip and predict its occurrence. They built a gripper for the GelSight and show a graph of the entropy when an object is being pulled from the grip which shows a clear rise in entropy. The authors claim this phenomena is present when a variety of different objects are pulled from the gripper however they don't use any form of 'online' control to react to the object being removed nor do they state whether the threshold for slip would vary from object to object. The simplicity of the model is useful but there isn't much evidence that it is very robust. It seems as if there would need to be prior knowledge of the object's shape and weight to know what the entropy threshold is, however the authors don't discuss this. Further work with the same sensor involved GelSight sensors integrated onto a two-fingered gripper used slip detection to determine whether a grasp was stable and regrasp if necessary [15].

A similar sensor, the FingerVision, also uses markers embedded in a soft gel to perform slip detection [14]. They use a convolutional LSTM neural network to detect slip and obtain a 97.62% classification success rate but do not detect slip in real time in grasping experiments. Meier et al. (2016) use a piezo-resistive tactile array [204] and train a convolutional neural network which can classify at 125Hz [13]. They claim a 97% success rate but don't perform any online experiments so it's unclear how it would perform in a real-world scenario.

Massalim et al. (2020) [205] use accerometers embedded in silicone in the fingertips of a Schunk EGN100 pinch gripper to detect slip. An object is slid over the fingertips and several methods including Deep CNNs, LSTMs and feed-forward networks are compared. In their work the CNN was most successful at detecting slip and was able to do so within 17ms of its onset.

Many of the previously mentioned tactile sensors were constructed for slip detection however there are commercially available tactile sensors which have been applied to the task including the BioTac which has been mentioned previously. Veiga et al. (2015) use a BioTac sensor and two

Figure 2.7: The BioTac securing a watering can against a wall. This was part of the data collection method undertaken by [197]. ©IEEE [2015].

machine learning classification methods to detect and predict slip [197] (Fig. 2.7). They collect data from objects slipping past the sensor and train binary classifiers using Random Forests and Support Vector Machines. The 'ground truth' for the slip was determined by filming the objects as they fell however the camera was running at a much lower frame rate than the BioTac (which was being used at 100Hz). They use Random Forests to perform 'online' slip detection on seven different objects including a box and a ball. They test each object ten times and achieved up to 100% success depending on the classifier used. No single classifier performed well for every object so despite the high success it lacks robustness. Additionally, they performed slip prediction by training the classifier on data up to twenty time-steps prior to slip onset.

Other work using the BioTac for slip has included Zapata-Impata et al. (2019) [206] who used a convolutional LSTM network to detect slip and its direction which could help to inform a corrective action. Additionally, Reinecke et al. (2014) [207] compare several methods including friction cones, a bandpass filter and a random forest. They note that all methods are able to detect slip but make no conclusion of which is best but also give very little quantitative analysis of their results.

Other research builds on slip detection methods by implementing more complex control systems for decision making when slipping. Heydarabad et al. (2017) compare Super Twisting Sliding Mode Control (STSMC) and First Order Sliding Mode Control (FOSMC) when preventing an object being dropped (or damaged) after the onset of slip [151]. Sliding Mode Control is a system where a controller will switch between different control schemes according to some input. The input in this case is the amount of object slippage - which the controller wants to minimise - and the output is the motor control. The experiment involves grasping an object with a one degree of freedom, two finger gripper and suddenly adding weight to test how well slippage is prevented. Both control modes perform well however FOSMC exhibits a severe 'chattering' where

the motor controlling the gripper is highly active and therefore not very efficient. STSMC does not exhibit this chattering which is its main benefit over FOSMC. For a more detailed description of Sliding Mode Control see [208]. Cirillo et al. (2017) presented a slip avoidance algorithm using a six-axis tactile sensor that measures both Force and Torque in three directions [209]. They have two separate control systems; one for quasi-static conditions and one for dynamic. The slip avoidance model defines a region of force-torque space where slip is prevented and depends on the coefficient of friction and the contact area.

2.5.2 Multi-fingered Manipulators

A further study to the initial slip detection study by Veiga et al. with a single BioTac [197] used up to five BioTac sensors on two different hands to stabilise grasped objects and prevent them from being dropped [183]. The control mechanism increased normal force on an object when slip was predicted and slowly released its grip to find the optimum grasping strength. This is useful in finding the sweet spot between grasping too tight and damaging an object and too loose causing slippage.

Vina et al. (2013) use wrist mounted force-torque sensors on a dual arm robot (model unspecified) with three fingers per hand to predict slip using Gaussian Processes (GP) [210]. They use GPs to determine the maximum torque and forces before slip onset given the current state of the grasp. This was tested by using one hand of the robot to push or rotate the object and see how the model predicted the onset of slip. Despite only being performed on a single object (cuboid cereal box) the model's strong prediction performance demonstrates that kinesthetic tactile sensing can be used in a similar manner to cutaneous tactile sensing when predicting slip.

An array based tactile sensor was developed by Wang et al. (2019) [211] where voltages across nine electrodes (in a 3x3 array) can be measured to determine grasping force. Three such sensors were attached to a RightHand robotics ReFlex three-fingered hand and by tuning the Wavelet coefficient on the discrete wavelet transform of the tactile date they were able to determine when slip was occurring. However, no regrasping takes place and the object set was limited to three objects so it is unclear how well the method would generalise.

Su et al. (2015), again, use a BioTac sensor to detect both rotational and linear slip but train a neural network as the classifier and claim an 80% classification success rate [198]. They also perform one experiment to determine grasping force required to lift a jar and maintain stability when more weight is added. This does demonstrate the methods ability to be used online but more than one test is required to make any claims about its successfulness.

Stachowsky et al. (2016) used contact force sensors to detect slip on a held object and also when picking up various objects to determine, in real time, the required grasp strength [212]. Li et al. (2017) used a Barrett three fingered hand with a 3x8 tactile array and a force sensor on each fingertip to detect slip. They used an SVM and achieved up to 96% success at detecting slip on a variety of objects, although the hand did not react to prevent the object from being dropped

once slip is detected [213]

2.5.3 Incipient Slip

In an early study Canepa et al. (1998) developed a sensor consisting of two layers of PVDF which allowed for the measurement of normal and shear stress [214]. The sensor itself was flat but various differently shaped convex indenters were pressed against the sensor and incipient slip was detected using a neural network. Here, they detected the 'amount' of incipient slip occurring by defining it as the ratio of tangential force to the maximum tangential force prior to gross slip onset.

Dong et al. (2019) were able to detect incipient slip using the GelSlim sensor by observing the movement of markers on the periphery of the contact surface when grasping various objects in a pinch grasp [215]. By assuming that the periphery of contact is subject to the lowest frictional force and therefore liable to slip first. When a predefined number of peripheral markers moved - whilst markers closer to centre of contact remained static - incipient slip was defined to have occurred.

Su et al. (2015) observed vibration in BioTac sensors to predict slip was going to occur 30 ms before it was detected by an inertial measurement unit atop an object [198]; however, the authors provide no direct evidence that the mechanism allowing them to achieve this detection was indeed incipient slip despite their claims in the paper.

Rigi et al. (2018) used a DAVIS event-based neuromorphic camera to detect incipient slip. Neuromorphic cameras return 'events' which indicate which pixels in the image have changed between frames - rather than returning the raw pixel value as done by traditional CMOS cameras - and this effect is used to reconstruct the surface contact area and detect when parts of it move [216]. There is some question of how reliable the contact surface are reconstruction is which may place some doubt on whether incipient slip is occurring. No examination of the accuracy of the reconstruction in undertaken so this remains an open question.

Feng and Jiang (2019) use a Fiber Bragg Grating (FBG) embedded in flexible silicone. The grating consists of a series of small optic fibre sections within another optic fibre with lower refractive index [217]. The grating will only allow certain wavelengths to pass whilst reflecting the rest. As the wavelength of the reflected light depends on separation of the grating sections when the sensor undergoes strain the reflected light wavelength will change. When slip occurs, there is a notable shift in the wavelength of the reflected light and the authors declare this moment to be incipient slip onset. Again, no ground truth is provided showing partial movement of the sensor surface so the presence of incipient slip in this case remains unverified.

A novel sensor for detecting incipient slip was presented by Khamis et al. (2018) [218]. The PapillArray consists of a 3x3 array of silicone pillars of differing heights. When compressed and a shear force applied, the pillars further from the centre - which are shorter and therefore under a smaller normal force loading are encouraged to slip before the central pillars. By measuring

Sensor Name	Sensing Mode	Sampling Frequency	Sensor Resolution
N/A [214]	Piezoelectric	100 Hz	~0.6cm linear taxel separation
GelSlim [215]	Optical	30 Hz	640x480 pixels
BioTac [198]	Multimodal (Pressure)	2.2kHz sample, 300 Hz controller	N/A (Single sensor)
DAVIS [216]	Neuromorphic Optical	1 kHz	190x180 pixels
PapillArray [218]	Photodiode	17.9 kHz	3x3 square array 15mm separation
N/A [220]	Capacitive	100 Hz	3x3 square array 13mm separation

Table 2.2: Summary of sensors and studies for incipient slip. These results display the variety of sensing modes, sampling frequencies and resolutions which are able to detect incipient slip. Note that for the BioTac despite being multimodal it is the pressure sensor which is used to detect incipient slip. Additionally in the first row the sensor had taxels laid out linearly, not in a 2D array.

differing pillar deflection with an external camera the question of whether incipient slip actually occurs is definitively answered and this independent movement of pillars is sufficient to detect incipient slip. The PapillArray pillars can also be used to estimate the coefficient of friction and force, and are highly sensitive to vibration [219].

Similarly to the above, Narita et al. (2020) [220] developed a 3x3 tactile array which instead of being optical uses electrodes to measure the pressure at each taxel. They present a mathematical treatment of rotational incipient slip and use it to develop a grasping force control algorithm to prevent objects from falling when they are allowed to rotate from a pinch grasp. Whilst their results show flawless success at regrasping three slipping objects - including a delicate chocolate Eclair - they do not provide conclusive evidence that incipient slip is indeed what they are detecting.

These studies highlight the diversity of sensors used to detect incipient slip. A summary of the primary results can be found in Table 2.2 which shows the varying modes, sampling frequencies and resolutions. Due to multiple factors influencing the conditions when contacting an object (including friction, contact area, sensor morphology) it is hard to quantify the requirements for a sensor to detect incipient slip. However, this summary (Table 2.2) serves as a reference for future sensors to know what has been achieved by the state of the art.

2.6 Concluding Remarks

In this literature we have presented an overview of slip detection in the field of robotics paying particular care to the distinction between incipient and gross slip detection and the integration

of tactile sensors into robotic hands and grippers.

There are two consistent points that arise from the examination of the literature. First; under-actuated robotic hands have shown great success in recent years in reducing the complexity of manipulators and yet retaining high success levels when performing tactile tasks. Secondly; there is a significant, but not universal, issue with published works claiming to have detected incipient slip with insufficient verification that this is the case.

Both of these points provide an excellent stage for the work undertaken in this thesis and the questions it seeks to answer.

CHAPTER 3

SLIP DETECTION WITH THE TACTIP

This chapter concerns the initial work using the TacTip optical tactile sensor to perform slip detection. This includes modifications to the TacTip and the development of a method to detect slip in real time. This chapter begins by giving an overview of the TacTip, further to that presented in the literature review, followed by a description of the experimental hardware and software methods used. I then perform slip detection and stabilisation of 3D printed objects of varying curvatures followed by a short extension where the same experiment is conducted using several natural objects.

The work presented within this chapter has been published in the following peer-reviewed publications. For each publication, a contribution statement is included:

- J. W. James, N. Pestell & N. F. Lepora. (2018). Slip detection with a biomimetic tactile sensor. IEEE Robotics and Automation Letters, 3(4), 3340-3346.

  Contribution statement: J. James conceived of the presented idea, performed modifications to the sensor, developed the method, carried out the experiments, performed the analysis and wrote the manuscript. N. Pestell assisted with experimental setup. N. Lepora supervised the project and performed critical revisions of the manuscript.

- J. W. James & N. F. Lepora (2018). Slip Detection on Natural Objects with a Biomimetic Tactile Sensor. In Conference on Biomimetic and Biohybrid Systems (pp. 232-235). Springer, Cham.

  Contribution statement: J. James conceived of the presented idea, carried out the experiments and wrote the manuscript. N. Lepora supervised the project and performed critical revisions of the manuscript.

3.1 Motivation & Scope

When grasping an object, humans are able to prevent dropping it by constantly adjusting their grip [1]. This is possible due to our highly sensitive slip detection capabilities. Slip causes local movement of the skin surface, activating the Meissner corpuscles that are densely concentrated in our fingertips [9]. These mechanoreceptors initiate a reflexive action to minimise unwanted object motion [221]. Replicating this behaviour in a robotic hand will yield a more sophisticated sense of touch and enable complex object manipulation by reducing the likelihood of an object being dropped [222].

Slip detection has been an active research area since the 1980s when Howe & Cutkosky presented a solution using an accelerometer embedded in an artificial skin to detect slip [12]. They also highlighted the importance of slip detection in allowing successful manipulation. Despite many studies being performed since, slip detection is yet to be commonplace on commercially available robotic hands [197, 209, 151, 125].

The development of a slip detection method with minimal data preprocessing and fast classification speed would allow for slip to be checked with each data collection cycle, which means processing power could be dedicated to computationally intensive tasks such as in-hand manipulation. Ideally, such a method would require minimal training and be robust to changes in experimental conditions, so individual tactile sensors could be easily calibrated to perform slip detection accurately.

The aim of this work is to develop a simple, fast and robust classification method to detect slip using a biomimetic optical tactile sensor, the TacTip [3]. The TacTip operates by measuring the positions of internal pins embedded in its compliant skin surface, analogous to mechanoreceptors embedded around the dermal papillae in the glabrous skin of our fingertips [2]. Here we propose that pin motion is a strong signal of slip. We validate this proposition by showing accurate and robust discrimination between static and slipping objects using a support vector machine (SVM) applied to pin velocity data. Its effectiveness and utility are validated by performing experiments where an object is allowed to slip, the slip is detected and the object caught in real time and, crucially, before the object falls.

We build to this by performing three experiments. Firstly, we collect data of an object slipping across the sensor surface and use this to train and validate a slip detection classifier. This is known as 'offline' testing as its purpose is to provide a benchmark of how well the method works prior to deployment in a more realistic setting. The second and third experiments involve 'online' testing with a set of bespoke 3D-printed and real-world objects respectively to test both the classifier and experimental pipeline in real time. This is in pursuit of the first research question posed in the introduction: *Can a simple method be used with the TacTip biomimetic optical tactile sensor to detect slip and prevent total loss of contact with an object?*

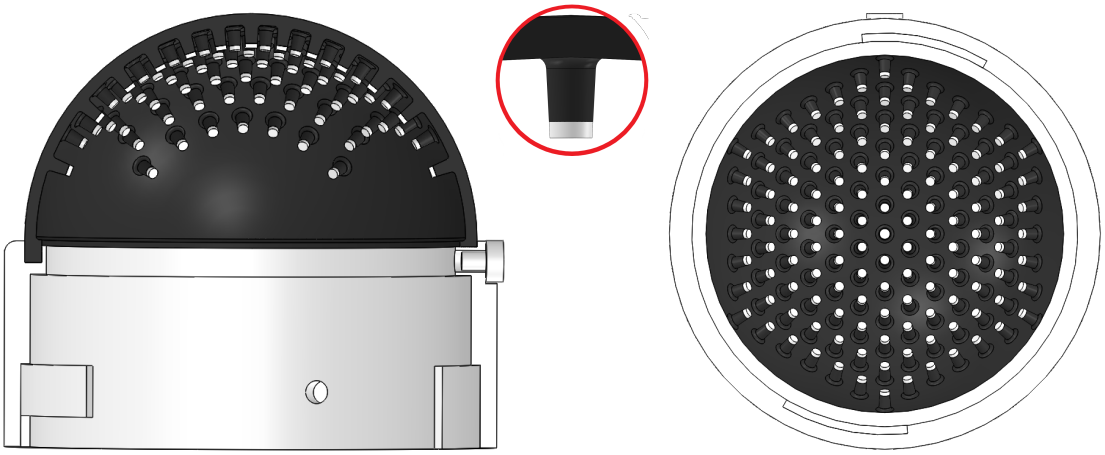

(a) (b)

Figure 3.1: (a) Cutaway view of 3D-printed TacTip showing the construction of the pins (b) Pins are laid out in a uniform hexagonal pattern when viewed from above to enhance the ability to resolve each individual pin. The inset image (red circle) shows the construction of a pin where a cap of VeroWhitePlus is placed on top of TangoBlackPlus towers.

3.2 Hardware Methods

3.2.1 The TacTip

The fundamental design principle of the TacTip was to create a tactile sensor which mimics the Merkel cell complex in the intermediate ridges in the human fingertip [3]. The intermediate ridges are protrusions of the epidermis into the dermis of the fingertip and the Merkel cells sit at the base of the intermediate ridges. These were initially mimicked by moulding rubber into a hemisphere with a series of pillars on the inside. The top of these pillars were then painted white to make them easily detectable by a camera. The hemisphere was sealed with a clear acrylic lens and the resulting cavity filled with silicone gel [2]. The skin was stretched over and bound to a plastic tube and the inside illuminated by LEDs.

The most significant change in the design has been to 3D-print the sensor which provides significant advantages including rapid prototyping of designs and the ability to create near-identical units in larger quantities. By using a multi-material polyjet 3D-printing process the

Property	Value
Tensile strength (MPa)	0.8-1.5
Elongation at break (%)	170-220
Shore Hardness (A)	26-28

Table 3.1: TangoBlackPlus Properties [223]

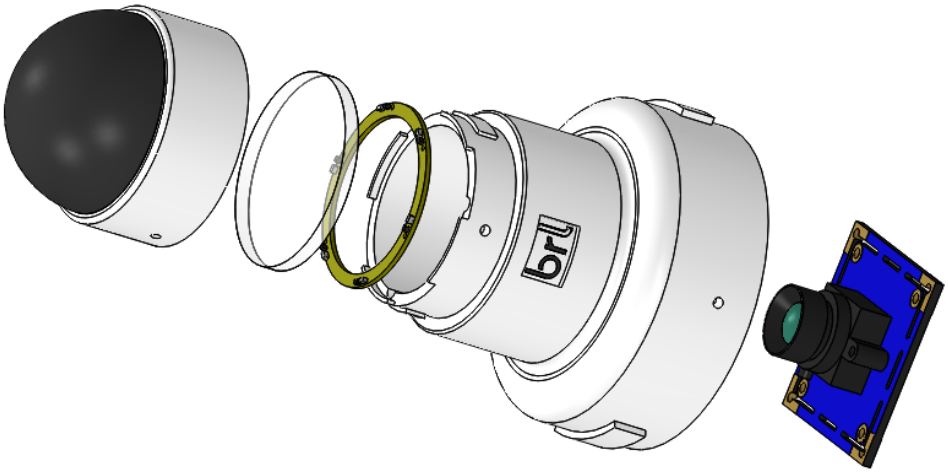

Figure 3.2: Exploded view of the TacTip. The entire unit can be mounted as an end effector to a robotic arm. All experiments here are conducted using a Universal Robots UR5. Will add labels later

solid elements of the design (pin caps, sensor base) and the flexible elements (skin, pin towers) can be printed as a single piece thus removing elements of the construction process (Fig. 3.1). The solid elements are printed in VeroWhitePlus and the flexible elements are printed in TangoBlackPlus, a rubber-like material whose relevant properties are summarised in Table 3.1:

These properties allow the skin to stretch without breaking as the TacTip is deformed by contacting objects of varying shape. One downside of TangoBlackPlus compared to the moulded material is that it is less opaque. This means external light leaks into the tip which can make resolving the pins difficult.

The remaining aspects of the construction remain the same. A clear acrylic lens is glued in place and the cavity filled with silicone gel (Techsil RTV27905) and illuminated with a ring of LEDs. The completed tip is attached to a mount containing the camera using a bayonet fitting which can in turn be mounted as an end effector to a robot arm (Fig. 3.2).

3.2.2 TacTip Modifications

Detecting and reacting to slip is all about reaction time. An object in someone's hand can go from securely grasped to falling in a fraction of a second. Previous work with the TacTip has never required high speed processing or reactions. For applications such as contour following [224, 102] several frames of data are processed and a decision is made. This is acceptable for contour following as the environment remains static but this is not the case when detecting slip.

The first change was replacing the camera. Previously the camera was a Microsoft Lifecam Cinema USB webcam that runs at 30Hz. As highlighted in chapter 2 previous slip detection methods have used a data stream running at approximately 100Hz and above. Many of these

rely on systems where achieving a fast data stream is not difficult, however due to the size of images being transferred (640x480 px) over USB the frame rate of USB webcams is limited.

A simple calculation can be performed to give an idea of the gains achievable by increasing the frame rate. Assuming an object 5cm in height is being held in a pinch grip and using

$$t = \sqrt{2as} \tag{3.1}$$

where t is freefall time, a is acceleration (taken to be $9.81ms^{-2}$) and s is freefall distance (5cm in this case) gives 0.1s to catch the object. In reality we will have more time because we are neglecting air resistance and friction, however, in many cases you would not be able to form a secure grip at every point on the object and minimising the slip is essential to be able to regrasp it. If we wanted to secure the object within 2cm (a more realistic distance) the time drops to 0.06s which is less than two frames of a 30Hz camera. Rearranging equation 3.1 shows that freefall distance $s \propto t^2$ so halving reaction time will quarter freefall distance.

However, there is another consideration. With higher frequency sensing the data load on a computer increases which means processing speed is necessarily affected and may become the rate limiting step in the pipeline. Therefore, a balance must be struck between increasing frame rate and increasing processing time such that the benefit of the former is not affected by the latter.

With this in mind an ELP USB camera module (model ELP-USBFHD01M-L21) was selected which runs at 120 Hz, significantly faster than the previous camera. Other benefits include maintaining USB connectivity allowing the new camera to slot into the existing software pipeline and it remaining small enough to be mounted as the end effector of a robot arm (base size 40x40mm). A new mount was developed to contain the camera module that eased integration into the existing TacTip sensor design (Fig. 3.3). Previously the Lifecam had to be partially disassembled to fit inside the camera mount, a procedure which is time consuming and involves handling sensitive electronic equipment. The new design involves screwing the camera onto the mount through four existing holes in the camera PCB which minimises any relative movement of camera and mount whilst also easing construction. Finally, the camera is also low cost (~£50). One of the key design principles of the TacTip is that it's very cheap to produce; costing less than £100.

3.2.3 Experimental Apparatus

To perform a rigorous analysis of slip, a custom apparatus was designed for automated collection of slip detection data. The rig was designed with several criteria in mind:

1. Allow an object to fall under gravity with minimal friction.
2. Allow any experiments to be repeatable with high precision.
3. Have the experiments be performed entirely without human input after initial setup.

4. Allow a variety of object shapes and weights to be easily tested.

The apparatus utilised a low friction rail system with a slider to which multiple objects can be attached (Fig. 3.4). Four tactile stimuli with different radii of curvature were made to represent differently-shaped objects (Fig. 3.5), which can be easily interchanged for testing. Because the objects remain secured to the rail when dropped, the entire data collection procedure can be performed autonomously.

3.3 Software Methods

This section provides an overview of the classification method chosen for much of this thesis, Support Vector Machines (SVM). We then discuss the data processing which takes place to convert the camera images from the TacTip into an input to the classifier.

3.3.1 Support Vector Machines

As gross slip is defined as the entire contact surface area of the sensor moving relative to the object it is contacting. To detect slip we utilise a binary classification method which will be able to reliably and quickly distinguish between the **static** phase where an object is securely held and the **slip** phase where sensor surface movement should be distinct. Support Vector Machines were chosen as the classification method as they satisfy several criteria:

1. Fast classification speed

2. Ability to handle data with high dimensionality (up to 254 dimensions for this work)

3. Fast to train over small data sets

SVMs are a binary classification method that works by plotting (labelled) training data and drawing a hyperplane which best separates the two classes of the data. New data is plotted and is classified according to the side of the hyperplane on which it falls [225].

To best separate the two classes, two parallel hyperplanes are drawn and the distance between them is maximised. The final hyperplane that is used as the class boundary is the hyperplane midway between the two original hyperplanes. A general hyperplane can be defined by

$$\vec{w} \cdot \vec{x} - d = 0 \tag{3.2}$$

where $\vec{x}$ represents the points in the hyperplane, $\vec{w}$ is the vector normal to the surface and d is the distance from the origin to the plane. The two planes used to define the maximal class separation are given by

$$\vec{w} \cdot \vec{x} - d = \pm 1 \tag{3.3}$$

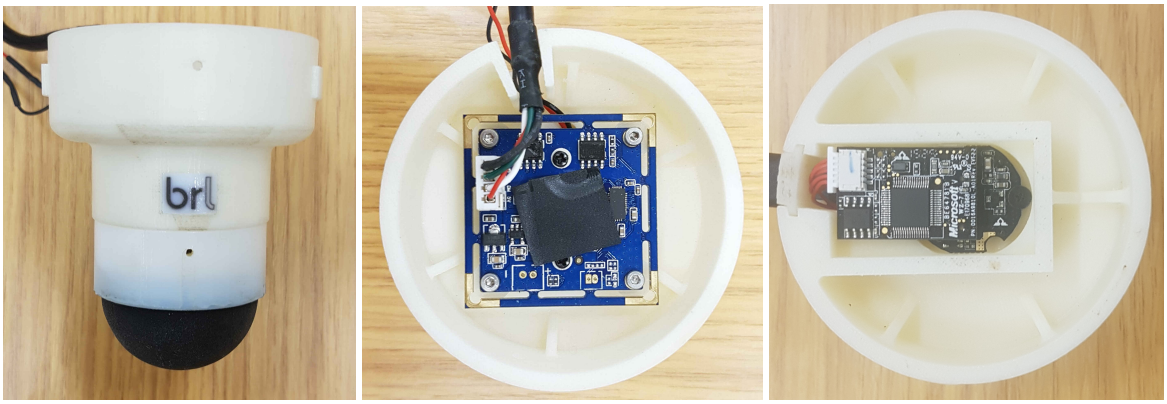

(a) (b) (c)

Figure 3.3: (a) TacTip attached to newly designed mount. (b) The new ELP camera module secured to the mount with screws to minimise movement of the camera. (c) Previous TacTip camera layout. The mount is attached to the UR5 via a bayonet cap.

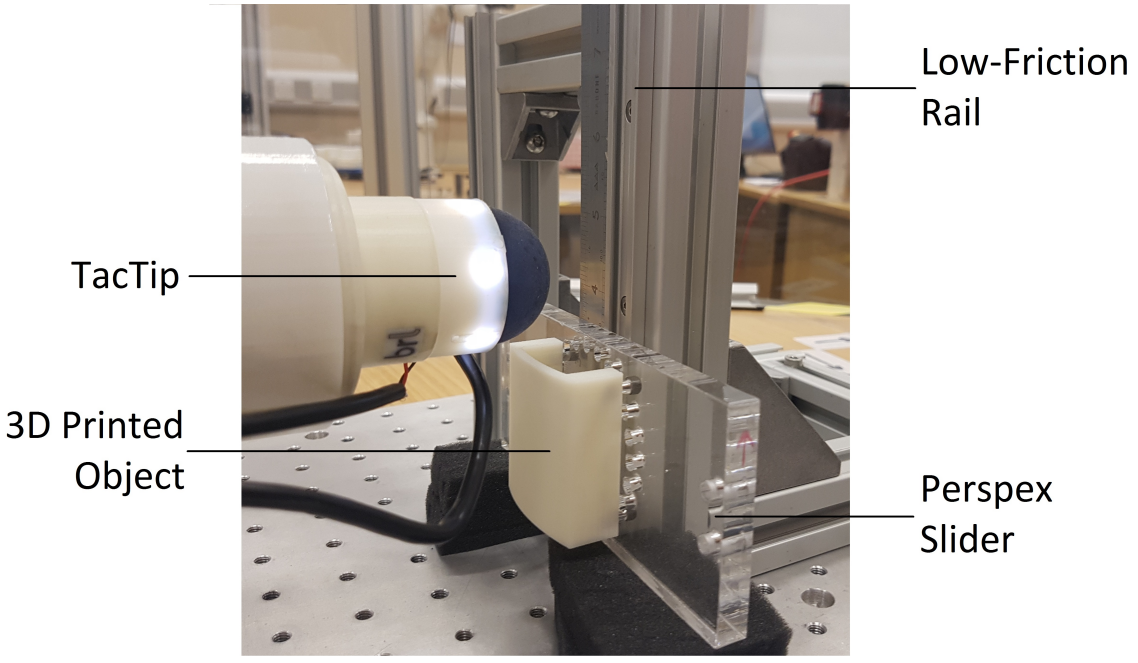

Figure 3.4: The rig used to collect data of a slipping object. A rectangular acrylic object, to which stimuli may be attached, is able to freely slide in the rail to simulate falling under gravity in a controlled environment

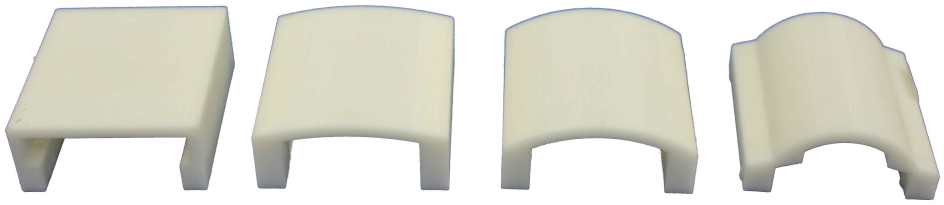

Figure 3.5: 3D printed stimuli created for this work. Each has a different radius of curvature to test ability to cope with objects of different shapes. From left to right, radii of curvature: ∞ (flat), 80, 40, 20 mm. The apex height of each object is the same (20mm).

meaning that the distance between them is given by $\frac{2}{\|\vec{w}\|}$. To maximise this distance $\|\vec{w}\|$ must be minimised. Each training data point $\vec{x}_i$ is given a label $\vec{y}_i$ of 1 or -1 according to its class. All of these data points must lie (if possible) the correct side of the two hyperplanes. The constraint for each data point $\vec{x}_i$ can be given as

$$\vec{y}_i(\vec{w} \cdot \vec{x}_i - d) \geq 1. \tag{3.4}$$

$\|\vec{w}\|$ can then be minimised according to this constraint. Training data points that lie on the two maximally separated planes are called support vectors and can completely describe the hyperplane that divides the two classes. This is called a hard-margin SVM where all the training data points fall the correct side of a hyperplane. This is not always possible as some values of one class may lie very close to values from another class and therefore a plane may not be able to completely separate two classes. In this situation the hyperplane that separates them gives an indication of whether it is more likely for new data to belong to one class or the other. This is called a soft-margin SVM. In such a scenario we introduce a *hinge* loss function

$$\max(0, 1 - y_i(\vec{w} \cdot \vec{x}_i - d)). \tag{3.5}$$

If $\vec{x}_i$ lies on the correct side of the line then the function evaluates to zero and if not it is proportional to the distance from the margin. By minimising

$$\left[\frac{1}{n}\sum_{i=1}^{n} \max(0, 1 - y_i(\vec{w} \cdot \vec{x}_i - d))\right] + \lambda\|\vec{w}\|^2 \tag{3.6}$$

the hyperplane $\vec{w}$ is determined. In this equation λ is a hyperparameter used to strike a balance between getting as many x_i on the correct side of the boundary and keeping the margin size large enough to separate the two classes.

The reason that SVMs are so fast for classification is that with any new data, $\vec{X}_i$, one merely needs to calculate the result of $\vec{w} \cdot \vec{X} - d$. If positive it belongs to class 1 and if negative class -1.

Not all classes will be effectively separable by a hyperplane. Thankfully a kernel trick can be used to draw a curve that can separate two classes in the non-linear case [226]. What we wish to do is transform the space using a kernel function such that the two classes are linearly separable.

The training data points in the new space are transformed by

$$\vec{x_i} \rightarrow \phi(\vec{x_i}) \tag{3.7}$$

and the kernel function $k(\vec{x_i}, \vec{x_j})$ is given by

$$k(\vec{x_i}, \vec{x_j}) = \phi(\vec{x_i}) \cdot \phi(\vec{x_j}). \tag{3.8}$$

$\phi(\vec{x_i})$ then replaces the $\vec{x_i}$ in equation 3.6 which is then minimised.

An example kernel function is the Gaussian kernel which is given by

$$k(\vec{x_i}, \vec{x_j}) = \exp(-\gamma \|\vec{x_i} - \vec{x_j}\|)^2) \tag{3.9}$$

and is a commonly chosen kernel when training non-linear SVMs [227].

3.3.2 Software Pipeline

Before being used by a classifier data from the camera must be processed such that it is in the required format. At this point one has two choices; some prior work with the TacTip has involved simply using the raw images from the camera which are downsampled and a thresholding operation used to binarise the image and thus reduce the dimensionality. Raw images used to train Convolutional Neural Networks (CNNs) have shown strong results in tasks such as contour following [106] and object classification [228]. The other option is to use the pin positions. The OpenCV function *SimpleBlobDetector* is used to detect the 127 pin centres, giving coordinates (x, y) in pixels. Multiple conditions on the properties of 'blobs' in the image such as size, shape and pixel intensity value can be set to detect only the pins (Fig. 3.6). Calculating the Euclidean distance travelled by each pin between frames allows for pins to be tracked from frame to frame. In certain frames the pin detection algorithm may fail to detect all pins; in such cases the positions from the previous frame are kept. In either case the result of the image processing can be used as the input to a classifier, regressor or as part of a control loop used to perform experiments with a robotic arm.

In this work we start with the pin positions as our features which are passed to MATLAB for further analysis. The main reason for using pin positions over raw images is that we are trying to observe physical movement of the sensor and the pins act as fiducial markers for determining the location of the sensor surface. We can, therefore, be confident that when a pin moves the surface of the sensor is also moving and we can learn the pattern of pin movement which corresponds to slip. When using raw images it is harder to be interpret what the sensory basis of the learned features from a CNN is. Visualisation of CNN activation is possible with tools such as *Grad-CAM* [229] however it is far from a solved problem [230].

As slip involves an object moving relative to the sensor, having a time-dependent component is useful for robustness. For this work the difference in position of each pin between consecutive frames—the pin velocity—was chosen. Velocity was chosen because a change in velocity will

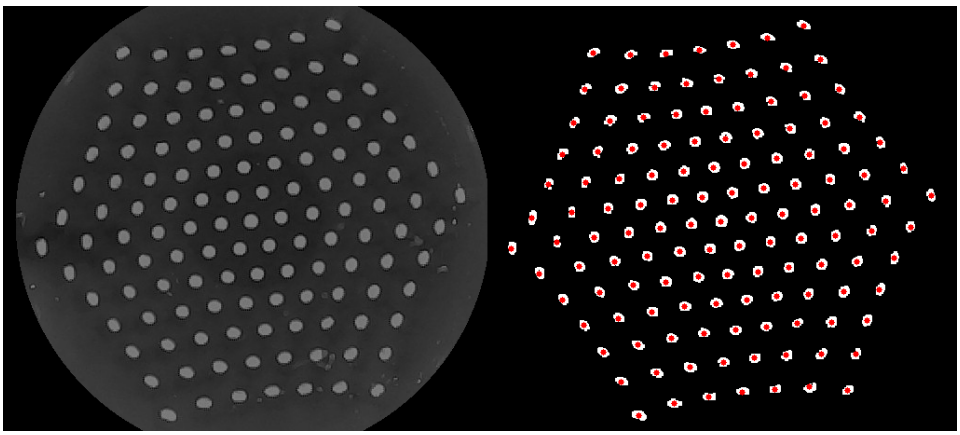

(a) (b)

Figure 3.6: (a) Raw greyscale camera image. (b) Identification of the pins (red dots) after image processing.

always be present when an object starts to slip and it is easily inferred from the pin positions. The pin velocities can also be seen as analogous to RA-I (rapidly adapting type I) mechanoreceptors in the human fingertip. These Meissner corpuscles have been shown to play a role in the detection of slip in humans by having a spike in activity when slip occurs [9]. When holding an object, the surface of the TacTip stretches downwards due to the object weight. When that object begins to slip, the coefficient of friction changes from a static to kinetic value that is generally lower [231]. Hence, the frictional forces decrease and the elastic force from the stretched sensor surface causes it to move back towards its non-deformed shape, shifting the pins upwards. We hypothesise that when slip occurs we will see a spike in pin velocities in much the same way Meissner corpuscles spike in humans.

To obtain pin velocities we begin with the list of pin positions which is collected in Cartesian coordinates $(\Delta x_i, \Delta y_i)$ for $1 \leq i \leq 127$. Positions are transformed by: $\Delta r_i = \sqrt{\Delta x_i^2 + \Delta y_i^2}$ and $\Delta\theta_i = \arctan(\Delta y_i / \Delta x_i)$. The angular component $(\Delta\theta_i)$ of the pins is shifted to have a mean of zero with respect to the x-axis of the camera, removing all angular bias in the data. This yields a 254-dimensional time-series input $(\Delta r_i, \Delta\theta_i)$ to the classification method.

3.4 Experiment I: Offline Slip Detection

The first experiment involves collecting data using the rig described in section 3.2.3 and using this to train an SVM. In this section I will describe the data collection procedure followed by an analysis of the data, SVM optimisation and finally offline testing of the SVM.

3.4.1 Data collection

For all of the tests in this Chapter the TacTip is attached to a Universal Robot UR5. This is a 6 DoF linear robotic arm with a 125 Hz interface and a maximum repeatability of ± 0.1mm allowing for the position to be controlled accurately and frequently. Using the rig described in section 3.2.3 the data was collected as follows:

1. Press TacTip against the flat stimulus (Fig. 3.5) normal to the surface
2. Raise arm 50mm to lift object
3. Retract at a speed of 0.1 mms^{-1} until stimulus falls
4. Return arm to bottom of rail

This procedure allows for rapid and autonomous collection of data. The camera is activated and data recorded throughout stage 3. The data collection routine was performed 40 times.

3.4.2 Inspection of slip training data

The training data demonstrates how drastic an effect a slip event has on the tactile data. Fig. 3.7 shows the pin displacements relative to their initial positions and the frame-to-frame pin velocities, over a typical data collection run. Each coloured line represents a different pin. There is a clear spike in the pin velocities at around the 1200th frame and a step-change in the pin positions, both of which strongly signal the onset of slip. This pin velocity spike is present in all pins. Therefore, slip affects the entire TacTip skin surface.

Given that we will apply an SVM classifier to the velocity of pin positions, Fig. 3.7 shows how noticeable the slip onset is and indicates that the classifier should work well. The width of the spike in the velocity data is approximately 0.2s (~20 frames) and includes the onset of slip to the object completely losing contact. This is evidenced by the flat line seen in the pin positions data after the spike. Hence, to prevent a slipping object from falling, the data must be collected, classified and the robot moved in a very brief period of time.

If we look at a vector field of pin velocities we can see this effect even clearer (Fig. 3.8). Prior to slip only a few of the pins are seen to move and this is mostly associated with noise (Fig. 3.8(a)). When we focus on a frame from the beginning of the spike in pin velocities we see a very different story; the pin velocity magnitude is large for almost all pins and is in a co-linear upwards direction (Fig. 3.8(b)). This is consistent with the expected signal and the significant difference between 'static' and 'slipping' data will allow us to accurately label the data for SVM training.

A few frames after slip onset the clear slip signal becomes messy (Fig. 3.8(c)). This may be cause by elastic effects from the sensor as the surface rapidly moves or from the object losing contact with the sensor. This complicates the data labelling procedure as it is hard to class these

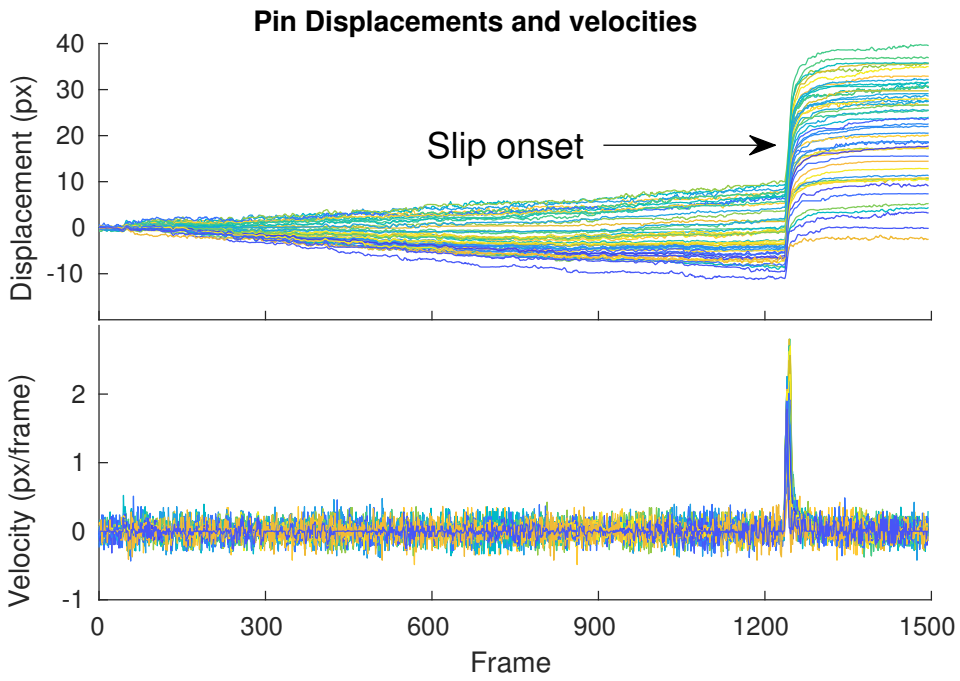

Figure 3.7: Top: Pin displacements during a data collection run. Bottom: Pin velocities obtained by differentiating the top graph. The sharp spike around 1200 frames is when slip occurs. For clarity a subset of the pins are used and a 5 frame moving average has been applied to the pin displacements.

frames as 'slip' with certainty. However, as we are currently interested in the accurate detection of the *onset* of slip to allow for a prompt reaction the cessation of slip is of less importance. Nevertheless, in the forthcoming section we explore how varying the number of frames we label as slip affects classification accuracy.

3.4.3 SVM Training

Binary classification splits the training data into two classes. For this work these classes will be referred to as 'slip' and 'static'. The ground truth labels were set by manually looking at the vector fields for each frame and identifying the frames with the alignment of vectors consistent with slip. We class all frames as 'static' until the clear slip signal from Fig 3.8(b) can be seen. Both linear and non-linear (Gaussian) kernels were tested with parameters chosen—for the non-linear case—using Bayesian optimisation (using the MATLAB function *fitcsvm*). Two parameters were optimised; the Kernel Scale and the box constraint.

The kernel scale (γ in eqn. 3.9) can be seen as setting the complexity of the class boundary. For small values, γ will have little effect on the data and the decision boundary will be drawn as for a linear SVM; for large values the decision boundary can be very complex by fluctuating greatly to put individual data points on one side of the boundary, and therefore has the tendency

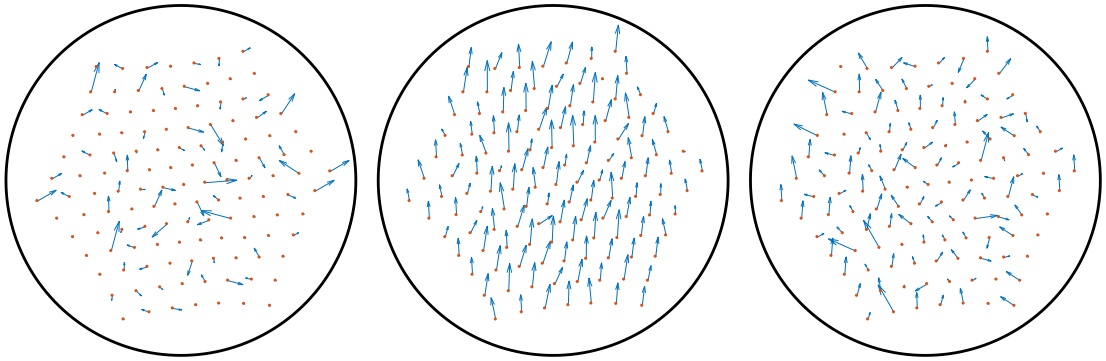

(a) (b) (c)

Figure 3.8: An example of the vector field of pin velocities. Each arrow corresponds to the velocity of one pin and each red dot corresponds to a single detected pin. (a) Typical vector field for a frame where the object is securely held. (b) The characteristic alignment of pins when slip occurs. (c) Showing the same slip event 5 frames after slip begins. The slip signal has already become very noisy. The difference in vector alignment and magnitude between (b) and (c) demonstrates the clarity of the slip signal. The direction of vector alignment depends on the slipping angle relative to the surface of the TacTip.

to overfit.

The box constraint (λ in eqn. 3.6) is a regularization parameter that gives the trade-off between correctly classifying data and maximally separating the two classes: a small λ results in a narrow boundary (distance between separating hyperplanes) but many misclassifications, and vice versa for large λ.

Two analyses were performed to identify the best classifier:

1. a comparison between linear and non-linear kernels

2. the effect of varying the number of frames in the training data 'slip' class

This second test is important because the initially-clear slip signal becomes noisy after only a few frames (see Fig. 3.8(c)). The classifiers were trained on half of the collected data with the remaining data used for testing.

3.4.4 Results

Offline testing classifies previously collected data and compares the output to the ground truth labels for the data. Crucially, this data has not been used for training the classifier. This will allow us to obtain the best classifier, which will then be used to identify slip in real time. The first classifier comparison was between the use of a linear and a non-linear (Gaussian) kernel. The dimensionality of both kernels were also varied. We compared using changes in both magnitude and angle, $(\Delta r_i, \Delta\theta_i)$, to sole changes in angle, $\Delta\theta_i$ and sole changes in magnitude,

Kernel	Dimensions	KS	BC	Success (%)
Gaussian	$(\Delta r, \Delta\theta)$	38.8	686.6	99.11
Gaussian	Δr	23.4	4.3	98.95
Gaussian	$\Delta\theta$	8.5	76.5	97.21
Linear	$(\Delta r, \Delta\theta)$	N/A	N/A	95.07
Linear	Δr	N/A	N/A	94.66
Linear	$\Delta\theta$	N/A	N/A	70.58

Table 3.2: Comparison of kernel types and dimensions used in the classifier. The classifiers using both magnitude and angular data perform best. The Gaussian kernel also performs notably better than the linear kernel. Columns three and four represent the optimised parameters kernel scale (KS) and box constraint (BC).

Δr_i, corresponding to 254, 127 and 127 dimensional data, respectively. For this first comparison, a total of six classifiers were tested, with the results expressed in terms of the percentage of correctly classified frames (summarized in Table 3.2).

Two observations are drawn from Table 3.2. The first is that using both the changes in magnitude and angle $(\Delta r, \Delta\theta)$ gives better performance than just magnitude or angular data. Both the magnitudes and angles are useful for slip classification, justifying the use of the transformation from Cartesian coordinates to magnitude and angle. As an aside, the magnitudes give better classification than the angular data on both tests.

The second observation is that the Gaussian kernel outperforms the linear kernel. All three of the classifiers trained with a Gaussian kernel outperform all three with the linear kernel. The best performing Gaussian SVM has a score 4% higher than the best scoring linear SVM method. Clearly a linear hyperplane is not able to effectively separate the two classes, but the use of an optimised non-linear kernel is sufficient to drastically increase the classification success.

The second set of offline tests involves varying the number of frames in the 'slip' class. Previously for training, every frame was assigned manually to the class 'slip' or 'static'. For the first test, all ground truth frames in the slip class were used to train the classifiers; the number of which varied from run-to-run. However, the pattern becomes noisy after only a few frames (see Fig. 3.8(c)). Choosing the appropriate number of frames in the slip class would ensure that only the data with a clear signal indicating slip would be kept, which would give a better separation between the two classes.

Testing demonstrated that that using 4 frames in the slip class increases classification success from 99.11% to 99.88% (Table 3.3). Therefore, using the cleanest slip signal allows the SVM to better discriminate between slipping and static objects, although this only marginally outperformed using 3 or 5 frames. For the remaining tests, only the 4-frame classifier in the 'slip' class is used. It should be noted that the classifier is able to detect more than the slip onset and can detect upwards of 10 frames after onset, albeit with lower accuracy.

Frames in 'slip' class	Success (%)
All	99.11
5	99.87
4	99.88
3	99.87
2	99.85
1	99.87

Table 3.3: Comparison of classifiers with varying frames in the 'slip' class. The first row is the best performing classifier from Table 3.2 where all the manually identified 'slip' frames were used to train the classifier. Having only four frames in the 'slip' class results in an improved classifier compared to using all frames.

3.4.5 Discussion

In this section we have trained an optimised SVM which is capable of distinguishing between the static and slip states of the TacTip with high accuracy. Initially, we showed that a non-linear kernel significantly improves the accuracy of the classifier and that using both the changes in magnitude and angle of pin velocity is beneficial as well. The latter point is perhaps unsurprising as we are simply giving the classifier more information to go off. However, it does show that both the distribution of pin velocity magnitudes and angles contains information which aids in discriminating between the slip and static states. Finally, reducing the number of frames in the 'slip' class when training meant that only the data with the cleanest slip signal was used to inform the decision boundary which resulted in improved classification accuracy.

In a study by Veiga et al. random forests were deemed to be marginally better at detecting slip than support vector machines [197]. However, here offline testing yielded comparable results between the two studies with a classification success of 99.88%.

Despite the apparent success of offline testing, there remains some unanswered questions. Is the manual labelling of frames into 'static' and 'slip' classes physically accurate and have we therefore developed a classifier which can detect the onset of slip or is this another feature in the data with another physical cause? Additionally, is the classifier - and indeed the entire experiment pipeline - capable of detecting slip in real time and reacting to catch the slipping object? These are the questions we seek to answer in the next section.

3.5 Experiment II: Online Slip Detection & Grasp Recovery

3.5.1 Experiment Description

The main goal of this research is to detect slip and react in real time. The offline testing above (Section 3.4) allowed us to identity the best-performing classifier, which not only detects

slip with minimal error but also has a low false-positive rate. A false positive in this case involves classifying static data as slipping and therefore reacting to an incorrect impulse. In most circumstances, this would be less costly than a false negative–where an object would fall without the robot reacting—but reacting unnecessarily could still be harmful. This is why we use a success rate based on classifying both static and slip frames rather than only detecting the slip frames.

For online testing in real time, a similar experiment is used as for the offline tests: the TacTip is pressed horizontally against a stimulus until it was secured, lifts the stimulus, and then the arm is again slowly retracted. However, in the online test, when slip is detected, the arm moves immediately back to prevent the object from falling. Data which is received in real time is classified using the best-performing classifier from the offline tests. To minimise the effect of false positives, two consecutive frames must be classified as slip before a response is triggered from the robot arm.

Two online tests were performed. Firstly, the flat stimulus was tested under the same conditions as the data collection, but we varied the speed at which the robotic arm is retracted to discover whether the classifier can generalise to changes in experimental conditions. Secondly, the three curved stimuli were tested to determine the ability to detect slip of differently-shaped objects (Fig. 3.5).

To determine whether a test was a success an ArUco marker was attached to each stimulus, with a camera (Canon EOS 600D) recording its position (Fig. 3.9)[232]. The ArUco marker is used to record the height of the stimulus: it thus determines whether the stimulus has been caught or dropped when slip begins, and how far the stimulus fell before being caught. Calibration is achieved by lifting an object 50 mm at the start of each test to calibrate the pixel-to-distance ratio.

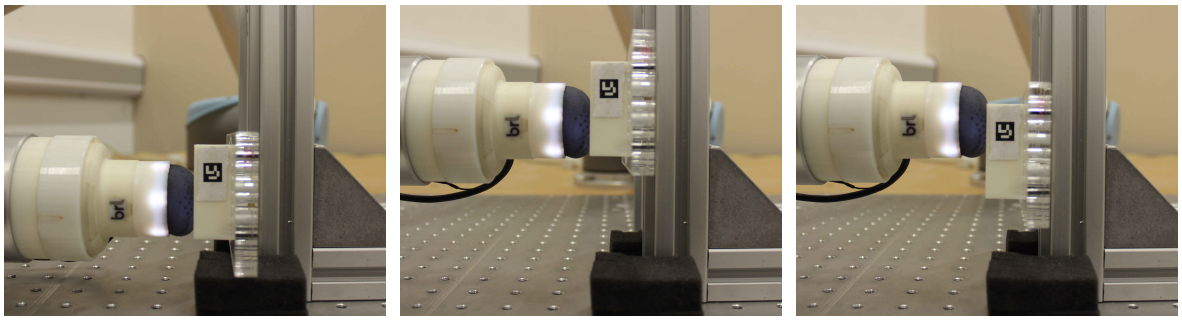

(a) (b) (c)

Figure 3.9: Figure showing the three steps of the online experiment procedure. (a) TacTip makes contact with object at bottom of rail. (b) Object slides 5cm up the rail and then arm begins to retract. (c) When slip is detected arm moves back in to secure the object. A clear drop in height can be seen between (b) and (c). This process then repeats. The height of the object is tracked by the ArUco marker attached to the stimulus.

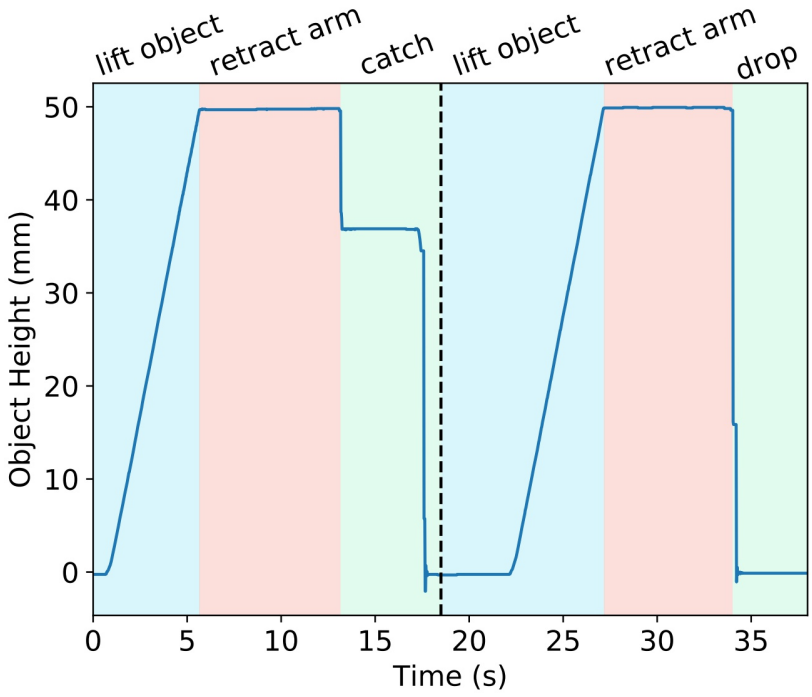

Figure 3.10: The height of an object during two tests - separated by the dashed line. Each test has three sections; lifting object, arm retraction and finally, what happens after slip. The first test has a clear drop followed by a plateau after the slip has been detected and successfully stopped. The second test, a failure, only has a large drop as slip was not detected and the object fell.

3.5.2 Results

The initial online tests were performed with the flat stimulus, which was also used for data collection and analysis. Therefore, online and offline performance can compared. The speed at which the arm was retracted was varied to evaluate performance under different slipping conditions. Validation was achieved by tracking an ArUco marker (Fig. 3.9); thus, we can determine whether an object has been successfully caught and calculate the falling distance (Fig. 3.10).

A test is deemed to be a success when there are two distinct plateaus separated by a clear drop in height. This means the object was held steady as the arm retracted (first plateau), began to slip (drop in height) and was then stopped by the arm (second plateau). Overall the systematic error in this method is estimated to be ±0.1mm, with standard error in the mean and systematic error summed in quadrature to give the total error.

Eleven different arm retraction speeds varying from 0.1 to 20 mms^{-1} were performed. Each speed is tested twenty times (Table 3.4). Seven of the eight lowest retraction speeds have a success rate of 100%, with the success rate of catching the object decreasing above 3 mms^{-1} retraction speed. The average success over the 220 performed tests is 95%.

There is a positive correlation between retraction speed and stopping distance, with the

Speed (mms^{-1})	Success (%)	Stopping Distance (mm)
0.1	100	15.5 ± 0.5
0.2	95	15.1 ± 0.4
0.4	100	15.5 ± 0.5
0.6	100	16.5 ± 0.5
0.8	100	16.0 ± 0.5
1	100	17.6 ± 0.4
2	100	18.8 ± 0.7
3	100	18.7 ± 0.7
5	85	22.0 ± 0.9
10	80	24.8 ± 1.6
20	90	26.9 ± 1.3

Table 3.4: The success of the SVM classifier at detecting slip and then moving the robot to catch the object. Each speed was tested 20 times. Best performance was for the lowest speeds but success is high across all tests.

RoC (mm)	Success (%)	Stopping Distance (mm)
∞ (Flat)	100	15.5 ± 0.5
80	90	14.9 ± 0.5
40	100	15.6 ± 0.5
20	95	14.3 ± 1.1

Table 3.5: The success of slip detection with objects with distinct radii of curvature (RoC). 20 tests are performed per object and their success percentage given. The first row is for the flat stimulus (from Table 3.4).

slowest speed giving a stopping distance of 15.5 mm and the fastest 26.9 mm. These results demonstrate that the method developed offline (Section 3.4) performs well in real time to secure a falling object; moreover, this performance at detection is invariant to changes in arm retraction speed. Meaning, ability to detect slip was unaffected by retraction speed. Fig. 3.11 shows the height of the object over twenty test runs. In this case, each test was successful. The entire computational loop including image capture, processing and classification runs at 100 frames per second. Classification was clocked at 3 milliseconds, less than the time between frames (~10ms).

The second online test uses three other stimuli with different radii of curvature to test robustness to object shape. Each stimulus was tested twenty times to investigate how the classifier generalises to objects with different curvatures. The stimuli were mounted such that their curvature was aligned to the vertical axis, with retraction speed 0.1 mms^{-1}.

Table 3.5 shows the classifier is able to detect slip on all the curved objects, with only 3 failures from the 60 tests performed. For two stimuli, the stopping distance is less than that for the flat stimulus; however, this is within the margin of error. Testing on these objects mimics a range of situations that would be encountered when deploying slip detection in real-world scenarios. We emphasise that these curved objects are entirely novel to the classifier, which was trained only on a flat object.

3.5.3 Discussion

In this section we have obtained the first real-world indication of the TacTip's ability as a slip detector and in the process answered the questions which remained at the end of Experiment I.

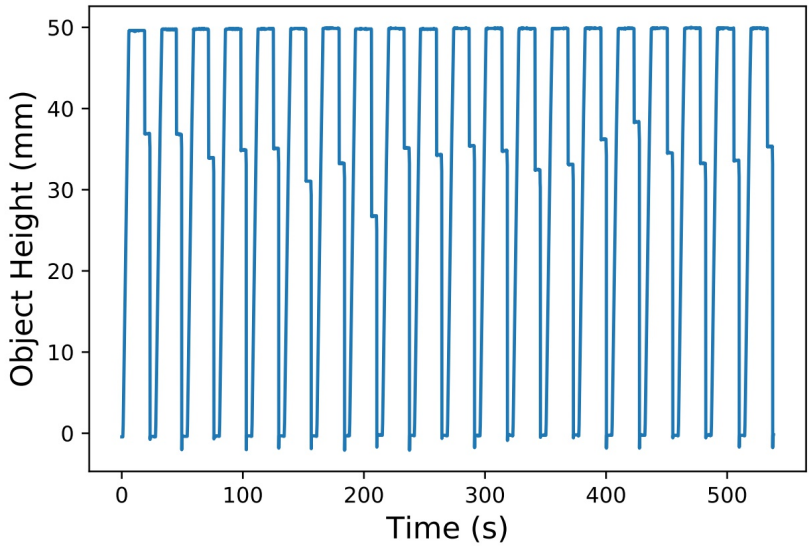

Figure 3.11: Graph showing the height of an object during twenty tests. Using the success criteria described in Section 3.5.2 it can be determined that each slip was successfully detected and the object prevented from falling. It also shows that there is a variability in the stopping distance.

Data coming from the TacTip was classified, slip detected, a response initiated and the object stabilised after slipping as little as 15.1 mm with up to 100% success. Results were consistent over a range of arm retraction speeds and with varied stimuli. This shows that not only is the experimental pipeline fast enough to react to slip but the manually labelled data used to train the classifier does seem to be using features which correspond to slip as it is highly successful at preventing objects from being dropped.

The classifier was trained on just one retraction speed, yet generalizes to over 220 tests with speed varied from 0.1-20 mms^{-1} with success rate of 95%. Veiga et al. (2015) achieved an average success of 74%; however, this was over a wider variety of different objects.

Again, as we leave the experiment a significant question which needs to be answered. When detecting slip, is the classifier limited to the artificial stimuli created here which vary little in weight and texture or will it generalise to natural objects? Addressing this is the subject of the next section where we extend this experiment to test on a small set of real world objects.

3.6 Experiment III: Slip Detection with Natural Objects

This experiment is a short extension to Experiment II where several natural objects were tested to determine if the slip detection method presented above generalises to objects that haven't been artificially designed (Fig. 3.12).

3.6.1 Experiment Description

Each experiment proceeds similarly to Experiment II with the main exception being that the objects are no longer attached to the rail. Instead, the UR5 robotic arm presses an object against one of the upright supports on the data collection rig . The arm then begins to slowly retract (0.2 mms^{-1}) until the object slips (Fig. 3.13). This speed was chosen as it was associated with the smallest slipping distance in the previous experiment (Table 3.4).

The experiment is considered a success if the object is visually seen to start falling, the classifier detects the slip, the arm moved forward and the object is secured against the wall without further slippage. Any other outcomes such as slip being detected but the object still being dropped is classed as a failure. Note that we were unable to reliably track the objects using an ArUco marker as certain objects rotated when slipping.

The five objects chosen were; a paper box containing a plastic cube, a metal coffee container, a mustard bottle, a water bottle (approx. 1/3 full) and a plastic banana (Fig. 3.12). The objects were chosen as each has a different shape, weight, compliance and texture as well as being common objects and shapes that one might encounter day-to-day.

3.6.2 Results

Each object was tested ten times in the manner described above and the results are summarised in Table 3.6. The results show that four of the five objects are stopped from falling with a high success of up to 90%. The only low scoring object is the banana which was only stopped 30% of the time. For this case the classifier was able to detect the onset of slip but the shape of the banana meant that moving to re-secure it mostly pushed the banana out of the way and onto the floor.

Each object used was novel to the classifier and no parameters of the object were known

Figure 3.12: The five different objects that were tested for this study. The objects were chosen due to their different shapes, weights and compliances so that an indication of the slip detection method's ability to generalise to random objects can be tested.

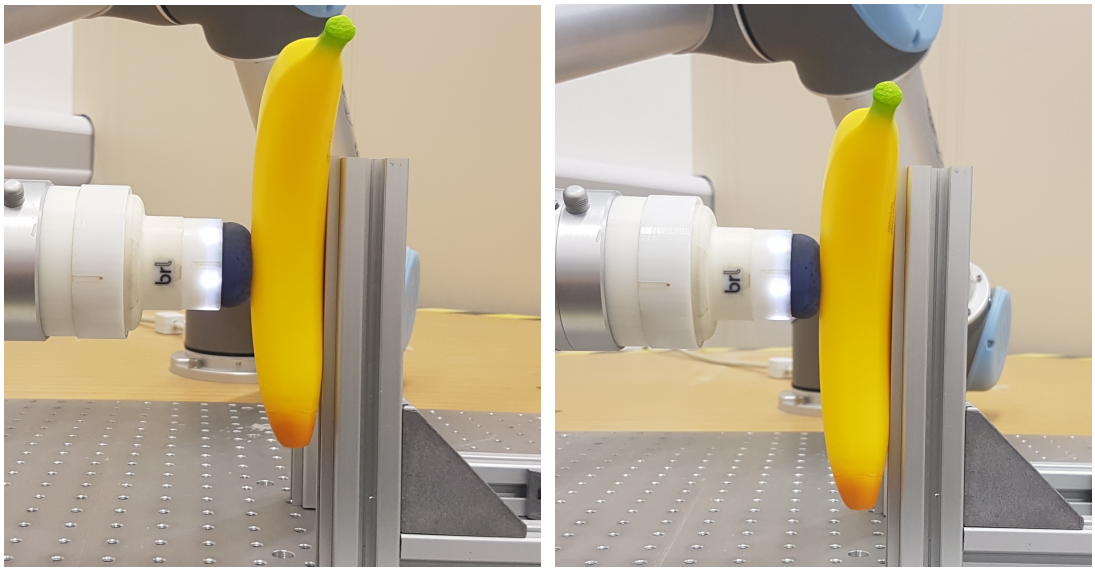

(a) (b)

Figure 3.13: The experimental setup for natural objects. An object is secured above the ground by using the tactile sensor to press it against a vertical metal plate. When slip is detected the sensor moves in to prevent the object from falling. A clear drop in height of the plastic banana between (a) and (b) is evident.

Object	Success (%)	Mass (g)
Box	90	145
Mustard	80	47
Water Bottle	90	186
Coffee	90	97
Banana	30	66

Table 3.6: The success of the slip detection method at generalising to a variety of objects. Each object has a different shape, compliance and weight and the slip detection method still performs well.

to the classifier prior to each experiment. This demonstrates the versatility of the classifier to generalise to previously unseen objects.

3.6.3 Discussion

The purpose of this short extension was to see whether the features which allowed the SVM to accurately classify slip on the 3D printed objects were present in a set of real world objects. Not only was this possible, as slip was accurately detected across all objects, but with four out of five objects the UR5 reacted quickly enough to stabilise them. This apparent generalisation is

likely due to the characteristic similar motion of pins as the sensor tries to relax from a highly deformed state (section 3.3.2). However, given the limited dataset true generalisation cannot be assumed and methods such as incremental learning using SVMs [233] or transfer learning techniques to improve generalisation under different settings [234].

All the different objects used here will indent the sensor to different depths and with a different force profile across the surface. This raises an interesting question as to how the depth to which the sensor is compressed affects the lateral movement of the pins when slip occurs. This was not investigated in this study but determining whether knowledge of the amount of sensor compression could be used to better inform a slip onset classifier is an interesting avenue of future study.

Slip was induced by retracting the arm to a position where normal force was insufficient to maintain the grasp. This was done for comparison to a study by Veiga et al. (2015) where data was collected the same way [197]. The method may be susceptible to false positives when lifting an object and the sensor surface is stretching under a load. There are multiple other scenarios in which slip could occur such as slipping under external load and at multiple angles relative to the surface of the sensor. However, here the scope of our study encompassed training only over a single angle (downwards under gravity). Furthermore, we did not consider the re-detection of non-slip, which would be an interesting extension of the method to detect when slip has stopped so that a precise action to minimise slip can be chosen. Slip can also be induced by pulling the objects but the success of the SVM when slip occurs in this fashion was not tested so the affect on performance is unknown.

3.7 Concluding Remarks

In this Chapter we have presented a method of detecting slip using the TacTip and demonstrated that it is able to reliably catch slipping objects before they are dropped.

Detection Method: We hypothesised that using the velocity profile of the internal pins would be a reliable indicator of slip in a manner similar to the RA-1 mechanoreceptors in the human finger. When slip occurs the velocity vectors of the pins display a clear alignment and this was used to train a Support Vector Machine. Transforming the velocity data into magnitude and angular components allowed the SVM to reliably discriminate between slipping and stationary objects. This required minimal training data and preprocessing.

Fast classification speed coupled with camera upgrades and streamlined processing means that the TacTip tactile sensor is capable of running at 100 fps, over three-fold faster than previous studies using the TacTip. As discussed in section 3.2.2 the increase in processing time from higher frame rate should not become a significant bottleneck. Given that the camera is capable of 120 fps there may be little benefit to further increasing the frame rate. Furthermore, classification speed was a major factor in the choice of an SVM.

Object Stabilisation The TacTip was able to detect slip on a variety of objects including novel curved and real world objects and prevent them being dropped. The ability of the classifier to cope with the variation of the arm retraction speed—when inducing slip—demonstrates a robustness to changes in experimental conditions. Different shapes deform the surface of the TacTip in distinct ways; however, by examining properties common to all slip events—here, the pin velocity distribution—it is possible to still reliably detect slip for differently curved objects. The minimal processing of our method allowed for slip to be detected in real time.

Having a single tactile sensor moving with a single degree of freedom means that the ability to handle complex objects is severely limited. However, the fact that slip was reliably detected, even on the banana, means that using a gripper with more degrees of freedom is likely to be successful at preventing slipping objects from being dropped.

The aim of this Chapter was to determine whether the TacTip is suitable for slip detection. Using a simple detection method with small modifications to the sensor we have shown that it is highly suited to the task. The main limitation of this work is that having only a single sensor limits the number of objects on which slip detection can be performed. This question allows us to segue into the next Chapter where we explore the integration of the TacTip into a multi-fingered robotic hand.

CHAPTER 4

THE TACTILE MODEL O - DEVELOPMENT AND TESTING

This chapter contains the work pertaining to the development of the Tactile Model O (T-MO) and its initial testing. The T-MO is based upon a GRAB Lab Model O [159] and here we discuss the modifications to the TacTip required to make it suitable for integration onto the hand and the validation of the grasping performance of the T-MO using a standard object set [140].

The work presented within this chapter forms part of the work included in the following peer-reviewed article:

- J. W. James, A. Church, L. Cramphorn & N. F. Lepora. (2020). Tactile Model O: Fabrication and testing of a 3D-printed, three-fingered tactile robot hand. Soft Robotics, ahead of print. doi.org/10.1089/soro.2020.0019.

  Contribution statement: J. James conceived of the presented idea, modified the TacTip, modified, designed and built the Tactile Model O, performed the tactile perception benchmark, assisted with the grasping benchmarks and co-wrote the manuscript. A. Church performed the grasping benchmarks and co-wrote the manuscript. L. Cramphorn assisted with the TacTip modifications and benchmarking. N. Lepora supervised the project and performed critical revisions of the manuscript.

4.1 Motivation & Scope

Tactile afferents in our hands provide information about the state of a grasp and, crucially, whether the grasp is failing [1]. Therefore, bringing tactile sensation to robotic hands will allow for more effective grasping, along with the wide range of benefits of human-like touch to perform tasks we take for granted yet robots are presently incapable of achieving.

Although robotic hands with integrated tactile sensors are becoming more common [222, 69], the vast majority of research on robotic hands still focuses on vision-guided grasp planning. In part, this is because there are a limited selection of commercial tactile-enabled hands, which are expensive and behind the development curve of the most advanced tactile sensors. Thankfully, the advent of fast, precise 3D-printing technologies now means it is inexpensive and relatively simple to adapt tactile sensors and robotic hands into new integrated platforms. Scaling to multiple sensors on a robotic hand presents several challenges, such as how to control the hand with integrated sensor feedback. With those challenges in mind, the presented platform offers a balance of dexterous capability against relative simplicity in its underactuation and fabrication.

The aim of this work is to modify a three-fingered robotic hand, the OpenHand Model O [159], to house the TacTip, an optical biomimetic tactile sensor [2, 3]. Prior work on integrating this sensor with 3D-printed hands has involved two 2-DoF, two-fingered robotic hands: the OpenHand model-M2 gripper with a tactile thumb [171] and the GR2 gripper with two tactile fingertips [173]. The current work represents a major advance in the functionality of 3D-printed tactile dexterous hands to integrate three tactile fingertips within a 4-DoF hand with state-of-the-art grasping capabilities. We expect that the grasping capabilities of the Model O combined with the success of the TacTip as a tactile sensor will result in an effective platform – the tactile Model O (T-MO) – for a wide range of future tactile robot hand applications and research.

This work makes several contributions. We continue prior work on integrating optical tactile sensors with 3D-printed robot hands by:

1. Increasing the number of tactile fingertips from two to three, degrees-of-freedom from two to four.

2. Miniaturising the tactile sensor to a size suitable for this hand.

3. Improve sensor performance with a better camera (e.g. improving the frame rate up to 120 per second and allowing for multi-modal data collection).

We demonstrate effective performance with an autonomous grasping platform comprising an arm-mounted tactile hand with depth camera for initial pose estimation, which is used to test the hand on a standard (YCB) object set [176]. This lays the platform for us to answer the second research question in this thesis: *Does the addition of tactile sensing to a robotic manipulator enhance effectiveness of the system?*

4.2 Tactile Model O Development

This section contains the development of the T-MO including the modification of the TacTip, hardware selection and integration onto the Model O. When embarking on the task of developing a multi-fingered tactile manipulator we wanted to keep the design aligned with the goals of this

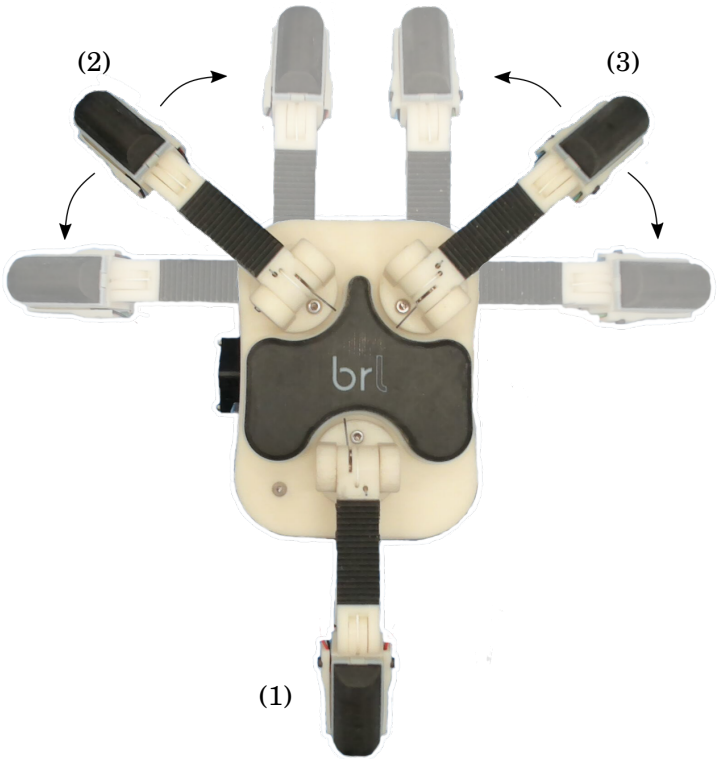

Figure 4.1: (a) The Tactile Model O (T-MO) with fingers labelled. Note the range of movement of fingers (2) and (3), which are mechanically coupled and thus constitute a single degree of freedom.

thesis as well as the ethos of the TacTip. With that in mind the following design goals were created:

1. Low Cost
2. Low Control Complexity
3. Strong Grasping Capability
4. Suitable for Slip Detection Experiments

4.2.1 Robotic Hand Selection

The first task was to select a robotic hand which could be modified to include a TacTip tactile sensor. The most widely-used platforms include the anthropomorphic iCub hand with integrated capacitive sensors [181], the Shadow hand with BioTac sensors placed at the fingertips [182] and with fabric and capacitive tactile sensors [74], the 4-fingered Allegro hand with PPS capacitive sensors [91] and with BioTac sensors [183] and the TWENDY-ONE hand with embedded force-torque sensors and a tactile skin [184]. These platforms are all expensive commercial offerings or research hands which are not open-source.

As discussed in the literature review a useful way to segment robotic hand research is into underactuated and fully actuated designs. Fully or highly actuated hands have the advantage of many actuatable degrees-of-freedom which allows for great grasping potential. However this comes with the added cost of requiring complex control systems for the hand to be successful. Underactuated robot hands greatly simplify the control systems required to grasp objects and are becoming increasing popular in research [139].

Another distinction mentioned in the literature review (Chapter 2) was between grippers and manipulators. Grippers, with only two fingers can be highly effective grasping platforms but they lack the capacity for manipulation inherent in systems with more fingers.

To summarise, the requirements of:

1. Open-source
2. Underactuated
3. At least three fingers

led us to select the OpenHand Model O as the platform. The Model O is the open-source counterpart of the i-HY hand [159] that won the ARM-H track of the DARPA manipulation challenge [160]. The Model O is a 3D-printed, three-fingered, underactuated hand that is one of several hands developed by the GRAB Lab's OpenHand project. It has four actuatable degrees-of-freedom which presents a nice trade-off between grasping capability and control complexity.

The three fingers are almost identical in that they contain two joints and a single degree of freedom, making each underactuated in the same way. A braided polyethylene wire 'tendon' runs the length of the finger and is connected to a Dynamixel MX-28T motor in the base of the hand. This allows the fingers to deform around objects for grasping without the object shape being known by the controller. Springs in both joints cause the finger to passively release when the active force from the motor is removed.

The only difference between the fingers is that one, the 'thumb', is fixed to the palm of the hand, whereas the other two fingers can rotate through 90 degrees from facing the thumb to facing each other (Figs. 4.1, 4.2, 4.3). The rotation of these two fingers is mechanically coupled and therefore constitutes only a single degree of freedom. This form of movement is known as abduction - coupled fingers moving perpendicular to thumb - and adduction - coupled fingers moving parallel to thumb.

The Model O was chosen over related hands - such as the Model M2 gripper [172] and Model T hand [158], which are both underactuated, 3D-printed hands with one and four fingers respectively and both having a single degree-of-freedom - as the extra degrees-of-freedom, particularly the coupled adduction/abduction of two fingers will allow the fingers to better conform to the shape of complex objects. This is with only a modest increase in control complexity.

To summarise, the choice of the Model O satisfies three of our design goals. It is low cost thanks to it being open source and much of it being 3D-printed. The underactuated design makes

Figure 4.2: Side view of the T-MO. Four Dynamixel servos and three JeVois machine vision modules are housed in the base unit with a marginal increase in size compared to the original Model O.

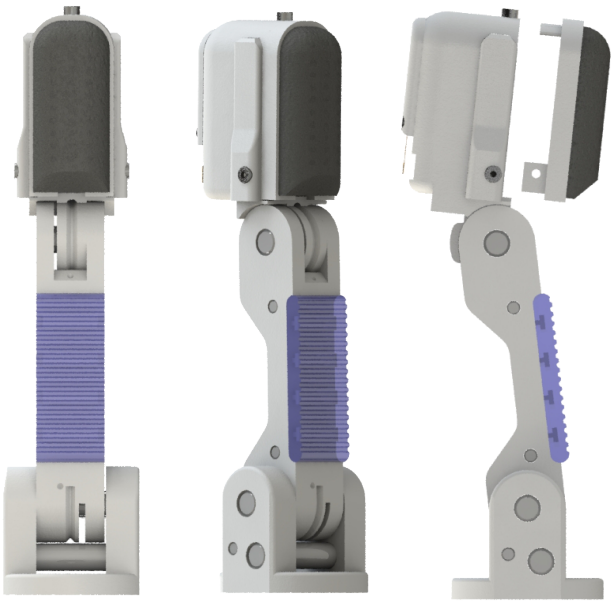

(a) (b) (c)

Figure 4.3: CAD renderings of the modified finger. (a) Front view of T-MO finger. (b) 45°view. (c) Side view showing how the smaller TacTip fits into the distal phalanx.

it easy to control and it has a strong pedigree when it comes to grasping; evidenced by its success in the DARPA manipulation challenge. All that remains is ensuring its suitability as platform for performing slip detection; this will be discussed in the next section.

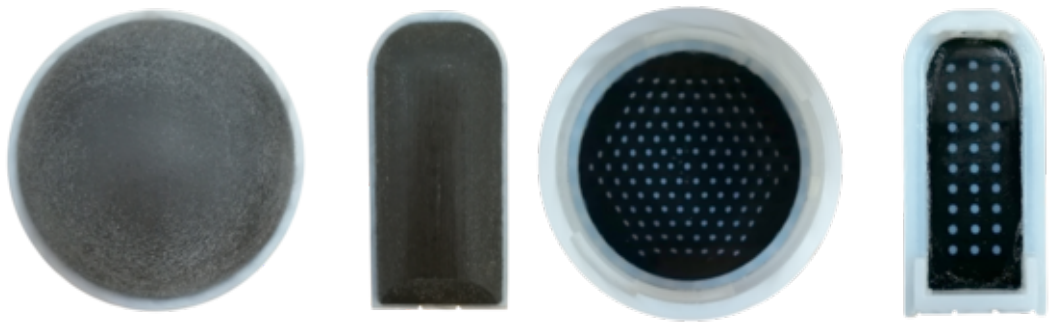

Figure 4.4: Comparing the form factors of the larger TacTip and the modified sensor used in this work.

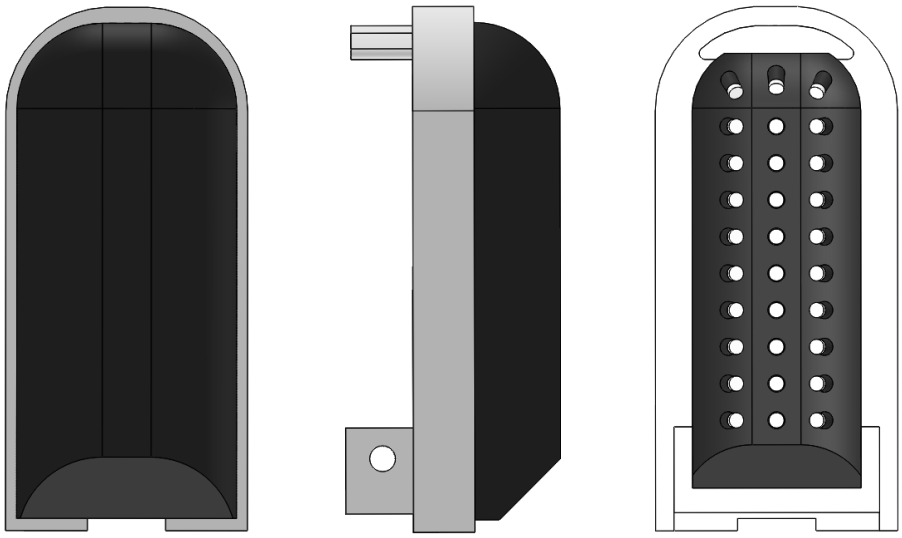

Figure 4.5: CAD renderings of the modified tactile sensor. (a) Top view of the sensor with dimensions. (b) Side view showing the chamfer at the base to prevent interaction of the sensor with the proximal phalanx when highly actuated. (c) New sensor pin Layout.

4.2.2 Tactile Sensor Modification

As evidenced by the work presented in Chapter 3 the TacTip has demonstrated strong capabilities as a slip detection sensor. The main aim of this study involves the integration of the TacTip onto the Model O, such that it is an effective slip detection platform yet retains strong grasping performance. As the TacTip previously used in Chapter 3 was a hemisphere with diameter 40mm and the distal phalanx is a rectangle measuring approximately 40x20mm a significant redesign of the tactile sensor is necessary.

The principles of the design remain the same. The sensor consists of a Tango Black+ skin with an array of pins printed on the inside. The pins are constructed by placing a small circular

blob of VeroWhite on top of Tango Black+ pillars. The new sensor is broadly semi-cylindrical with a fillet at the top. This results in the shape of the sensor being similar in both size and shape to that of the human fingertip. A chamfer is added to the base of the sensor which means that when the distal joint is highly actuated the sensor surface does not interact with the proximal finger linkage.

The sensor skin is embedded into a VeroWhite base which gives the sensor rigidity. The entire TacTip exterior is printed as a single unit, using both materials, which has allowed for rapid manufacture and prototyping. A lens is inserted into the sensor before being filled with silicone gel, as before. The sensor used here has 30 pins laid out in 3 columns of 10. The pins have a diameter of 1.2 mm and the pin centres are 3 mm apart. White LEDs are used to give uniform illumination inside the sensor and reduce the effects of any external light that bleeds through the Tango Black+ skin or Verro White base (both of which are not perfectly opaque).

A camera is mounted on the base of the sensor to view the pins as the sensor deforms, with each captured frame first processed in Python using OpenCV. Either the pin positions or the raw camera images can be used as the tactile information, for example as tactile inputs into supervised learning methods for regression or classification over labelled data.

4.2.3 Modification of Finger Design for Sensor Integration

4.2.3.1 Pin Layout

Each finger of the Model O has two joints and two phalanges with pads constructed from Vytaflex 30 to give a high friction surface suitable for grasping. We have replaced the distal phalanx of each finger with a tactile sensor such that three sensors are used in total (Fig. 4.2). This keeps the complexity of the modification low but still involves collecting data from more TacTips than has been tried before. The reduction in size and change of shape (40 mm diameter hemisphere to 20×10 mm rectangle) of the tactile sensor presents two challenges.

The first challenge is that the pin layout needs modifying to be consistent with the shape of the distal phalanx. As previously stated this led to the number of pins in the sensor being reduced to 30, arranged in three rows of 10, to ensure good coverage of the interior surface whilst also having sufficient separation of the pin tips to be easily distinguishable (Figs. 4.4, 4.5). Four LEDs are mounted above the sensor lens in two strips along the major axis of the finger (previously, six were used in a ring).

4.2.3.2 Camera System

The second alteration is to the camera system: the small size of the distal phalanx means that, to allow the camera to be attached directly above the sensor, the form factor of the camera board must be small and the lens must have both a wide field-of-view and a small focal length.

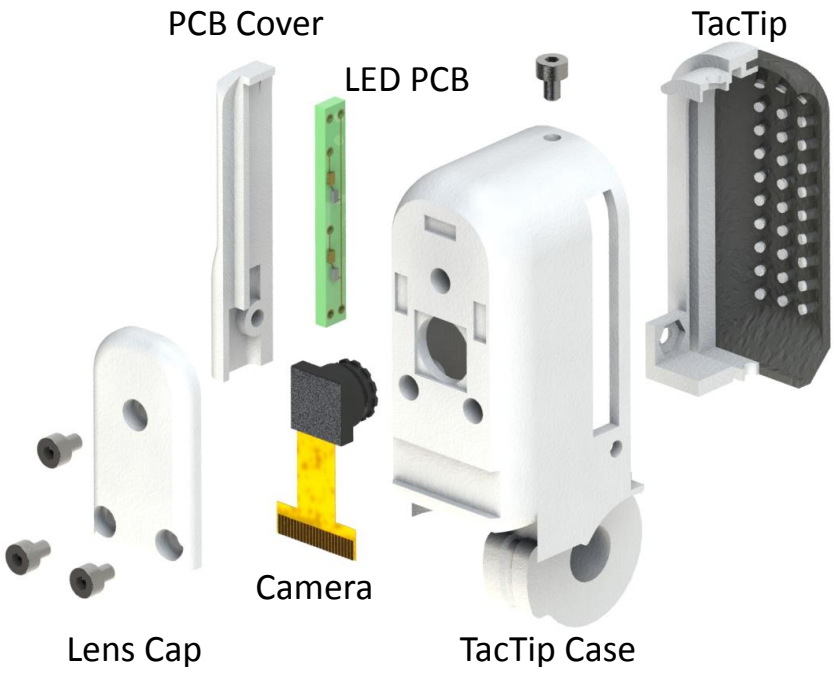

Figure 4.6: Exploded view of the distal phalanx in the T-MO finger.

Another desirable feature would be to have image processing performed on the hand to reduce computational load on the control PC.

These requirements led to the use of a 90° non-distortion lens connected to a JeVois machine vision camera system [235]. The camera module is connected to the finger (Fig. 4.6) and a ribbon cable connects it to the JeVois board which is housed in the 'base' of the hand (Fig. 4.7). The JeVois is able to capture frames and process them using OpenCV at a variety of frame rates and resolutions ranging from 1280 × 1024 (15 FPS) to 176 × 144 (120 FPS). TensorFlow Lite models can be loaded directly onto the JeVois, enabling processing by pre-trained deep networks within the hand itself.

There are many existing microcontrollers and single-board computers which are capable of driving a camera. Perhaps the most notable single-board computer is the Raspberry Pi; however, larger Raspberry Pi models such as the Model 3 B- which would be capable of driving a camera at high frame rates - would require a separate housing unit thus significantly enlarging the T-MO. Smaller models such as the Zero struggle to run a camera at a high frame rate. The JeVois' lack of other features such as GPIO is beneficial as it keeps size to a minimum. The JeVois is low cost (~£50) and allows some of the processing load to be transferred from the control PC to within the hand itself. We use a single JeVois module for each of the three TacTips. The small size meant the JeVois were able to be integrated into the base of the hand with minimal size increase (Fig. 4.7).

The camera is held in place by screwing a cap over the top of the board. The ribbon cable emerges from the rear of this cap and feeds directly into the base of the hand where the JeVois

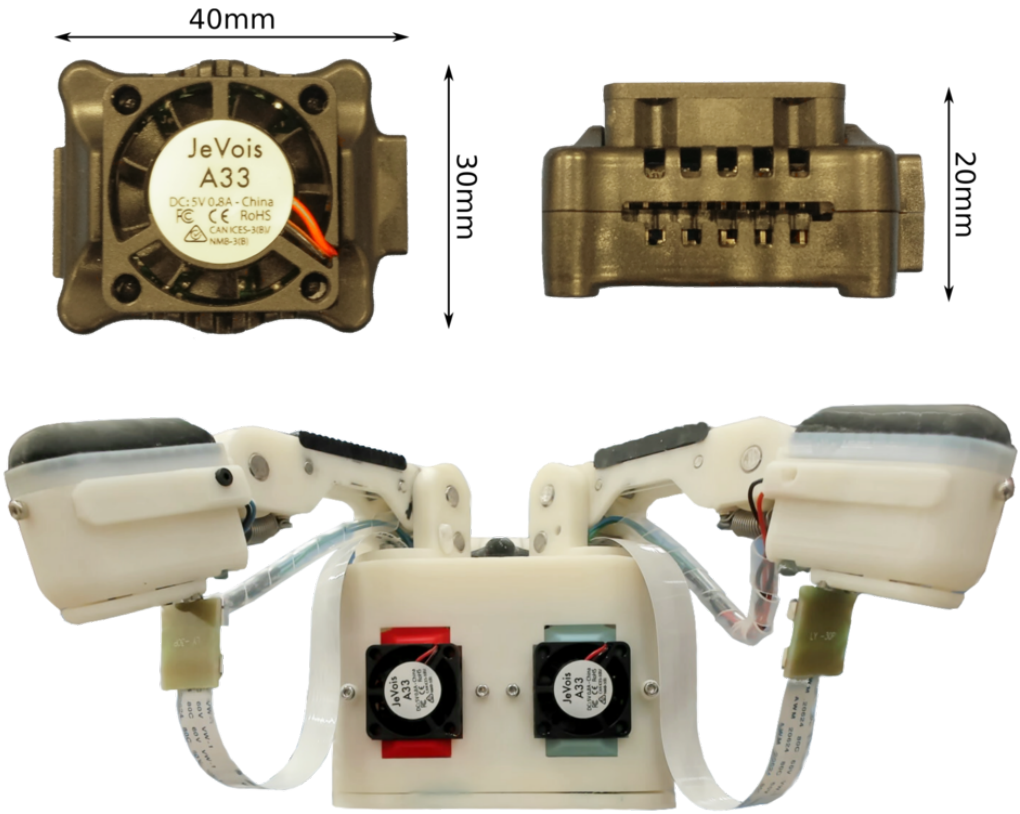

Figure 4.7: JeVois machine vision camera system. The lower image shows how the JeVois processors are integrated into the base of the hand. A ribbon cable runs from each JeVois unit to its camera module in the distal phalanx of each finger. A second cable on each finger supplies electricity to the LEDs.

processors are housed. The TacTip slots into the phalanx and is held by three screws. This makes replacing the sensor skin very simple when breakages inevitably happen. Overall, the integration of the tactile sensors makes the fingertips heavier, the effect of which is compensated by using stronger springs to hold the fingers in a fully relaxed position when the hand is held with the palm facing down.

Whilst the new fingers are roughly the same width and length as those of the original Model O, they are deeper because the use of a camera with a 90° field-of-view means that the lens must be at least 20 mm away from the TacTip to view the entire 40 mm surface. This makes the fingertips significantly thicker than those of the Model O which has the effect of removing the ability to slide the fingertips under objects to initiate grasps. For this reason, we expect that the larger size of the fingers presented here will have an impact on the ability of the hand to pick up very small flat objects, but otherwise the functionality of the hand should be similar.

As mentioned previously, either the pin positions or raw camera images can be used as tactile

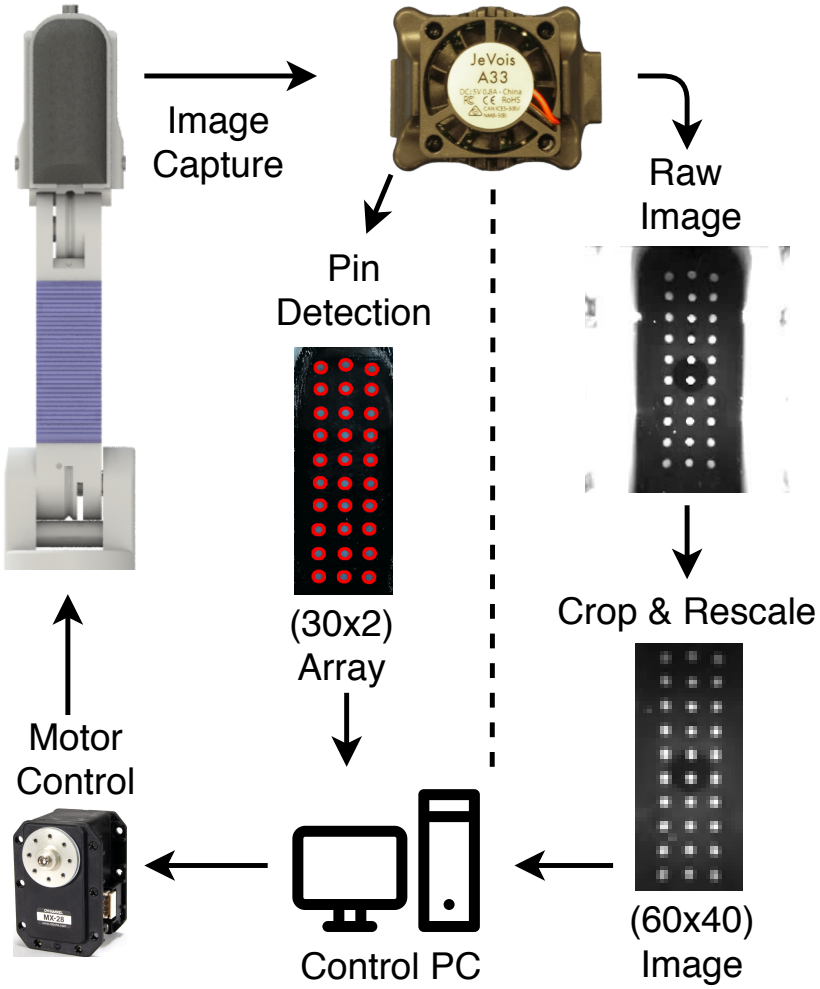

Figure 4.8: Flowchart showing the processes within the T-MO when images are captured by the JeVois. Either pins can be directly detected onboard the hand and sent to the control PC via a serial port or - as used here - raw images are cropped and rescaled before being passed to a classifier. Processes are the same for each of the three sensors. Note, the pixel dimension (bottom right in brackets) is an example and can be changed as required.

data. The images from each camera are captured and processed on its JeVois processor and sent to the control PC. For pin positions, a script on the JeVois is launched remotely that detects the pins (via the Python OpenCV function 'SimpleBlobDetector') and sends them over a serial connection. For raw images, Python OpenCV on the control PC can detect each JeVois as a video source and capture frames directly (Fig. 4.8).

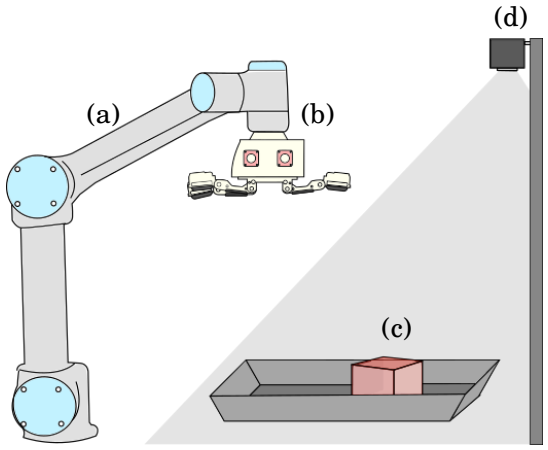

Figure 4.9: Diagram of the autonomous setup used for both collecting large amounts of data and for verifying grasping capabilities of the T-MO. (a) Universal Robotics UR5 robot arm. (b) Tactile Model-O. (c) Object to be grasped. (d) Microsoft Kinect2 RGBD camera.

4.3 Experimental Methods

The benefits of adding tactile sensors to robotic hands has been well examined in previous studies [4, 5] with a significant benefit being that touch provides information which vision cannot. However, clearly the purpose of a robotic hand is to perform grasping tasks and the addition of tactile sensors is moot if the grasping performance of the hand is significantly reduced.

Benchmarking protocols are provided to give a comparison between different platforms to quantify and encourage progress in the field of robot grasping and manipulation research. Here we perform four grasping validations:

- Grasp capability on all objects in the YCB object set [176]
- i-HY object benchmark [159]
- Gripper Assessment Benchmark [176]
- Extended Gripper Assessment Benchmark [140]

First, a description of the grasping platform is provided before further explanation of each benchmark is given.

4.3.1 Autonomous Grasping Platform

To facilitate testing and data collection, we utilise an automated grasping platform for the hand (Fig. 4.9). The T-MO is mounted as the end effector on a UR5 robot arm (Universal Robots, Denmark), controlled by the PC used to capture and store the tactile data. In addition, a Kinect 2 RGBD camera (Microsoft) is mounted above the workspace to provide a depth image of objects, which we process to give putative pose estimates of use for grasping. A tray is located in front of

the base of the arm into which a user can place an object and give the control PC an object label (currently the only human input into this system). This tray has steep sides to prevent objects falling off the platform and a soft (styrofoam) cladding to protect dropped objects.

This platform uses the Kinect depth images to estimate the pose of objects, which guide a simple planner for the arm-hand system to attempt to grasp and lift test objects. As the object covers only a small part of the tray, we are able to obtain the approximate depth of the tray by averaging the depth across an entire image. In other words, as the majority of the image will be the base of the tray the average value of the depth image gives a reasonable estimate of the location of the tray.

This depth estimate allows us to obtain the 2D extent of the object by subtracting everything in the image which is further away than the floor of the tray. To allow for errors a small threshold of 10 mm is subtracted from the estimate of the tray depth. Essentially, everything assumed to be the floor of the tray is removed from the image leaving only the object. By fitting an ellipse over the object we can find its centre of mass (x, y) and pose angle. These are calculated from the image moments corresponding to the major and minor axes of the best-fit ellipse. A z coordinate is also estimated from the minimum object depth to guide the initial vertical hand placement before grasping at 20 mm above the object.

The transformation from the camera frame to the robot frame is according to

$$\begin{pmatrix} x_{\mathrm{ur5}} \\ y_{\mathrm{ur5}} \\ z_{\mathrm{ur5}} \end{pmatrix} = \begin{pmatrix} y_{\mathrm{kin}} \\ -x_{\mathrm{kin}} \\ -z_{\mathrm{kin}} \end{pmatrix} + \begin{pmatrix} a_x \\ a_y \\ a_z \end{pmatrix} \tag{4.1}$$

with constant translation (a_x, a_y, a_z) found from an initial calibration (here $a_x = 643$ mm, $a_y = 0$ and $a_Z = 907$ mm) in which the hand is guided onto a known position. For this transformation to hold, the Kinect has been placed pointing vertically downwards with orientation aligned to the x and y axis of the UR5 robot arm.

4.3.2 Grasping Validation

Here we provide descriptions of the four grasping validation experiments conducted to evaluate the effectiveness of the T-MO.

4.3.2.1 Test 1: YCB Object Set

The Yale-CMU-Berkeley (YCB) object set was created to provide a standardised benchmark for robotic manipulation research. The set consists of 77 objects which can be divided into 5 categories including food items and tools [176]. The first experiment is merely to test which objects within the YCB set the T-MO is able to grasp.

For this test, objects were placed in the centre of the tray and a pre-determined grasp orientation was used to attempt to lift the objects. The T-MO was lowered to the objects and the

Figure 4.10: Example images of the T-MO hand grasping a variety of objects from the YCB Benchmarking Object Set. Each grasp is performed by placing the object on a flat surface in a fixed position and using a UR5 robotic arm to lower the hand over the object and raise to a specified height. This figure also shows how the rotation of the fingers can be employed to help grasp objects depending on their shape.

fingers were actuated to full torque. The T-MO was then lifted and visual inspection was used to determine if the grasp was successful. This test is the least rigorous of the four performed here and is included as it provides broad information about which objects the T-MO cannot grasp.

4.3.2.2 Test 2: i-HY Object Set

The i-HY hand, upon which the T-MO is originally based, demonstrated its grasping capabilities with a benchmark involving 10 unique objects where all objects were grasped 20 times [159]. Each grasp was performed in an automated manner by detecting the approximate centre of mass of an object using a depth sensor (a Microsoft Kinect, as used here) and an alignment performed to the major axis of the detected object. For a direct comparison to the i-HY hand, the same experiment has been performed here with our newly modified hand, using the method and platform described above in Section 4.3.1.

As the set of objects used to validate the i-HY was not standardised, it is difficult to recreate the experiment exactly, so instead a set of similar objects has been used. The list of objects was: a file, battery, hammer, two pens, torch, phone, screwdriver, small section of PVC pipe and a roll of electrical tape.

4.3.2.3 Test 3: Gripper Assessment Benchmark

The Gripper Assessment Benchmark uses a subset of the objects from the YCB object set split in four categories; round objects, flat objects, tools and articulated objects. The full list of objects is provided in Table 4.1.

To locate the object in this test we forgo use of the depth sensor and instead used a fixed position as described in the benchmark guidelines. Further control of the hand is available in the rotation of the finger joints. Fingers 2 and 3 can be jointly rotated from 0° (Cylindrical grasp), through 45° (Spherical grasp), to 90° (Opposed grasp). The grasp that is likely to be successful is then pre-selected selected from these distinct cases depending on the geometry of the object to be grasped (*e.g.* Fig.4.10).

A printable grid (provided with the benchmarking test) is used to consistently place objects and apply offsets to their positions. Four object locations are tested. Firstly, the object is centred on the grid and the T-MO oriented directly above the object facing down. For the remaining three tests the position of the T-MO is fixed and the object is shifted by 1cm in the x, y and z directions to make it more difficult to grasp. These four positions are hereafter referred to as SP1-4.

The experiment then proceeds as follows. The object is placed at SP1 and a grasp initiated. It is lifted and held for 3 seconds. The object is rotated 90 degrees about the x axis of the grid and if still held the test is a success. Only if SP1 is passed are positions SP2-4 attempted. For a more complete description of the benchmark and scoring criteria see [176].

Whilst, to the best of our knowledge, there is no available score on this benchmark for the original Model O hand, this will allow for a direct comparison to other available grippers.

4.3.2.4 Test 4: Extended Gripper Assessment Benchmark

An extension to the standard Gripper Assessment Benchmark was proposed by Jamone et al. 2016 [140] to include three more categories of objects: Cubic, Cylindrical and Complex. These objects are easier to grasp as, unlike in Test 3, none of them are small and flat - like the washers - nor overly heavy - like the drill. The full list of objects is provided in Table 4.2. The procedure for the benchmark is the same as for Test 3 with tests being performed at locations SP1-4.

4.3.3 Tactile Perception Task: Edge Detection

The T-MO has been developed as a platform for tactile tasks such as grasping, object identification and slip detection however it is important to see how the modified sensor compares to the 'original' TacTip on acuity tasks. One such task used by Lepora et al. (2019) [106] involved determining the position and orientation of the TacTip relative to the edge of a 12cm diameter circular disc. The TacTip was placed with the central pin on the edge of the circle and the major axis of the camera aligned tangential to the edge. For each tap radial position and angle relative the the edge were varied randomly. Radial positions were sampled from [-6,9] mm (where negative distances

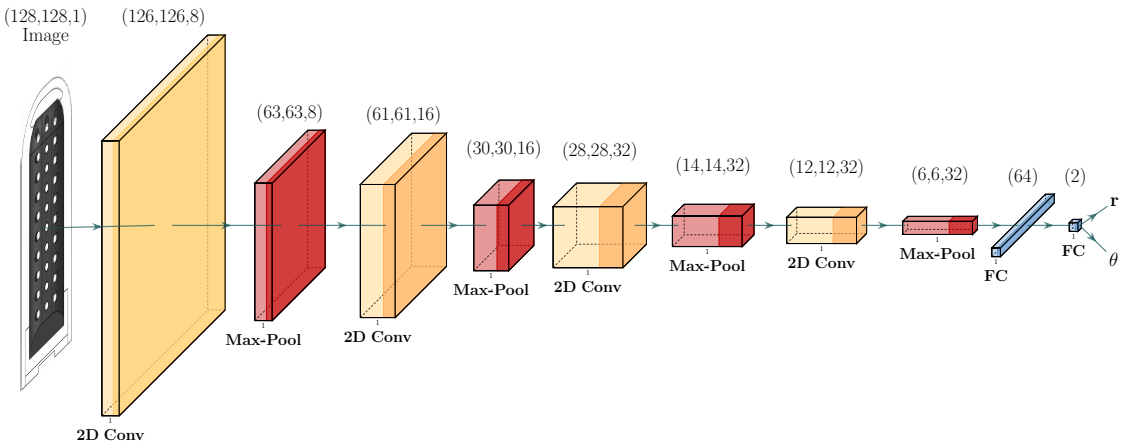

Figure 4.11: Architecture of the regression CNN used to predict sensor position and orientation relative to the edge of a circular disc. The input is a 128x128px greyscale image. Each layer has type labelled below and the size of the output from that layer above. For example, the first convolutional layer has 8 filters with a kernel size of 3x3 resulting in an output of (126,126,8) to the first max-pool layer.

(a) (b) (c)

Figure 4.12: Adaptor for connecting the T-MO sensor to the ABB IRB120 for tactile acuity testing. As for the regular TacTip it is connected to the robot arm via a bayonet fitting (c).

indicate the sensor being closer to the centre of the disc) and angles from [-45,45] degrees. Each tap compressed the TacTip to a distance of approximately 3.5mm and seven frames were selected.

A regressor was trained using a convolutional neural network (CNN) which contained four convolutional layers with max pooling inbetween. Finally two fully connected layers were used to provide a two dimensional output for radial position and angle. Here, the same procedure as Lepora et al. is followed for data collection and the same network architecture is used (Fig. 4.11). 1000 taps are collected for training the CNN, split in a ratio of 80:20 for training and validation. A further 500 taps are collected for evaluating the trained network. As this is solely a test of the *sensor* not the entire T-MO hand the sensor is attached to an ABB IRB120 6-DoF robot arm via a custom adaptor (Fig. 4.12). Before training the image is downsampled from (640,480)

(a) (b)

Figure 4.13: (a) Items from the YCB object set that the T-MO was able to grasp. (b) Items from the YCB object set that the T-MO was unable to grasp.

to (128,128) to reduce the number of parameters which need to be optimised. The use of the same conditions - stimulus, robot, data collection and CNN architecture - is done to allow for a reasonable comparison between the sensors.

4.4 Results & Discussion

4.4.1 Grasping Validation

The first test was assessing the grasping capability on the entire YCB object set. The T-MO successfully grasped the majority of the objects in the set only struggling on the larger heavier objects and the smaller flat ones (successful/unsuccessful objects shown in Fig. 4.13).

Due to the thickness of the redesigned distal phalanges the technique of driving the hand into the table in order to perform a power grasp was no longer possible. In the human distal phalanx the nail not only serves to improve finger sensitivity by providing a counter force to pressure applied to the fingertip (in addition to the solid bone) but it is also useful in executing precision grasps [236]. In human grasping this is useful for tasks such as picking up small objects or removing splinters. The T-MO's tactile sensor has a solid base which provides the necessary counter force but is too thick to allow for the precise pinch mode to be deployed to grasp small, flat objects.

Similarly the compliance of the tactile sensors and inability to provide high forces results in pinch grasps being more subject to failure when given high torsional forces. As the method of grasping was to find the centre of the object located using the depth camera, objects with a non-uniform weight distribution - such as the hammer - would rotate out of the grasp. Images showing the deformation of the tactile sensor can be found in Figure 4.14.

The second test was a comparison to the i-HY hand using ten objects. The grasping weaknesses identified from the first test resulted in reduced performance for the hammer, file and pen, where

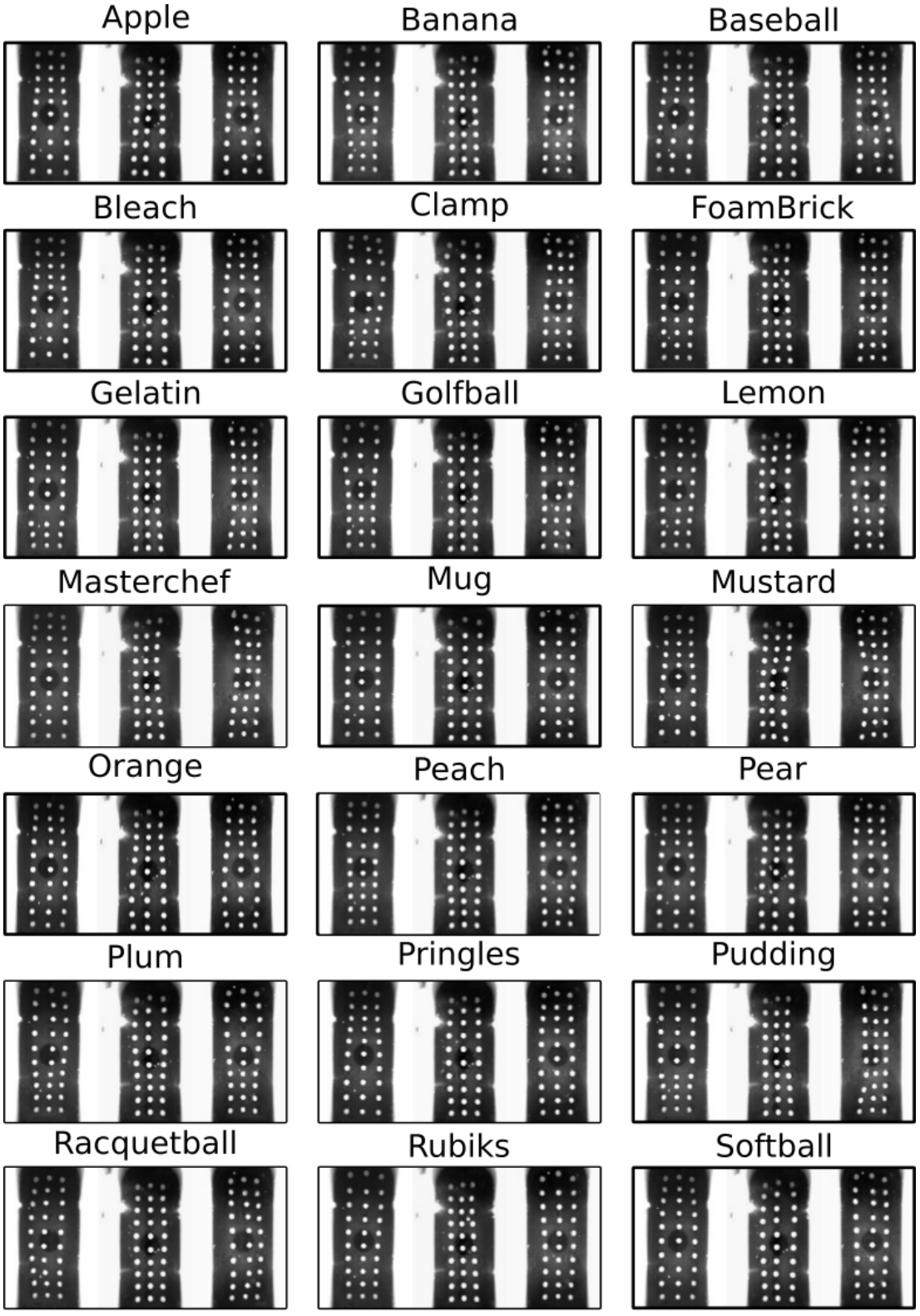

Figure 4.14: Tactile sensor internal view when grasping various objects. Significant deformation of the sensor is clear and differently shaped objects provide noticeably different indentation.

Table 4.1: Scoring of the Tactile Model O hand at four set points (SP) in the Basic Gripper Assessment Benchmark provided by [176]. F.O. and A.O. stand for Flat Objects and Articulate Objects. Total score for this test is 202.5 out of 404.

	Object	SP1	SP2	SP3	SP4
Round Objects	Soccer Ball	4	4	4	4
	Soft Ball	4	4	4	4
	Tennis Ball	4	4	4	4
	Racquet Ball	4	4	4	4
	Golf Ball	4	4	4	4
	Marble XL	4	4	4	4
	Marble L	4	4	0	4
	Marble M	4	0	4	0
	Marble S	4	4	0	0
F.O.	Washer 1-6	0	0	0	
	Credit Card	0	0	0	
Tools	Marker L	4	0	4	0
	Scissors	0	0	0	0
	Hammer	0	0	0	0
	Flat Screwdriver	2	0	0	0
	Drill	0	0	0	0
	Clamp XL	4	4	4	4
	Clamp L	4	4	4	4
	Clamp M	4	4	4	4
	Clamp S	4	4	4	0
A.O.	Rope	8.5			
	Chain	0			

the hand was unable to successfully perform a grasp. However, the remaining 7 objects had similar results to the i-HY tests, with at least 18 out of 20 trialled grasps being successful. The i-HY only struggled with the pen. It should be noted that the i-HY hand used in this test was endowed with MEMS barometric TakkTile sensors, to give a basic array of 4 pressure-sensitive taxels on each fingertip [159] although it's unclear whether these were used in the test to assist with grasping.

To further validate the grasping capabilities of the T-MO hand, a standardised benchmark, the Gripper Assessment Benchmark, provided by [176] was employed. This test is performed using the platform and setup described in Section 4.3.1. Overall, the total score achieved for this benchmark is 202.5 out of 404 and the complete scores for this benchmark are available in Table 4.1.

The performance of the T-MO hand is competitive with other hand designs, surpassing the iCub (173/404) and Model T (122/404) Basic Gripper Assessment scores. Other GRAB Lab robotic hands do achieve better scores on the standard benchmark. These include the Model B, Model T42 and Model S which score 270, 379 and 402.5 out of 404 respectively. None of these hands have

Table 4.2: Extended scoring of the Tactile Model O hand in the Basic Gripper Assessment Benchmark as proposed by [140]. Total score for this test is 176 out of 208.

	Object	SP1	SP2	SP3	SP4
Cubic	Pudding Box	4	4	4	4
	Foam Brick	4	4	4	4
	Coloured Wood Block	4	4	0	0
	Dice	4	4	0	0
Cylindrical	Pringles Can	4	4	4	4
	Plastic Wine Glass	4	4	4	4
	Cup L	4	4	4	4
	Cup M	4	4	4	4
	Cup S	4	4	4	4
Complex	Plastic Pear	4	4	4	4
	Plastic Strawberry	4	4	4	4
	Plastic Bolt	4	4	0	0
	Plastic Nut	4	4	0	0

yet been equipped with tactile sensing. To the best of our knowledge, the T-MO is the highest scoring hand with tactile capabilities.

The final comparison was the Extended Gripper Assessment Benchmark. The T-MO scores for this extended benchmark are available in Table 4.2, with total score 176 out of 208. This surpasses the score of the iCub (164/208) which was being tele-operated by a human controller. Again, flat objects prove a significant challenge for this hand and result in a drop in overall score. Whilst it would be possible to modify this hand with a nail design to help grasp flat objects, this would require significant modification of the tactile sensing part of the design for the sensors to remain effective.

4.4.2 Tactile Perception Task: Edge Detection

The Convolutional Neural network described in Section 4.3.3 and Figure 4.11 was optimised using Adam [237]. An initial learning rate of 10^{-4} was used with a decay rate of 10^{-6} per epoch. A dropout rate of 0.25 is used on the first fully connected layer and training takes place over 100 epochs although early stopping with a patience parameter of 5 epochs is used to prevent overfitting.

When testing on 500 taps randomly sampled in the same angle and radius range as the training data (Fig. 4.15), the T-MO sensor was able to resolve radius and angle with mean absolute errors of ~0.2mm and ~2 degrees. This compares well to the hemispherical TacTip which obtained mean absolute errors of ~0.3mm and ~2 degrees [106].

Whilst this appears to be marginally better at resolving radial position there are a couple of points that require clarification. Firstly, in Lepora et al. [106] this was tested on a larger test dataset of 2000 taps making it a more reliable test set. As the purpose of the tactile perception

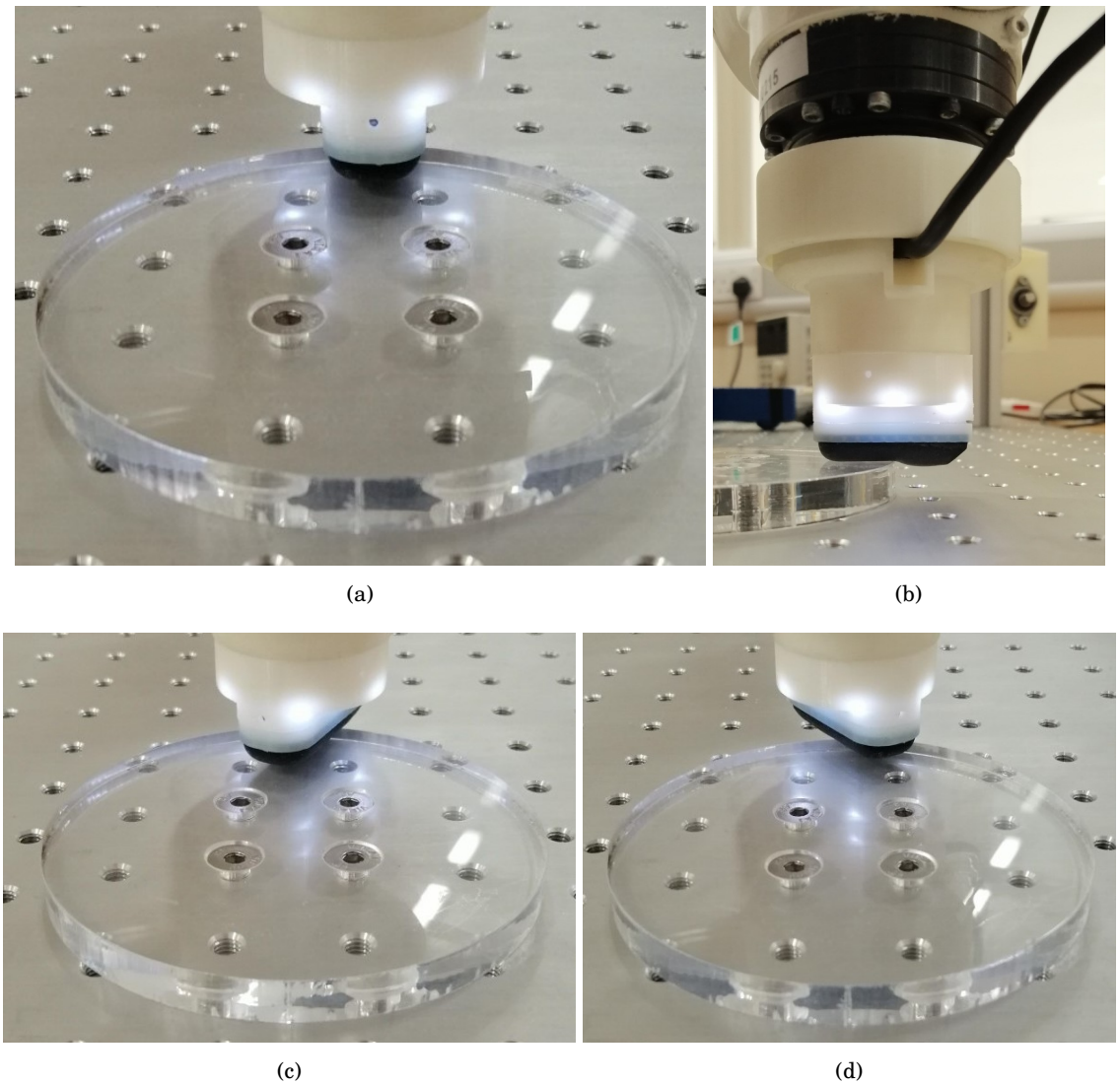

(a) (b)

(c) (d)

Figure 4.15: Tapping in at various positions and orientations relative to a circular object. (b) shows the attachment to the ABB IRB120 6 DoF robot arm.

study is to determine whether the T-MO TacTip has significantly lost tactile sensing performance, a smaller dataset is acceptable.

Secondly, being hemispherical, when the TacTip is moved away from the edge of the disc (and away from the centre) less of the tip contacts the surface during the 3.5 mm tap. However, with the flat surface of the T-MO means that throughout the range of radial motion in this task part of the flat surface will always be in contact with the edge leading to similar deformation. This provides an advantage for radial resolution which is not present in the angular data where errors are the same.

The purpose of this test was to determine whether the new design of sensor retained the hemispherical TacTip's strong tactile acuity. Despite comparable performance in radial and

angular perception it can only be concluded that the T-MO does retain strong tactile acuity but we cannot make a fair judgement about relative performance between the TacTip and the T-MO. This is mainly due to small differences in the experiment and not conducting all the tasks performed by Lepora et al. [106] such as contour following by tapping and sliding.

4.5 Discussion & Limitations

4.5.1 Tactile fingertip morphology and Actuation Method

Modifying the finger morphology to integrate tactile sensors within an already very capable grasping system (the Model O) was expected to result in impeded performance, as we have seen with a modest drop in grasping capability compared with the original i-HY hand (Section 4.3). Due to the thickness of the redesigned distal phalanges, the technique of driving the hand into the table in order to perform a power grasp was no longer possible. Even so, the tactile hand still managed to successfully grasp most objects it was presented with.

Future design improvements to the tactile fingertips will focus around a more compact design that would help grasp small objects with a 'fingernail' and larger objects by sliding under them to establish a power grasp. At present, to avoid distortion of the tactile image we use a 90°field-of-view lens, which constrains the camera to be mounted quite high above the sensing surface. One redesign strategy would be to adopt mirrors that enable the camera to be mounted nearer the joint, as in the Gel Slim [129]. That said, camera technology is going through a stage of rapid miniaturization, and it may be a combination of smaller camera with a wide-angle lens would be a more effective solution. These remain open design questions that are subjects for future work.

The stronger springs required to provide the extension force to relax the fingers - which are heavier due to the sensor assembly - means that the maximum grasping force that can be applied is lower. Whilst we are not able to quantify the frictional differences between the TacTip and the Vytaflex which comprised the distal finger pad in the original Model O the inability to grasp heavy objects such as the drill may be explained by the TacTip skin being less frictional than the Vytaflex finger pads. When performing a force closure grasp a lower friction surface means that the risk of an object slipping is necessarily higher as a higher force needs to be applied to maintain a stable grasp. Therefore, whilst an underactuated hand makes attempting to grasp objects simple, a more complex manipulator may be able to compensate for any increased risk of object slip by establishing a more stable grasp with a greater contact area. However, as demonstrated, the T-MO design retains strong grasping capability across a wide range of objects.

The use of an underactuted platform makes responding to a grasp failing easy. The hand need only grip tighter in an attempt to secure the object. For the T-MO the success of this is dependent on the amount of time taken to detect slip and tension the cables to apply an increased force. Reducing this latency could be achieved by utilising a faster onboard computer to interpret the tactile data at a higher frame rate or reduce the resolution of the images which would have the

same effect. Replacing the tendon driven actuation with motors integrated into every joint would eliminate time losses when the cable is being tensioned and provide an opportunity for better grasp planning and in-hand manipulation. Regrasping slipping objects is explored in depth in the subsequent chapter.

Another future avenue of study could be integrating the TacTip into a robot hand with greater than three fingers. This would have the advantage of proving greater manipulation capabilities - particularly if the hand was fully actuated. In-hand manipulation carries many benefits including being able to reorient objects to find an optimally stable grasp [222]. Potential difficulties would be from increased computational load and expense from more cameras. Were this to be explored it may be of benefit to couple this with further shrinking of the TacTip to minimise any loss of grasping performance from adding tactile sensing; as was experienced here.

4.5.2 Tactile sensor design

Here we use the same 3D-printed skin as in other tactile sensors within the TacTip family, having an array of pins spaced approximately 3 mm apart developed originally for a 40 mm diameter, domed tactile sensor [3]. This design choice was for consistency in the absence of a good reason to customize those aspects, unlike for example the overall shape of the sensing surface which required customization to fit onto the Model O fingertip. However, it does result in relatively few pins (a 10×3 array) compared with others in the TacTip family (127 pins in the domed sensor). Since these pins are used as sensing elements, this may limit the tactile sensor performance.

This was partially addressed by determining the radius and angle of the sensor relative to the edge of a circular disc. Results were shown to be similar to the hemispherical sensor allowing us to conclude that the sensor does retain a high level of tactile acuity. However, this was not done with the entire T-MO system, instead the sensor was attached to a 6-DoF robot arm, but this does show that shrinking the form factor of the sensor does not significantly affect the ability to resolve edges. The effect on the tactile sensing capability when using the entire T-MO system is further explored in the subsequent chapter.

4.6 Concluding Remarks

We have presented a three-fingered tactile hand that comprises a GRAB Lab Model O modified to include three TacTip optical tactile sensors in its fingertips. Using small camera modules mounted in the the distal phalanx of each finger coupled with the JeVois vision system housed in the 'palm' of the hand and lightweight TacTip sensors, provided an integrated and sophisticated tactile sense that complements the grasping functionality of the hand.

To evaluate the capabilities of the tactile Model O (T-MO), we benchmarked its grasping performance using the Gripper Assessment Benchmark on the YCB object set [176]. In the Gripper Assessment Benchmark we scored similarly (202.5/404) to the Model T and iCub hands

(122/404 and 173/404) but were surpassed by other hands produced by the GRAB Lab [238]. This included a test where the iHY hand (on which the Model O is based) could grasp all 20 objects and the T-MO could reliably grasp 17 items. The reason for this performance drop is the change to the finger morphology needed to integrate our tactile sensors within the distal phalanx that can be improved in future design iterations of the hand (Section 4.5.1).

For a final comment, it should be noted that further tactile tasks including object classification and grasp success prediction were presented by James et al. (2020) [239] but not included in this thesis. It was shown that the T-MO provided comparable results to other, more expensive, robot systems such as the BarrettHand,[240] Schunk[241] and iCub[242] hands even though it has a much lower cost (costing less than £1100 to make). Most of the T-MO's cost is actually its motors, followed by the 3D-printing and camera costs, so it may be possible to reduce these costs still further. A benefit of building the hand ourselves is that we can quickly fix issues such as accidental damage or parts failure, while being 3D-printed means the hand can be adapted to various applications and we can fix design problems that only become apparent later in its use.

In summary, the Tactile Model O has modestly reduced grasping performance compared to the GRABLab Model O. However the smaller sensor retained high tactile acuity. It is unsurprising that altering the fingers to include tactile sensing would affect grasping performance. The question that remains is: given the T-MO is a capable grasping system, what are the advantages of tactile sensing in this hand when performing real-world tasks? This will be addressed in the next chapter when we investigate how the T-MO performs as a slip detection system.

CHAPTER 5

SLIP DETECTION WITH THE TACTILE MODEL O

This chapter contains the work testing the Tactile Model O's (T-MO, presented in Chapter 4) ability to detect and react to gross slip. I investigate how the TacTip fares for slip detection when it is scaled down in size and when the number of sensors is increased from one to three. This is followed by testing how well the T-MO performs in several 'real-world' scenarios where the slip detection functionality is required.

The work presented within this chapter has been accepted for publication in the following peer-reviewed journal. A contribution statement is included:

- J. W. James and N. F. Lepora, "Slip Detection for Grasp Stabilization With a Multifingered Tactile Robot Hand," in IEEE Transactions on Robotics, early-access doi.org/10.1109/TRO.2020.3031245.

  Contribution statement: J. James conceived of the presented idea, designed and constructed the robot hand, conducted all experiments and analysis and wrote the manuscript. N. Lepora supervised the project and performed critical revisions of the manuscript.

5.1 Motivation & Scope

Tactile sensing is used by humans when grasping to prevent dropping objects [1]. It is well known that tactile sensing is useful in robotic grasping and provides information complementary to vision [4, 5], such as contact forces and surface texture. To paraphrase Bajcsy et al. "Vision hypothesises, touch verifies."[6] With a sophisticated tactile system a robotic hand could replicate many of the complex tasks that humans perform with minimal conscious thought.

In Chapter 2 we discussed the importance of slip detection in the context of work presented over the last three decades. In Chapter 3 I presented a simple, but effective, method of detecting

slip with a single TacTip when objects were suspended by pressing them against a solid support. In reality, the utility of this in a cluttered human environment is limited; instead, a multi-fingered robot hand with slip detection capability is necessary to grasp objects and prevent them from being dropped. Scaling up from a single sensor to multiple sensors on a robotic hand presents difficulties such as how to combine control of a many degree-of-freedom (DoF) hand with sensor feedback. As stated in previous chapters, the TacTip has previously been integrated onto multiple existing robotic hands. This inculdes the OpenHand M2 [172, 171] and the GR2 [131, 173]. However, neither the T-MO nor any other hand using the TacTip or variants thereof have been used to perform slip detection.

The field of slip detection is diverse and growing with many new sensors and control methods proposed to aid its implementation in grasping and manipulation [69, 16]. This based on different technologies including optical [219, 243, 15], neuromorphic [216, 244] and force sensing [212, 13] to name but a few. The methods of detecting slip are also diverse with research into both model-based and model-free approaches. Model-based approaches have included use of beam bundle models [245] and friction cones [207] and model-free approaches have included everything from random forests [197, 185] to the increasingly popular deep learning [13, 170, 14, 206]. Rosset et al. (2019) compared a CNN to a model using sensor firing rates in a pick-and-place task with the model coming out on top [246]. Whilst interesting, this was far from comprehensive enough to stifle the debate on model-based vs. model-free. The aim of this chapter is to demonstrate the slip detection and grasp correction capabilities of the recently-developed Tactile Model O (T-MO) hand [228] using simple, methods. This system integrates the TacTip, an optical biomimetic tactile sensor [2, 3], onto a GRAB Lab Model O hand [159]. The principal contributions of this chapter are to:

1. Compare and understand simple slip detection methods based on pin velocity features, which can be scaled from one to three fingers of the Tactile Model O.

2. Test multiple slip scenarios, including responding to the onset of slip in real time with eleven different objects in various antipodal pinch grasps (e.g. Fig. 5.1)

3. Demonstrate the benefits of slip detection by testing two real-world scenarios: adding weight to destabilise a grasp and repeat detection of slip in real-time to perform first time grasping.

The chapter is laid out as follows. First, another brief overview of relevant literature is given to further motivate the work. Then the hardware and software methods are described before moving onto the experiments. The experiments undertaken in this paper are split into three distinct sections. Firstly, the slip detection capabilities of a single sensor are tested. Secondly, the capabilities of the entire hand is tested using several natural objects. Finally, the classifiers developed during the second test are deployed in two tasks which use slip detection to aid grasping performance. This chapter's work is to determine whether the Tactile Model O (T-MO)

(a) (b)

Figure 5.1: The Tactile Model O (T-MO) before and after catching a softball by detecting slip and reacting to prevent it from being dropped.

is able to detect when an object is slipping, react to stabilise the grasp, and can be deployed in several distinct grasping scenarios. Overall, this seeks to answer the third and fourth research question posed in Chapter 1: *can a low-cost multi-fingered manipulator be used to reliably detect slip?* And, *can slip detection be used as a metric to evaluate the stability of a grasp and improve grasping efficiency?*

5.2 Background

Much prior research involving slip detection on objects has used 1-2 sensors to hold an object in a two-fingered pinch or pressing an object against a wall with a single sensor. Veiga et al. (2015) used the latter with a BioTac tactile sensor [197]. Using a Random Forest classifier they achieved up to 100% success on multiple objects when detecting a slipping object and preventing it from falling. Dong et al. (2017) integrated two GelSight sensors onto a two-fingered gripper and used slip detection to determine whether a grasp was stable and regrasp if necessary [15]. Subsequently, Li et al. (2018) used visual and tactile information to evaluate the stability of a grasp. With the same hardware they obtained 88% accuracy compared to 82% when using tactile feedback alone [170].

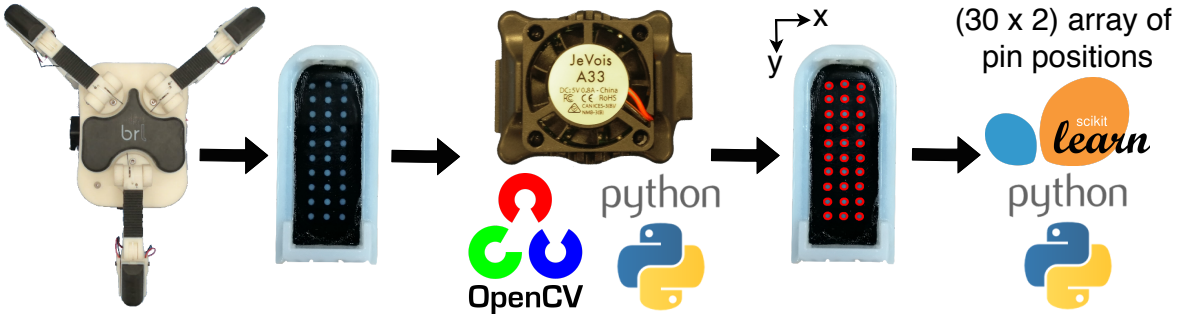

Figure 5.2: Data flow schematic of the Tactile Model O (T-MO). From left to right: T-MO with embedded cameras; TacTip sensor with 30 pins; JeVois vision system captures image of sensor; TacTip pins detected using Python and OpenCV (camera axes shown); (30x2) array of pin coordinates sent to control PC.

Dong et al. (2019) used a modified GelSight sensor, the GelSlim, to detect slip and to perform a task - screwing on a bottle cap [215]. The GelSlim uses a mirror array to reduce the size of the pinch gripper whilst utilising the same sensing technology as the GelSight. The GelSlim is a soft optical tactile sensor with markers embedded in a gel. By deforming around objects a high resolution image of an object's morphology can be obtained as well as using the markers to determine how the object is slipping. They used this ability to screw and unscrew a bottle cap. A similar sensor, the FingerVision, also uses markers embedded in a soft gel to perform slip detection [14]. They use a convolutional LSTM neural network to detect slip and obtain a 97.62% classification success rate but do not detect slip on-the-fly in grasping experiments.

Other work has involved increasing the number of sensors and the variety of slip scenarios. Stachowsky et al. (2016) used contact force sensors to detect slip on a held object and also when picking up various objects to determine, in real time, the required grasp strength [212]. Li et al. (2017) used a Barrett three fingered hand with a 3x8 tactile array and a force sensor on each fingertip to detect slip. They used an SVM and achieved up to 96% success at detecting slip on a variety of objects, although the hand did not react to prevent the object from being dropped once slip is detected [213]. Veiga et al. (2018) used up to five BioTac sensors on two different hands to stabilise grasped objects and prevent them from being dropped [183]. The control mechanism increased normal force on an object when slip was predicted and slowly released its grip to find the optimum grasping strength. Li et al. (2014) also use BioTac sensors to predict when a grasp is failing and deploy two strategies to find a stable grasp [191]. Our approach here is to consider a tactile-enabled manipulator that is midway in control complexity (the 4-DoF Tactile Model O) in combination with an simple slip detection method that extends naturally from one tactile fingertip to a many-fingered hand.

5.3 Hardware Description

5.3.1 Robotic Hand

For this experiment we are using the Tactile Model O (T-MO) discussed in Chapter 4. As a brief reminder this consists of a GRAB Lab Model O [159] which has been modified to contain three TacTip tactile sensors (Fig. 5.2). The sensors are significantly smaller than the original TacTip size but retain the same working principle.

It contains three JeVois machine vision systems [235] which are used to capture images at 60 frames per second (340x280 resolution) and track the pin positions (Fig. 5.2). The pin data is then sent to a control PC for input into a classifier or control system. The ability to perform onboard processing reduces the computational load on the control PC which would allow the T-MO to be used on a less powerful setup. This also opens up the possibility of using the T-MO on a fully autonomous mobile system where computational power is at a premium.

The hand contains three under-actuated fingers which each contain two joints but a single actuatable degree of freedom. This allows the fingers to conform to the shape of any object without needing a complex control framework to individually actuate each joint. Two of the fingers can also rotate through 90° about their base to allow for different grasping modes. This rotation is mechanically coupled so constitutes only a single degree of freedom. Overall, the T-MO retains much of the grasping capabilities of the original Model O whilst gaining a tactile sense.

5.3.2 Experimental Platform

The T-MO is attached to a Universal Robots UR5 six degree-of-freedom robotic arm. The majority of the experiments are conducted involve the T-MO grasping objects from the YCB Object Set [176] to test how the hand copes with slip detection experiments on natural objects.

Prior to this it is useful to compare the slip detection capabilities of the newly developed small tactile sensor compared to the 'traditional' larger TacTip. To test this we reused the slip detection rig used in James et al. (2018) [243] (and Chapter 3) which consists of a 3D printed flat shape which can move vertically in a low friction rail system (Fig. 5.3).

The purpose of the low friction rail system is two-fold. Firstly, it provides a very controlled environment in which to test how well a tactile sensor can perform slip detection. Secondly, it allows for direct comparison between different sensors using the same platform. The two rails are Igus Drylin N linear guides which prevent the object from rotating and falling out of the rails whilst minimising the effects of friction.

5.4 Software Methods

5.4.1 Tactile Data

One goal of this work is to develop and test a classifier that can accurately distinguish between when an object is slipping over the surface of a sensor and when it is static - i.e. is held securely. The first step towards doing this is to process the raw tactile data. As mentioned in the hardware section 5.3.1, the output from the sensor is a 2D list of the pin positions. Our use of pin positions, as opposed to using raw images [228], is because it gives a direct measure of slip from the movement of fixed points on the sensor surface. In previous work, these have been demonstrated to be an effective feature set for slip detection [243].

Before being passed to a classifier we prepare the data by converting the pin positions into velocities. This is done by subtracting the previous pin positions from the current positions; as the data is received at 60 Hz this gives the rate of change of pin positions per frame which is analogous to velocity. The vector of pin velocities is collected in Cartesian coordinates $(\Delta x_i, \Delta y_i)$ for $1 \leq i \leq 30$, and transformed by: $\Delta r_i = \sqrt{\Delta x_i^2 + \Delta y_i^2}$ and $\Delta\theta_i = \arctan(\Delta y_i / \Delta x_i)$. The angular component $(\Delta\theta_i)$ of the pin velocities is shifted to have a mean of zero with respect to the x-axis of the camera, which means that the data is independent of slipping angle and should thus allow the classifier to detect slip in any direction. This yields a 60-dimensional time-series input $(\Delta r_i, \Delta\theta_i)$ to the classification method.

5.4.2 Classifier Description

As described in the introduction, our approach here is to use a simple, interpretable slip-detection method that extends naturally from one tactile fingertip to a many-fingered hand. In prior work (James et al. 2018), we showed that a support vector machine is an effective detector of slip on tactile data preprocessed into pin positions for a single sensor [243]. However, that demonstration left unanswered questions such as why the SVM is an appropriate method or whether other classification methods would be better suited.

Here we justify the appropriate method by comparing three distinct binary classifiers that can detect slip: first, a threshold on the magnitude of mean pin velocity; second, a support vector machine applied to either linear or nonlinear combinations of pin velocities; and third a logistic regression (LogReg) method applied to individual pin velocities. These classifiers were chosen to progressively increase in their sophistication while maintaining an interpretation in terms of the pin velocities being a direct measure of slip occurrence.

5.4.2.1 Threshold Classifier

This first decision method simply takes the magnitude of the average pin velocities for each time sample and uses a threshold to decide whether slip is occurring or not. Since the pin speeds are expected to be higher and the velocities co-linear when slip occurs, data falling above the

threshold T is considered to be slipping. The vector of thirty pin velocities is reduced to a single dimension and determined to be slip if it exceeds a threshold T:

$$v = \sqrt{\left(\frac{1}{30}\sum_{n=1}^{30}\Delta x_i\right)^2 + \left(\frac{1}{30}\sum_{n=1}^{30}\Delta y_i\right)^2} \geq T. \tag{5.1}$$

This metric means that frames where the pin velocities have a wide angular distribution will give a smaller value than when they are co-linear. Intuitively, one might expect that this method would be effective at slip detection with the TacTip tactile sensor using the pin velocities, because these directly indicate slip. However, as we will see in the results, the classifier suffers from not rejecting false positives - i.e. detecting slip from changes of pin position not related to slip.

5.4.2.2 Support Vector Machine

SVMs work by separating multi-dimensional data into two classes, using a hyperplane that best separates the training data of the two classes. In practise, this decision boundary is constructed from finding two parallel hyperplanes that maximally separate the classes, then taking choosing the hyperplane midway between. If data cannot be linearly separated it can be transformed using a nonlinear kernel before constructing the hyperplanes. Here we test both a linear and a Gaussian-kernel SVM to find the best classifier. For the pin velocity data considered here, the SVM classifiers can be interpreted as detecting slip by where the vector of pin velocities falls relative to the hyperplane.

For the case of a Gaussian kernel, two additional hyperparameters must be optimised. The first is a regularization parameter C that gives the trade off between correctly classifying data and maximally separating the two classes: a small C results in a narrow boundary (distance between separating hyperplanes) but many misclassifications, and vice versa for large C. The second hyperparameter, γ, is the kernel scale, which can be seen as setting the complexity of the class boundary. For small values, γ, will have little effect on the data and the decision boundary will be drawn as for a linear SVM; for large values the, decision boundary can be very complex by fluctuating greatly to put individual data points on one side of the boundary, and therefore has the tendency to overfit. For a more detailed description on SVMs see [225].

5.4.2.3 Logistic Regression

LogRegs are an effective machine learning technique that are simple to implement and commonly used to provide a baseline when comparing to other methods [247]. They are binary classifiers which assign an observation to a class given a set of input variables, in this case pin velocities, by using the logistic function to give a hypothesis based on a decision boundary

$$h_\theta(\boldsymbol{x}) = \frac{1}{1+e^{-\boldsymbol{\theta}\cdot\boldsymbol{x}}} \tag{5.2}$$

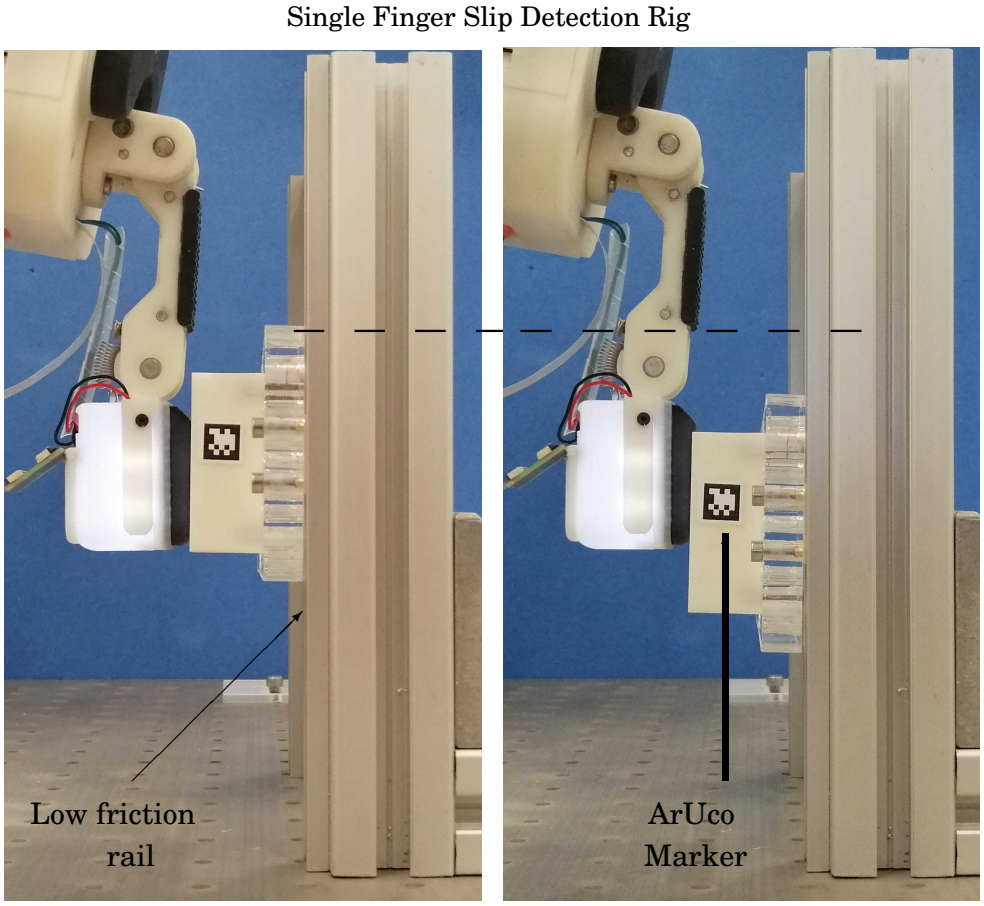

Figure 5.3: Low friction rail system for testing slip detection capabilities of a single sensor. (a) Flat object being held prior to slip occurring. (b) Object being caught after slip has been detected; a clear drop in height is present which is detectable by the ArUco optical marker.

where $\boldsymbol{x} = (1, x_1, x_2, ..., x_m)$ is a vector of observations and $\boldsymbol{\theta} = (\theta_0, \theta_1, \theta_2, ..., \theta_m)$ are the model parameters to be determined from optimizing the fit of h_θ to the class labels. Then the prediction will be class 1 (slip) if

$$\theta_0 + \theta_1 x_1 + ... + \theta_m x_m \geq 0 \tag{5.3}$$

As here these m observables are the pin velocities, the LogReg method may be considered as analogous to the threshold classifier above but using individual pin velocities.

To avoid overfitting we introduce a regularization parameter C that penalises large fluctuations in the model parameters. All the SVMs and LogRegs in this work are trained using Python's scikit-learn package with functions **SVC** and **LogisticRegression** respectively. Hyperparameters are determined using Bayesian optimization with the scikit-optimize function **BayesSearchCV**.

5.4.3 Classifier Evaluation

A subtlety in applying the above classifiers to slip/non-slip data is that there are usually more examples of non-slip than slip, but we do not want to discard data that could give a better classifier. Then the normal method of using accuracy to evaluate the classifier ceases to be a good method. A more reliable metric in such cases is the F1 score, which takes into account the Precision and Recall defined as:

$$P = \frac{TP}{TP + FP} \tag{5.4a}$$

$$R = \frac{TP}{TP + FN} \tag{5.4b}$$

where TP is the true positive rate, FP is the false positive rate and FN is the false negative rate. The F1-score is then:

$$F1 = 2\frac{P \times R}{P + R}. \tag{5.5}$$

As this does not take into account true negatives we calculate the F1 score for each class and average the result.

5.5 Single Finger

5.5.1 Experiment Description

The first task uses the slip detection rig (Fig. 5.3) to test the slip detection capabilities of a single sensor in the T-MO. The rotationally-fixed finger (bottom finger of left hand side of Fig. 5.2) held the 3D printed object at the top of the rail system by pressing against it and then retracting at a random speed between 0.1 and 5 mm s^{-1} to induce a slip. The tactile fingertip stopped recording when the UR5 robot arm had finished retracting and therefore, due to the variation in speed, each test has a different number of frames. For this test we collected data using only a single finger.

To label the data we placed an ArUco optical marker on the slipping object and recorded its height with another JeVois camera. Any frames from the TacTip that arrive after the ArUco begins to fall are labelled as belonging to the **slip** class and any that arrive prior to this are labelled as **static**. This makes the labelling process autonomous and contains no labelling bias that could have occurred if performed manually.

As the amount of time spent not slipping vastly outweighs the time spent slipping there is a large class imbalance between the **static** and **slip** classes. To have enough data in the **slip** class we ran the data collection procedure 100 times which will be evenly divided between training and test sets. However, there is another issue here. Whilst finding the boundary between **static** and **slip** is simple, finding the point at which the slip ends is somewhat arbitrary in this dataset. What we are interested in is confidently finding the boundary between non-slip and slip and

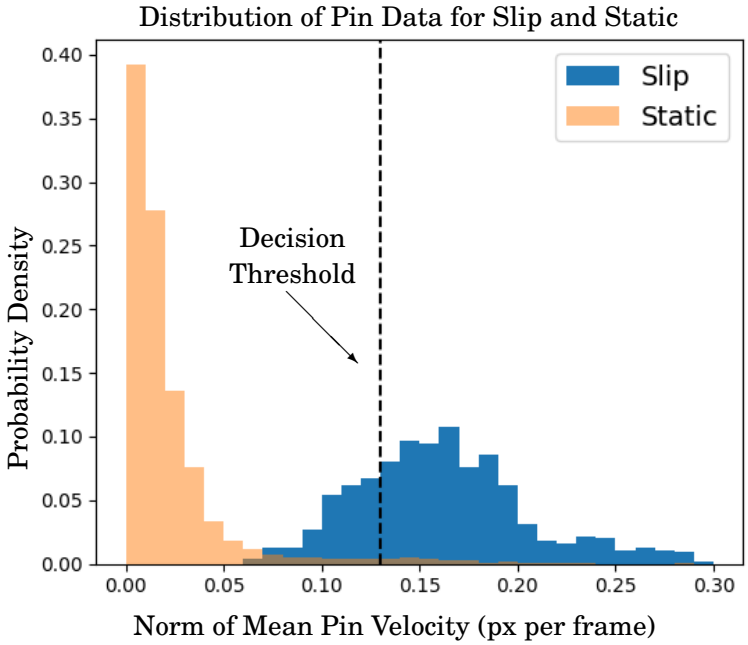

Figure 5.4: Probability density of magnitude of mean pin velocity for all slip and static samples in the training set with optimal decision threshold (T) marked. The static distribution has a long tail which is what causes the threshold to be unreliable. The long tail is barely visible due to the large imbalance in sample numbers therefore if the threshold were moved into the valley between distributions there would be an unacceptable number of false positives.

then reliably detecting the continuation of slip for as long as possible such that when detected an action can be taken to minimise slippage. Therefore, we varied the number of frames n_{slip} in the **slip** class from 1 to 15 to obtain the classifier which is most reliable at detecting slip for a given number of frames after slip commences.

We tested three methods to find the best offline classifier: a threshold on magnitude of average pin velocity, a logistic regression and a support vector machine (SVM). The threshold is attempting to identify whether the spike in all pins speeds when slip occurs can be accurately identified whereas the SVM and LogReg can be seen as looking at what happens to each pin individually and drawing a complex decision boundary to best distinguish slip from static.

As is common in many machine learning methods, large datasets can be difficult to handle (e.g. the time taken to optimize an SVM scales as the number of samples squared [248]). Therefore for efficiency, we tested the effect of downsampling this data. To find the best classifier offline, we vary the number of frames in the 'slip' class and randomly downsample the data before optimising each classifier. Downsampling by a proportion d leaves a dataset of size $N' = dN_0 + N_1$ for a dataset with N_0 samples in the static class and N_1 samples in the slip class. Note, we do not downsample the slip class as the effect of varying the slip samples is already being considered. The optimised classifiers are then tested on the entire test set.

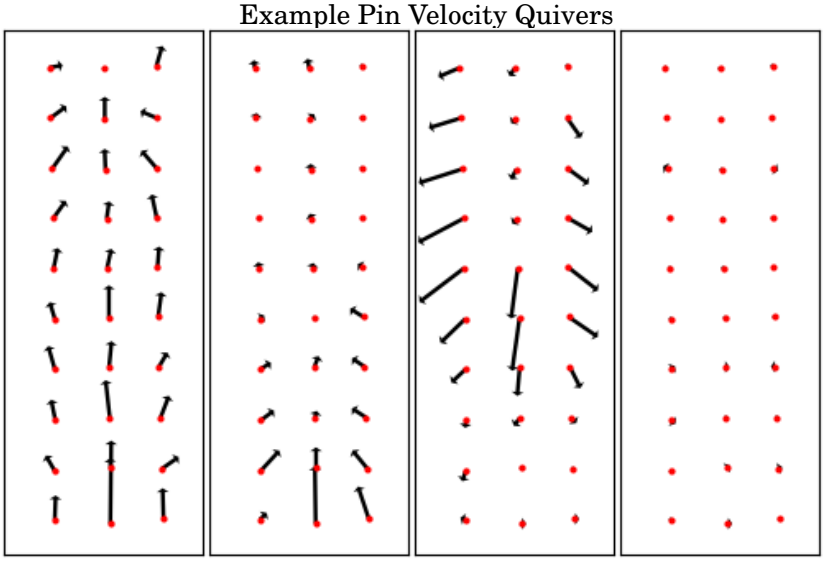

Figure 5.5: Example pin velocities: (i) slip - right of T; (ii) slip - left of T; (iii) static - right of T; (iv) static - left of T. (iii) has large arrows with a sufficiently large mean vertical velocity component to place it on the wrong side of the boundary leading to an incorrect classification. (ii) is a sample from several frames after slip onset where the velocities have shrunk resulting in a value $< T$ and incorrect classification.

5.5.2 Results

5.5.2.1 Offline performance

The first test was the offline performance of the slip detection using pre-collected data with the single finger.

Threshold method: The threshold was chosen by testing ten values between the magnitude of mean pin velocity across all static samples and all slipping samples. The best performing threshold was an average of 0.13 pixels per second which had an $F1$-score of 0.753 on the complete dataset with eleven frames in the 'slip' class. As we will see, this is significantly worse than the SVM and LogReg classifiers (typically above 0.9), and so demonstrates that a more sophisticated classifier is necessary to capture the complexities of the boundary between slipping and static.

The threshold was selected by optimising F1-score which is useful when evaluating classifiers trained on imbalanced data [249], as is the case here. The poor performance of the threshold method seems to be due to the optimal threshold significantly overlapping with the slip class (Fig. 5.4). This can be seen in pin velocity quiver plots (Fig. 5.5), where Fig. 5.5(iii) is from the static class but would be misclassified as slip with the threshold classifier.

This signal may be caused by initial contact with an object which is not slip and results in large pin velocities but the distribution remains significantly different from slipping. Similarly, Fig. 5.5(ii) is slip but would be misclassified as static as it occurs around eight frames after slip onset where fewer pins are still moving leading to a weaker slip signal. We want the classifier to

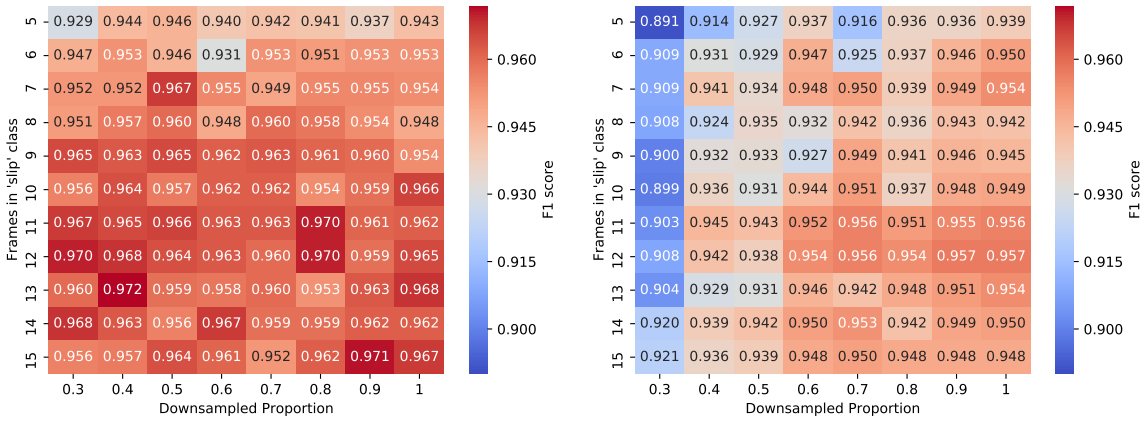

(a) SVM F1 Scores

(b) Logistic Regression F1 scores

Figure 5.6: Heatmaps of F1 scores of (a) Logistic regression and (b) SVM when altering the amount of data in the 'static' class by randomly downsampling and altering the number of frames used in the 'slip' class. The SVM is not significantly affected by downsampling and consistently outscores the logistic regression. Both methods trail off significantly when downsampling below 30% and with fewer than 5 frames in the 'slip' class; these results are omitted for clarity.

be robust to such effects and thus the basic threshold method is not appropriate.

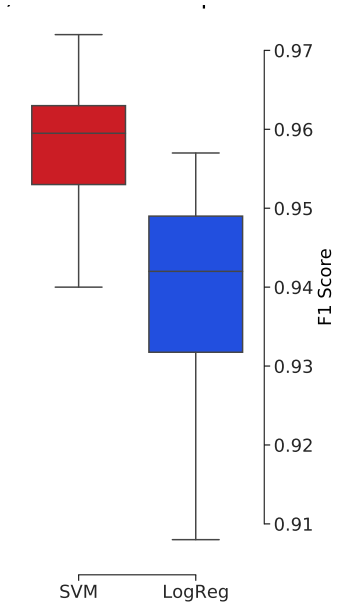

Figure 5.7: Boxplot showing comparison of SVM and Logistic Regression.

It seems as though the threshold should be placed in the gap between classes (Fig. 5.4) but due the imbalance in the number of samples in each class this would lead to an unacceptable number of false positives. The distribution of the 'static' data has a long tail which is scarcely visible in Figure 5.4 due to the class imbalance.

SVM and LogReg methods: We tested these two classifiers under the effects of downsampling the training data and varying the number of frames in the 'slip class. We retained 10% to 100% of the data in 10% increments and varied the number of frames in the 'slip' class from one to fifteen.

The SVM outperformed the logistic regression across all tests (Fig. 5.6) giving peak $F1$ scores of 0.972 (SVM) and 0.957 (LogReg). The logistic regression showed a noticeable drop in performance when downsampling the data below 60% whereas the SVM performed well until just 30% of the data was kept; even scoring best when downsampled to 40%. The mean $F1$-score from all SVM classifiers in Fig. 5.6 (a) is 0.960 which outscores the best score for the LogReg (0.957) which demonstrates the SVM is the superior method for detecting slip using

Classifier	**Kernel**	γ	C	DS	n_{slip}
SVM	Gaussian	1.104	3.989	0.4	13

Table 5.1: Parameters of the Support Vector Machine (SVM) which scored best in offline testing using a single finger. γ is the kernel scale, C is the box constraint, DS is the downsampling rate and n_{slip} is the number of frames used in the 'slip' class per test.

the TacTip (Fig. 5.7).

However, classification performance is not the only important factor: a fast reaction time is also critical for catching a slipping object quickly. Therefore it was also important to ensure both the SVM and LogReg classification methods can classify new data quickly. We verified that both are able to classify in sub-millisecond time, which is much smaller than the response time of the hand (>5ms). This allows us to select the method going forward based purely on score.

Classifiers using n_{slip} from 11-15 frames performed best for both methods, so it was hard to select with confidence the ideal number of frames to choose for future tests. That said, the best scoring classifier's parameters can be found in Table 5.1. These parameters will be used for online testing and to train any future classifiers.

5.5.2.2 Online performance

Having trained the best classifier offline we test the ability of the platform to detect slip in real time. We used the same rig and experiment setup as for collecting data except this time we want the finger and UR5 to perform an action to minimise slippage when it is detected.

Again, the object is held in the low friction rail and the UR5 is retracted. When slip is detected the UR5 moves 1.5mm further forward and the torque on the finger is increased slightly. These were justified as once the object starts moving more force is required to stop it than to hold it without slipping, but moving too far forward risks damaging the sensors by over compressing them. 1.5mm was therefore chosen as it gives sufficient additional force without damaging the sensors.

Two reaction strategies were used: first, if any frame was classified as slip we performed the predefined action to catch the object; second, we required two consecutive frames to be classified as slip before the action was taken. The latter reduces the likelihood of false positives triggering an action too early at the cost of slower response times. We tested each scenario 50 times. The ArUco marker was again attached to the object to track how far the object slipped before being caught and to independently verify whether a test failed or an action was taken before slip occurred.

Table 5.2 shows similar catch success between the two scenarios. The major difference is in false positive rate which drops from 20% to 0% when using two consecutive frames to trigger an action rather than a single frame.

N Frames	Caught (%)	FP (%)	Dropped (%)	d (mm)
1	74	20	6	21
2	72	0	28	29

Table 5.2: Online slip detection and catch success. High success at catching the object was achieved in both tests but waiting for two consecutive frames to be classified as 'slip' greatly reduces the false positive responses. In the second scenario slip was correctly detected in each test but the single finger was unable to provide enough force to stop the object in time. **N Frames** refers to the number of consecutive frames classified as slip before an action is taken. **FP** is false positive (action triggered before slip) and **d** is the average distance slipped before being successfully caught.

It should be noted that in the second scenario it never failed to detect the slip and the lower catch rate was due to it being unable to stop it in time. This is probably due to needing a large amount of force to stop the object slipping once it builds up some downwards momentum and the object being quite small. The finger also has a some flexibility that gives a small latency between moving the motors and a force being applied. We anticipate that there will be additional subtleties when using all three fingers to grasp an object rather than using a single finger and a low friction rail system, which examine next.

A related prior study by James et al. (2018) [243] demonstrated that a larger TacTip could perform slip detection and react to catch an object sliding in a rail (same setup as Fig. 5.3) after only 16mm of falling. Under the same conditions we obtained distances of 21mm and 29mm depending on the strategy used to respond to slip. These reduced scores are most likely explained by the cameras here running at 60FPS compared to 100FPS in the TacTip and the flexibility of the T-MO's fingers leading to a reduced force being applied to stop a falling object. Nevertheless, the T-MO's demonstrated ability to successfully stop slipping objects within a short distance and the ability to deploy slip detection in realistic scenarios represents a significant advance.

5.6 Whole Hand Testing

5.6.1 Experiment Description

Having determined the single finger performance we then need to test how effective the T-MO hand is at performing slip detection and re-grasping natural objects with all three fingers. This gives a good indicator of how well the T-MO will perform when slip detection is deployed in realistic scenarios.

For consistency, we follow a similar approach to the previous section in regards to training data collection and testing. We therefore select objects that can be easily grasped and tracked by an ArUco marker: five objects from the YCB Object Set [176] which vary in shape, weight and surface smoothness and yet could be reliably tracked to detect the onset of slip for training data labelling (Fig. 5.8).

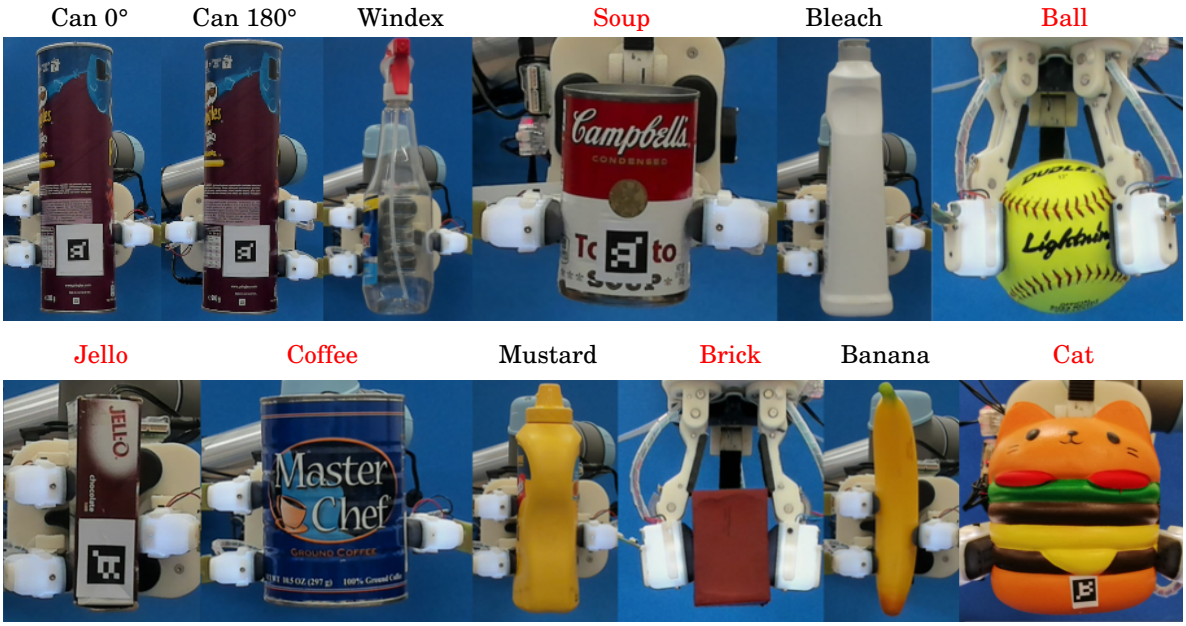

Figure 5.8: Grasps used for online testing with eleven different natural objects. We tested with the hand in various orientations and used different number of fingers in contact with the object to demonstrate robustness. The left two images show the crisps can held at 0°and 180°for testing in Section 5.6.2.2. Objects in black were used for collecting training data. All objects (including the remaining six novel objects, in red) were used for testing.

The primary added difficulty when scaling up from one finger to three is that the dynamics of the onset of slip become more complex. For example, when a grasp is relaxed one finger may begin to slip before another and, crucially, before the object starts to drop and is registered by the ArUco marker. To combat this we used a constant finger movement speed when deliberately dropping the object ($\approx 0.5\%$ of the maximum finger movement speed which is approximately 0.07 rad s^{-1}) which we found to be a good compromise between moving too slow (which contaminates the dataset labels when some sensors slip before others) and too fast (resulting in slip onset occurring before sufficient tactile data is collected). To find the best classifier for use in real-time scenarios we trained classifiers under two conditions.

Firstly, we trained a distinct classifier for each finger, each using training data from that single sensor alone. Each of these three classifiers would then be used to classify new data from the sensor from on which it was trained. The justification for this is that, although extremely similar, each manufactured TacTip will have slightly different properties that may lead to a one-size-fits-all classifier being inappropriate. We will refer to these three classifiers collectively as the **local** classifier from here on. The drawback of training classifiers on a per-sensor basis is that in different grasps the load will be distributed differently among the three sensors.

The second approach we tested, therefore, was to train a single classifier on all the data from all sensors to encapsulate a more general picture of what constitutes slip and ultimately be more

versatile. We will refer to this classifier as the **global** classifier from here on. This global classifier has the advantage of having knowledge from multiple grasp loads without the disadvantage of needing collect data in many different orientations. In each case we deploy a classifier on data from each sensor individually so that each can independently determine if it is slipping. For the **local** it is a different classifier for each sensor and for the **global** it is the same. This is necessary as, at any time, some sensors can be slipping whilst the others are not. Additionally each sensor's frame rate can vary slightly which so classifying on each sensor separately reduces classification latency.

In total we have four classifiers, three for the local case and one for global. The best classifiers, trained offline, in both of the above cases can then be tested online using the five objects used for data collection and with another five novel objects from the YCB dataset to determine the success of the T-MO at real-time slip detection and grasp recovery. A sixth novel object is also used; a highly deformable cat which we test both on its own and with a 100g mass adhered to the underside.

As demonstrated in the single finger case we can change how we react to slip to combat limitations in the classifier such as false positives. With three sensors we increase the parameters at our disposal for developing a strategy to respond to slip and this should be sufficient to balance any drop in classifier performance that may occur when scaling up from a single sensor to three.

The parameters we can vary are

1. Number of consecutive frames detecting slips: N_{Fr}
2. Number of sensors detecting slip: N_{Sen}

The first variable allows each sensor to gain more information before deciding that slip is occurring in the hope of reducing false positives. The second variable allows us to wait until more sensors are slipping before the hand responds. Both variables determine how cautious we should be with the first setting the cautiousness on the single sensor scale and the second on a global scale.

5.6.2 Results

5.6.2.1 Offline Performance

The training data for this section was collected from five different objects selected from the YCB object set (Fig. 5.8). We held each object in a cylindrical pinch grasp - thumb opposed to other two fingers - by closing the fingers until the object was stable and then released the grasp until the object slipped. We performed this twenty times per object split equally between training and testing sets.

As for the single finger case we have a total of 50 training runs (10 per object) and 50 test runs. The ArUco marker on each object allows us to label each frame as either slipping or static.

We, again, downsample the number of frames in the **static** class to 40% of its original size to bring the balance of frames in each class closer together and also reduce training times. We again use thirteen frames in the **slip** class which was previously shown to perform best.

In total four classifiers were trained; one for the global classifier and three for the local. The first was trained on the data from all three sensors to provide a one-size-fits-all classifier (global classifier) and the remaining three were trained on the data from a single sensor to account for any small differences between sensors (local classifier). As expected, the local classifier performs better with an average F1-score of 0.833 as against 0.822 for the global classifier. Note that for comparison we also tested the classifier trained previously on just a single finger using the slip rig (Sec. 5.5): this scored 0.627, which demonstrates that the data is different when grasping an object with the entire hand.

Looking at the three classifiers in the local case individually gives $F1$-scores for the three sensors of 0.869, 0.824, 0.805 respectively. The finger of the first sensor is opposed to the remaining two in these tests so has to provide enough force to balance the force from the other two. This means that the sensor will be more compressed, causing the pins to move more and therefore providing more tactile information which may explain the higher score.

Another notable issue here is the large drop in $F1$ scores when going from the single finger to the whole hand. This is most likely due to the increased complexity of the dynamics when slip occurs in the whole hand and demonstrates the difficulty in scaling up from one sensor to three. With the single finger the object is either slipping or it is static so labelling the data is easy. Once the ArUco marker registers a drop in height we can be certain that slip is occurring. With three fingers the object could slip on one or two fingers before the ArUco registers that the object is falling. This can confuse the stick-slip boundary and therefore reduce the success of the classifier. However, the real test of the hand's ability to detect slip will be when performing slip detection online.

5.6.2.2 Online Performance

The first online test was performed on a single object, the crisps can, to determine how well the offline results work in real time and to develop a strategy to respond to the onset of slip. The test conditions are the same as for the single finger case. We grasp the object and slowly release until slip occurs. When detected we close the fingers to a tighter position than the start to counteract the momentum of the falling object. This position is 2% of the finger motion range and was chosen to add more force but not grasp the object too tight. We, again, record the height of the object with an ArUco marker to calculate falling distance and identify any false positives.

Primarily, we want to determine which of the two classifiers developed in the previous section performs best online: the **global** (trained on data from all sensors) or the **local** (three classifiers each trained on a separate sensor). To do this we tested two different grasps: the first is the same as the training data and for the second we rotated the hand through 180° (Fig. 5.8). Grasps

SVM	Strategy	Grasp	TP	FP	FN	D (mm)
Local	$2_{Fr}3_{Sen}$	0°	100	0	0	39
Global		0°	100	0	0	40
Local	$2_{Fr}2_{Sen}$	0°	100	0	0	25
Global		0°	100	0	0	28
Local	$1_{Fr}3_{Sen}$	0°	100	0	0	35
Global		0°	100	0	0	35
Local	$1_{Fr}2_{Sen}$	0°	60	40	0	17
Global		0°	80	20	0	16
Local	$2_{Fr}3_{Sen}$	180°	70	0	30	63
Global		180°	100	0	0	38
Local	$2_{Fr}2_{Sen}$	180°	90	0	10	45
Global		180°	100	0	0	27
Local	$1_{Fr}3_{Sen}$	180°	100	0	0	34
Global		180°	100	0	0	24
Local	$1_{Fr}2_{Sen}$	180°	50	50	0	21
Global		180°	70	30	0	12
Local Average			83.75	11.25	5	35
Global Average			93.75	6.25	0	28
All Average			88.75	8.75	2.5	31

Table 5.3: Results from all classifiers (SVM), grasps and strategies when testing in real time the slip detection capabilities of the T-MO hand. TP: True positive, FP: False positive (reacted before slip), FN: False negative (item dropped) all (%). D is average slipping distance in mm.

hereafter referred to as **0°** and **180°**. Both are three fingered cylindrical pinches but by rotating the hand the force distribution on the second and third fingers will be distinct which should inform us which classifier copes better with variation.

Additionally, we want to discover how changing the slip response strategy affects performance. As mentioned in Section 5.6.1 we can vary the number of consecutive frames classified as slip before a sensor will be confident that slip is occurring and we can vary the number of sensors simultaneously detecting slip before a response is taken. It was quickly determined that using just a single sensor to trigger slip was going to lead to greatly reduced performance compared with waiting for 2 or 3 to slip therefore this was omitted from further testing. The remaining four strategies used are:

1. Two consecutive frames, three sensors, $2_{Fr}3_{Sen}$.

2. Two consecutive frames, two sensors, $2_{Fr}2_{Sen}$.

3. One frame, three sensors, $1_{Fr}3_{Sen}$.

4. One frame, two sensors, $1_{Fr}2_{Sen}$.

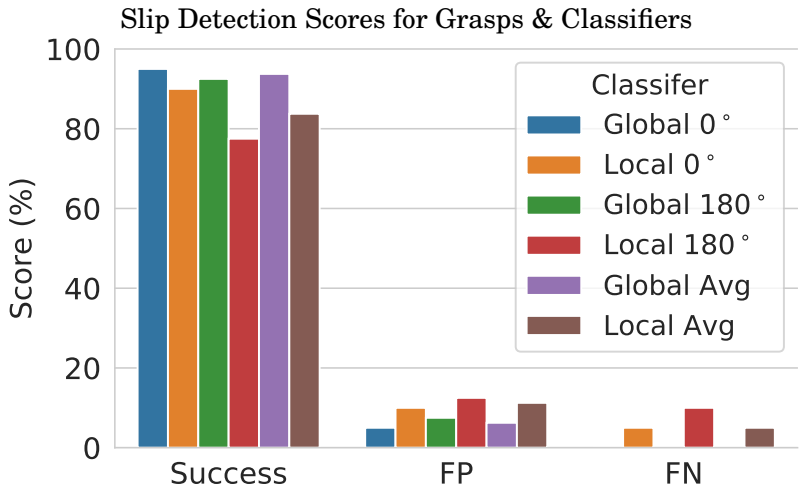

Figure 5.9: Comparison of successes, false positives (FP) and false negatives (FN) when reacting to the onset of slip with two classifiers in two orientations. Both classifiers score highly but the local classifier's inability to generalise to the rotated orientation makes the global classifier the better choice going forward.

The strategies will henceforth be referred to by the code in the final column of this list. We did this for both grasps giving a total of 8 different scenarios per classifier.

For each scenario we performed ten trials and the results are summarised in Figs. 5.9 & 5.10 and Table. 5.3. Most of the scenarios scored highly with many scoring 100% and three quarters scoring 80% and above. A trial is considered a success if the object is seen to fall briefly before the hand responds and successfully reestablishes a stable grasp.

In general, false positives (reacting before slip visibly occurs) are low across the board (8.75% across all trials, Fig. 5.9) with all of them coming in the trials where only one frame was required to be considered a reliable slip signal and only two sensors simultaneously detected slip to trigger a response (strategy $1_{\text{Fr}}2_{\text{Sen}}$). This is the most sensitive strategy so it is unsurprising that this leads to the occasional false positive. All the false negatives (object dropped) occurred with the local classifier when the hand is rotated. This is a different grasp to the training data collection and the local classifier struggles to generalise but, again, the false positive rate is low (2.5% across all trials).

When testing in the same grasp configuration as for training data collection (hand 0°) the classifiers score very similarly with scores of 95% and 90% for the global and local classifier respectively (Fig. 5.9). When the hand is rotated (180°) the global classifier, again, scores well with 92.5% which is only a 2.5% drop. The local classifier suffers more here scoring 77.5%. This explains much of the difference in classifier score when averaged across the 8 trials where the global classifier - 93.75% - outscores the local - 83.75% (Table 5.3).

The slipping distances (Fig. 5.10) show that the the global classifier performs well in both

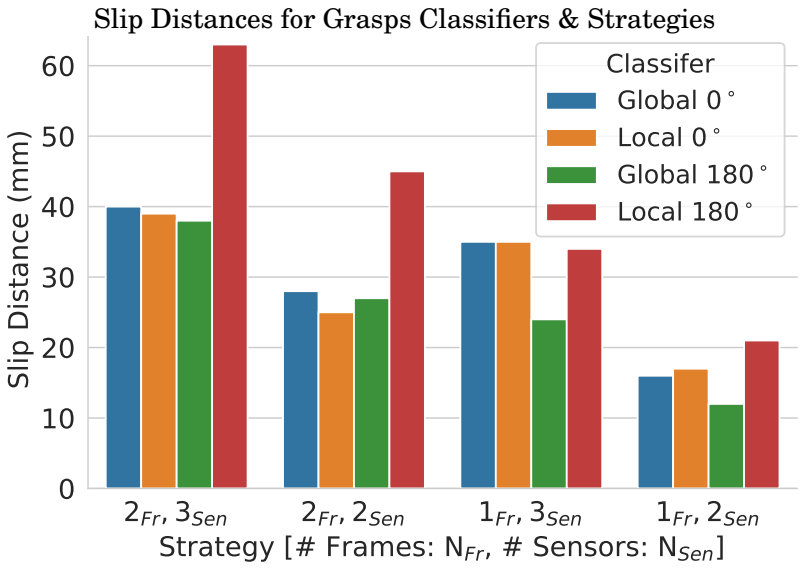

Figure 5.10: Slipping distance of the can for each strategy when regrasped after slip detected. The local classifier struggles in the rotated orientation as it fails to generalise to different grasps. The most sensitive strategy ($1_{\text{Fr}}2_{\text{Sen}}$) has the smallest slipping distance as it requires the least evidence before it acts to minimise slip.

grasp orientations and all strategies with similar slipping distances for both (30 mm normal, 25 mm rotated). The local classifier in the normal orientation performs similarly however the performance drops significantly - using all but one of the strategies - when the hand is rotated 180° (29mm 0°, 41mm 180°).

When each sensor only requires one frame classified as slip to give a signal and only two sensors are required to trigger a response (strategy $1_{\text{Fr}}2_{\text{Sen}}$) the slipping distance is greatly reduced as against the other strategies - 17 mm across all trials for $1_{\text{Fr}}2_{\text{Sen}}$ compared to 31 mm for $2_{\text{Fr}}2_{\text{Sen}}$ which is the next best (Fig. 5.10). This is, again, unsurprising as this strategy is the most sensitive and therefore reacts fastest to the onset of slip.

What these results show is that the global classifier outperforms the local classifier as it is able to generalise better to a different grasp and that the more sensitive response strategies are more likely to result in false positives but will stop a slipping object quicker. For the remaining tests with the other four objects from the training dataset and the five novel objects we will use the global classifier - a single SVM trained on data from all three sensors. We also have four different strategies that can be deployed depending on how sensitive we want the hand to be when detecting slip and initiating a response.

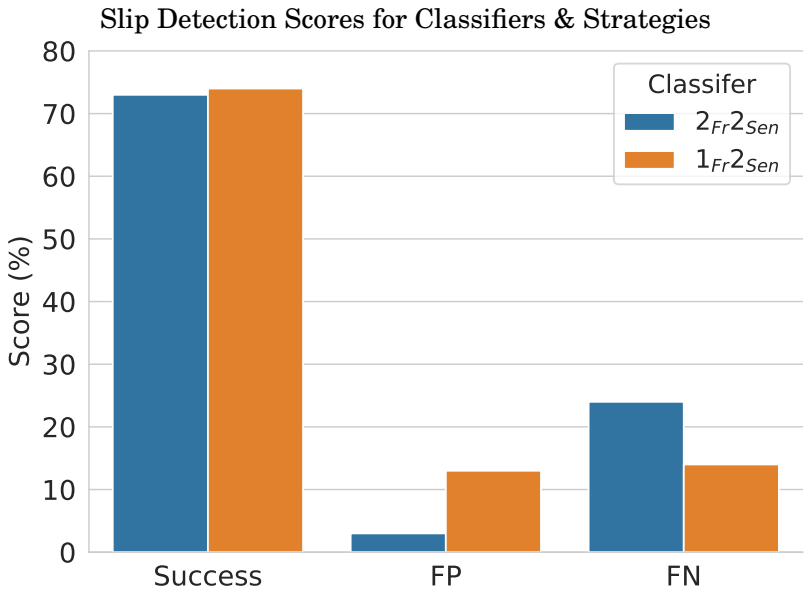

Figure 5.11: Average results for each strategy across all eleven objects (six of which were novel) when doing slip detection and grasp recovery.

5.6.2.3 Other and Novel Objects

The final test was using the remaining four objects from the training dataset as well as six novel objects that are completely new to the classifier, two of which are deformable (Fig. 5.8). This tests how well the classifier generalises to new objects. We test strategies $2_{\text{Fr}}2_{\text{Sen}}$ and $1_{\text{Fr}}2_{\text{Sen}}$ from the previous test for each object with ten trials for each strategy. These are chosen as they gave the smallest slipping distance when regrasping an object (Fig. 5.10). Results are presented in Table 5.4 and summarised in Fig. 5.11.

Both strategies score highly with $2_{\text{Fr}}, 2_{\text{Sen}}$ marginally outscoring $1_{\text{Fr}}, 2_{\text{Sen}}$ with successes of 74% and 73% respectively (Fig. 5.11). When $2_{\text{Fr}}, 2_{\text{Sen}}$ fails it is overwhelmingly due to it dropping the object (false negative) rather than reacting before slip occurs (false positive) - 3% FP, 24% FN across all trials. False positive and false negatives are much closer for $1_{\text{Fr}}, 2_{\text{Sen}}$ which has 13% FP, 14% FN across all trials. As $1_{\text{Fr}}, 2_{\text{Sen}}$ is the more sensitive strategy these results are to be expected. $2_{\text{Fr}}, 2_{\text{Sen}}$ is less sensitive so requires more evidence before it will initiate a response therefore more objects being dropped is unsurprising.

Fig. 5.8 shows the variety of grasps used in this experiment. This includes two and three finger pinches and having the hand in different orientations. As the classifier was only trained with the hand in one orientation it shows that the classifier is able to detect slip independent of hand orientation.

Some objects perform worse than others; notably the sponge brick and the cat (Table 5.4). These are both deformable objects which shows that a more complex response strategy may be

needed to deal with such objects. However, when a 100g mass was attached to the cat the score raised from 45% to 70% across all trials. The coffee, windex, bleach and banana score highly with one method ($\geq 80\%$) but struggle with the other. The remaining objects score highly when using both strategies. The objects in the training set score higher (84%) than the novel objects (70%), however this is skewed by the Jello which is thin so contact area is small; and the brick which is light and compliant and therefore caused difficulties.

One final comment that should be made is that there may be a concern that the slip response could damage very fragile object. However using a force meter it was determined that the peak force of the slip response was measured to be ~3N which was less than the approximate forces to crush a cardboard tube (4N), a strawberry (3.5N) or an eggshell (20N) with the sensor - objects chosen for their perceived fragility. This indicates that the slip response is unlikely to damage objects.

5.7 Application Scenarios

5.7.1 Experiment Description

The motivation for developing an effective slip detection method using the Tactile Model O (T-MO) was to use the classifier in real scenarios where slip detection can be used to improve grasping performance or the effectiveness of the hand. To test this for the T-MO we have deployed the slip detection capabilities in two scenarios.

Object	Strategy	TP	FP	FN
Ball	$2_{Fr}2_{Sen}$	100	0	0
	$1_{Fr}2_{Sen}$	90	10	0
Banana	$2_{Fr}2_{Sen}$	90	0	10
	$1_{Fr}2_{Sen}$	60	20	20
Brick	$2_{Fr}2_{Sen}$	30	0	70
	$1_{Fr}2_{Sen}$	50	0	50
Coffee	$2_{Fr}2_{Sen}$	100	0	0
	$1_{Fr}2_{Sen}$	50	50	0
Jello	$2_{Fr}2_{Sen}$	20	0	80
	$1_{Fr}2_{Sen}$	60	10	30
Mustard	$2_{Fr}2_{Sen}$	90	0	10
	$1_{Fr}2_{Sen}$	90	10	0
Bleach	$2_{Fr}2_{Sen}$	100	0	0
	$1_{Fr}2_{Sen}$	70	30	0
Soup	$2_{Fr}2_{Sen}$	100	0	0
	$1_{Fr}2_{Sen}$	100	0	0
Windex	$2_{Fr}2_{Sen}$	60	30	10
	$1_{Fr}2_{Sen}$	100	0	0
Pringles	$2_{Fr}2_{Sen}$	100	0	0
	$1_{Fr}2_{Sen}$	80	20	0
Cat (66g)	$2_{Fr}2_{Sen}$	30	0	70
	$1_{Fr}2_{Sen}$	60	0	40
Cat (166g)	$2_{Fr}2_{Sen}$	60	0	40
	$1_{Fr}2_{Sen}$	80	0	20

Table 5.4: Results from all objects. TP: True positive, FP: False positive (reacted before slip), FN: False negative (item dropped) all (%).

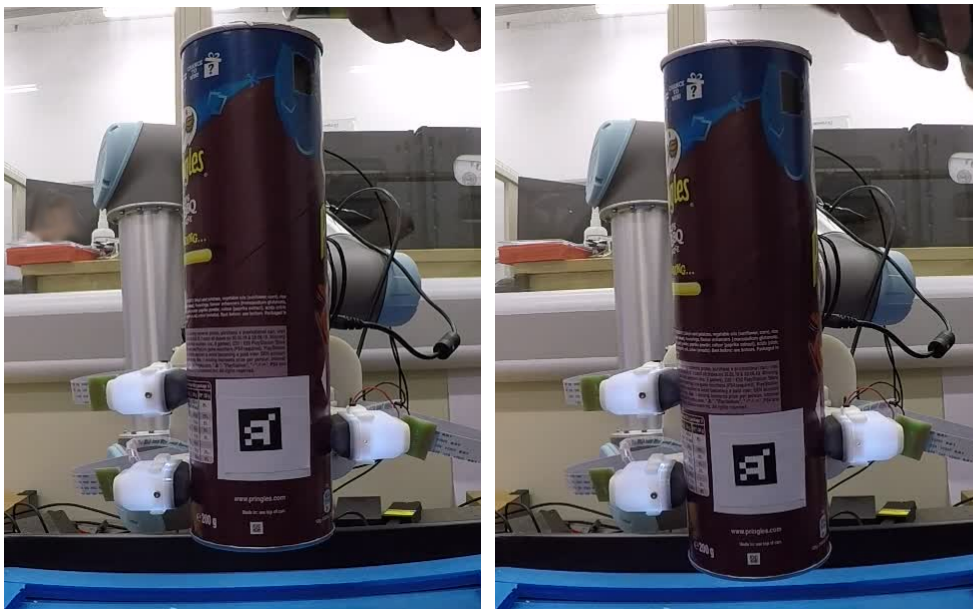

(a) (b)

Figure 5.12: Grasping object before (a) and after (b) adding rice to destabilise. Slip is detected and the object is caught after slipping a short distance.

5.7.1.1 Grasp Destabilisation

Firstly, we use it to adjust the grasp strength when weight is being added to an object which is already being securely held. This is a situation that humans encounter often and handle with ease such as when liquid is being poured into a glass. By detecting when slip is occurring the T-MO can increase the grasp strength to compensate for the added weight (Fig. 5.12).

For obvious reasons we avoided using water to add weight and instead we poured rice into an empty crisps can which has been used in previous tests. This gives a more gradual increase in weight rather than dropping larger masses in one by one which could be enough to cause a slip but may not cause the object to fall. This could, incorrectly, appear as though the slip detection is stopping the fall. A steadier weight increase will eventually cause the object to fall.

5.7.1.2 First Time Grasping

The second scenario is to use slip to find the minimum grasp strength required when lifting an object. In reality, most solid objects are unlikely to be damaged by most robotic hands on full power. The user need only establish a candidate grasp, squeeze as tightly as possible and hope it is stable. This would be disastrous when handling fragile or deformable objects (soft food, thin plastic cups, etc) and therefore finding the sweet spot between securely grasping an object and not damaging it is essential.

We close the hand until it is in contact with the object and then raise the UR5 arm. If slip is

(a) Establish Light Contact (b) Lift Arm; Object Slipping (c) Grasp tightened; Object Grasped

Figure 5.13: The stages of picking an object up first time using solely tactile data. (a) Initial contact is made with the object. (b) Arm is raised, slip is detected and hand is gripped tighter. (c) Sufficient force is applied and the object is securely lifted off the table. The difference in finger position on the can shows that the sensors did slip and the initial grasp was insufficient to lift the object. This verifies that the slip detection is sufficient to determine the minimum required force to lift an object of unknown weight.

detected the hand will increase its grip strength and this is repeated until the object is lifted, first time, without grasping too tight. This allows the T-MO to lift objects of unknown weight first time using only tactile information (Fig. 5.13).

To establish a grasp with no prior knowledge of the object and no vision system requires the hand to know when initial contact occurs. By calculating the mean absolute difference between individual pin positions at time 0 when there is no sensor contact and time t:

$$d(t) = \frac{1}{30} \sum_{p=1}^{30} \sqrt{(x_p(t) - x_p(0))^2 + (y_p(t) - y_p(0))^2} \tag{5.6}$$

where x_p and y_p are the Cartesian pixel coordinates of a pin; we can get a crude measure of sensor deformation.

Using equation 5.6 we can set how firmly to set the initial grasp by slowly closing the hand until the deformation reaches the desired value. We want to choose this value such that the sensors are deformed enough that slip is reliably detectable but not so deformed that the object will be picked up without having to further increase grip strength.

The other variables that we have to consider are the slip detection strategy and the length of pause after triggering a response to slip. As the fingers are initially not in contact with the object we want to use the most sensitive slip detection strategy. This would be only a single frame from a single sensor giving a slip signal to trigger a response $1_{\mathrm{Fr}}1_{\mathrm{Sen}}$. This was not previously used because it resulted in an action being taken before an object could be detected as falling by the ArUco marker. When slip is detected the hand is closed a small amount corresponding to 1% of its entire range. If the movement here is too small then many slips have to be detected before the object is secure; using this value each increment in grasp position is small enough to not damage an object but minimises the number of slips required to lift an object. The time delay

after a response was chosen to be 0.1s which gives enough time for the hand to actually move and therefore the classifiers now operating on data from the new state to determine if further squeezing is required.

Determining the amount of excessive force applied when lifting is important to ensure fragile/deformable objects aren't being crushed. As the T-MO has no force sensing we estimate this by measuring the grasp position at which both objects (at all weights) could be lifted and compared it to the position when using slip detection. We consider the grasp strength as proportional to the increase in finger position between initial contact with the object and the grasp position. We therefore define overgrasp as

$$o = \frac{(g_{\text{slip}} - g_{\text{cont}}) - (g_{\text{min}} - g_{\text{cont}})}{g_{\text{min}} - g_{\text{cont}}} = \frac{g_{\text{slip}} - g_{\text{min}}}{g_{\text{min}} - g_{\text{cont}}} \tag{5.7}$$

where g_{cont}, g_{min} and g_{slip} are the grasp positions for contact with the object, minimum position to lift the object and the position obtained using slip detection to select the grasp. g_{min} was determined for each object mass by systematically increasing the grasping strength until the object could be lifted.

To verify that the object was successfully lifted and that the initial grasp was insufficient to lift the object we attached an ArUco marker to both the object and the T-MO and tracked their heights throughout each experiment.

5.7.2 Results

5.7.2.1 Grasp Destabilisation

The first experiment, where rice was added to an empty can, was repeated five times and was successful in each one. Here we used strategy $2_{\text{Fr}}2_{\text{Sen}}$ which cuts a nice balance between avoiding false positives and having a small slipping distance. A clear slippage was noticed prior to the hand responding and the can was never dropped. The only negative as that in two of the trials a small slippage was visible where no response was triggered and then soon after another, larger slippage did result in the hand gripping tighter. However, as the success criteria is that the object is not dropped this is insignificant.

Figure 5.12 shows a grasped object before and after slip is induced and detected. A graph of the height of the object shows that the object moved slightly downwards as rice is added before a rapid drop in height is notable. This initial small drop is most likely due to the sensors sagging as they cope with the extra weight rather than a false positive when slip is taking place. Heydarabad et al. (2017) performed a similar experiment but added weights in larger increments rather than in small rice grains trying to simulate a fluid as was done here [151]. They successfully detected slip and prevented the object from being dropped however dropping in a mass to induce slip gives a much greater signal than slowly adding weight in the form of rice.

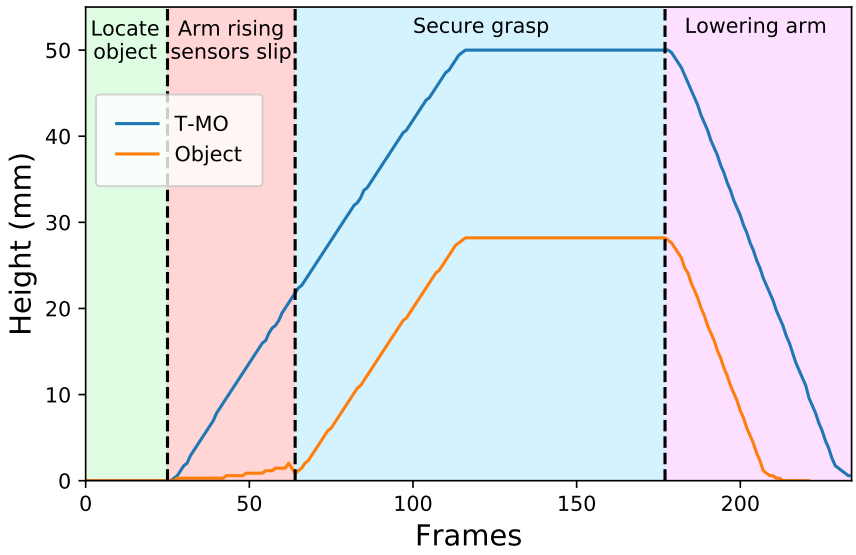

Figure 5.14: Height of the T-MO and the object above the ground when attempting to lift the object first time. The four stages indicated by background colour: (1) Hand makes initial contact (2) Arm lifts with insufficient contact force to lift object, slip is repeatedly detected and hand tightens (3) Object held (4) Object lowered. Heights recorded using ArUco markers (Fig. 5.13).

5.7.2.2 First Time Grasping

In the second scenario we are establishing a stable grasp at the first attempt. We used seven different crisps can masses from 50g (empty) to 500g and performed ten trials per mass. We also tested a deformable object, the cat, both on its own and with a 100g mass attached. We set the deformation coefficient (Eq. 5.6) at 0.5 - this was the minimum sensor deformation which reliably triggered slip - and raised the UR5 at 17mms^{-1}. To be successful the arm must be rising noticeably before the object (Fig. 5.14).

The 50g crisps can was right on the lower mass limit and we could not be certain that the can slipped before being lifted. Each of the remaining weights and the deformable cat (at both weights) were successfully lifted first time in each of the ten trials. Using Eq. 5.7 we determined that at masses between 100-300g the grasping position on the solid object was on average 39% too tight (Fig. 5.15, red line). At larger masses the overgrasp becomes more significant (105%). The deformable cat was overgrasped by 34% and 74% when unweighted (66g) and weighted (166g) respectively.

Intuitively, the heavier the object the more the hand would have to close to pick it up and therefore more slips should be detected. This is reflected in the results (Fig. 5.15, red line) where the number of independent slips detected - i.e. the number of times the hand gripped tighter - directly correlates with the mass of the object; therefore the heavier the object the harder the hand is gripping. These results demonstrate that the T-MO is highly capable at picking up objects

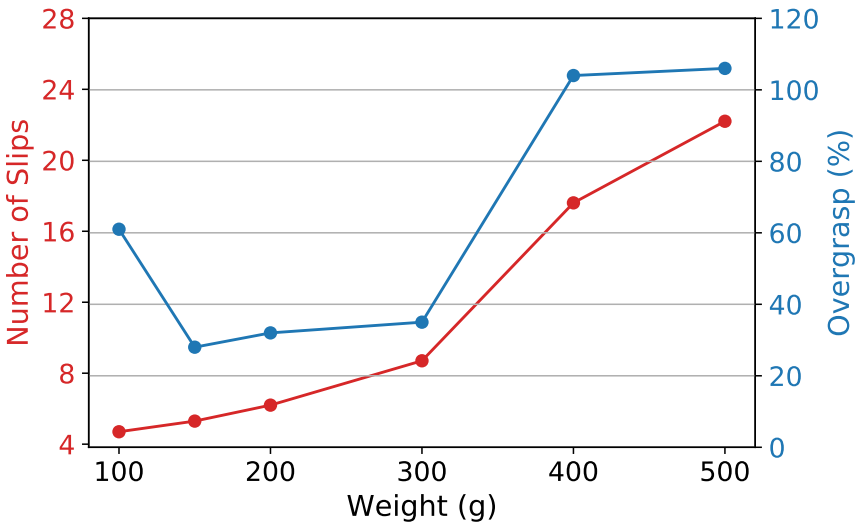

Figure 5.15: Number of slips detected (red) and overgrasp percentage (blue) when lifting an object at different masses. The overgrasp is an approximate measure of how excessively tight the grasp is when lifting. For low mass overgrasp is low showing that the object is picked without grasping too tight.

of unknown mass first time using only tactile data.

Grasping an object first time without excessive force is an important consideration as it minimises energy use, increases longevity and does not damage the object. Humans have been shown to add a safety margin of between 10-40% when preventing objects from slipping [46] and the results here do not greatly exceed this; although we do acknowledge that the overgrasp figure can only be seen as a very basic approximation of excessive force. We anticipate that a bespoke classifier for lifting up objects would perform better but we have demonstrated that objects will likely be undamaged when lifted by the T-MO. A similar experiment was performed by Stachowsky et al. (2015) who successfully lifted a deformable cup ten times without damage [212]. However, they only performed this with a single cup weight. It was also successful when the gripper's surface friction was reduced but this still only constitutes two scenarios. Furthermore, our strategy of repeatedly detecting slip in real-time allows for continuous evaluation of the state of a grasp resulting in first time success rather than a single decision after a candidate grasp has been initiated [239] or attempting grasps multiple times [15].

5.8 Limitations and Future Work

5.8.1 Objects for Testing

As investigated in James et al. (2020) the thickness of the fingers on the Tactile Model O (T-MO) means that the hand struggles to pick up very small and flat object from a surface [239]. This

restricts the number of objects on which we can perform tests. Given that the purpose of this paper is to test the slip detection capabilities of the T-MO we deliberately selected objects that we had previously determined were easily grasped. There would be little point trying to test how well the T-MO could react to slip on an object that it could barely grasp in the first place. However, given the objects chosen the method can only be considered applicable to objects which are graspable with an antipodal pinch.

We have demonstrated that the T-MO is highly capable at slip detection and grasp stabilisation, and have used these skills in tasks involving slip detection that could be encountered in real world scenarios. This, coupled with the T-MO's strengths as a low-cost manipulator, provide a solid motivation to refine the design to improve grasping performance and subsequently widen the range of objects on which slip could be detected.

5.8.2 Classification Method

One of the advantages of the onboard processing units, the JeVois, encased within the T-MO is their ability to reduce computational load on the control PC. By processing their own data into either pin positions the PC does not need to process three high bandwidth video streams and can communicate with the JeVois over low bandwidth serial ports.

Prior work with the T-MO (when using raw images) operated at a low frame rate (20fps) to allow for high resolution images to be captured and had significant latency given the classification time when using a deep convolutional neural network. We do not use those methods here as the high frame rate (60fps) and low latency from using pin positions is beneficial when responding to events which happen on a very short time scale. We have demonstrated that using pin positions provides an effective tactile signal for slip detection and gives the T-MO hand the ability to perform grasping tasks. Further work exploring the use of high frame rate image capture and using the JeVois' onboard processing to run small TensorFlow Lite models on raw images would be interesting however it is beyond the scope of this study.

The dimensionality of the classifer was chosen to match the 60-dimensional output of the JeVois after pin detection. It is possible that the spatio-temporal pattern relating to slip exists in lower dimensional space and the SVM is overfitting. Indeed, it is well known that, after a certain point, the addition of more dimensions to a classifier will start to hamper performance [250]. Therefore, learning a lower dimensional representation of slip *could* result in increased performance and may also provide faster inference times and faster training. However, as the number of dimensions matches the dimensional output from the sensor the choice of SVM dimensionality is justified.

Another possible choice of dimensionality would be to use a sensor which outputs a single dimension as input to a classifier. The primary advantage of this would be the ability to have a higher sampling frequency to provide a faster reaction time. For example, a previous study used the 2.2 kHz pressure sensor within the BioTac sensor for slip detection [198]. However, the

pins provide a fiducial marker for the movement of the sensor surface the movement of which is clearly visible when slip occurs whereas with a single dimensional sensor it may be difficult to physically interpret the slip signal. Even with the lower frequency pin detection the T-MO performs well at real-time slip detection and grasp recovery but nevertheless investigating ways to reduce reaction time is crucial for future performance improvements.

5.8.3 Incipient Slip and Slip Prediction

A significant area of research within tactile sensing is the detection of incipient slip where part of the contact surface is slipping and part is static - as opposed to gross slip where the entire contact surface is slipping which has been investigated here [16]. Incipient slip is a complicated phenomenon which is strongly influenced by the surface properties of the tactile sensor and the object being held including coefficient of friction and surface geometry. Depending on conditions it may only be present on a short timescale. This means the ability to detect incipient slip depends on the frame rate at which tactile sensors operate as well as the properties of the sensor's surface. A preliminary examination of the data did not indicate the presence of incipient slip and reliable detection of incipient slip with the T-MO would likely involve significant modification to the T-MO's hardware and therefore goes beyond the scope of this study.

Here, using gross slip detection, we have demonstrated strong performance at grasping objects, preventing novel object from being dropped and presented several control strategies which can be used depending on the task all without relying on incipient slip. We anticipate that making the necessary changes required to detect incipient slip would enhance performance and we will investigate this in the future.

5.9 Concluding Remarks

We have presented a method of using a three-fingered hand with integrated optical tactile sensors - the T-MO - to perform slip detection with a Support Vector Machine. Using various simple slip response strategies we grasped objects at the first attempt, performed slip detection on novel objects and regrasped slipping objects .

Scaling up from one to three sensors represents a significant challenge as the complexity of the interaction between the object and the sensors increases greatly. This means that there is no guarantee that the features present in the single finger case will be prominent or even present in the three finger case. Additionally, the robot hand platform must be capable of collecting tactile data, classifying it and react quickly. Therefore demonstrating that the T-MO is capable of preventing a slipping object from being dropped is the culmination of two distinct contributions.

The aim of this chapter was to determine whether a low cost manipulator can be used to reliably detect slip and whether that ability can provide a metric of grasp stability and improve grasping efficiency. This chapter has demonstrated that the Tactile Model O (T-MO) is a highly

capable slip detection platform when using a support vector machine as a classifier. The T-MO was able to detect slip in novel objects when an antipodal pinch grasp is used and was robust to changes in grasp and slipping direction. I also developed different strategies for reacting to slip detection which can be used depending on the scenario. This work demonstrates that a low cost manipulator can indeed be used to reliably detect slip.

The developed classifier was used in two realistic scenarios where the ability to detect slip allowed the T-MO to pick up an object of unknown weight with the approximate minimum necessary force and prevent it from being dropped when the weight was changed. This also demonstrated that the ability to detect slip serves as a useful and robust metric for determining grasp stability in several scenarios and by demonstrating first time grasping without excessive force it has also been shown that slip detection can improve grasping efficiency.

To summarise, this chapter has demonstrated that a low-cost multi-fingered manipulator can be used to reliably detect slip and that slip detection can be used as an metric to evaluate the stability of a grasp and improve grasping efficiency. This has therefore answered the third and fourth research questions posed in Chapter 1 and in doing so has settled the lingering question from Chapter 4 regarding whether the addition of tactile sensing to a robotic manipulator enhance effectiveness of the system. In the following chapter we will return to the single sensor to address an issue which was touched upon in this chapter, incipient slip.

CHAPTER 6

INCIPIENT SLIP

This chapter concerns two design iterations of the TacTip for inducing and detecting incipient slip. This includes modifications to the TacTip design, methods used to detect incipient slip and experiments performed in real time to prevent objects being dropped. This chapter begins by giving a brief overview of incipient slip, further to that presented in the literature review, followed by a description of the experimental setup. A separate section is devoted to the design and testing of each of the two sensors before a final 'online' test is performed where incipient slip is detected in real time.

Part of the work presented within this chapter has been accepted in the following peer-reviewed conference.

- J. W. James, S. J. Redmond & N. F. Lepora. (2020). A Biomimetic Tactile Fingerprint Induces Incipient Slip. 2020 IEEE/RSJ International Conference on Intelligent Robots and Systems (IROS), pp 9833-9839.

  Contribution statement: J. James conceived of the presented idea, designed the sensor, developed the method, carried out the experiments, performed the analysis and wrote the manuscript. S.J. Redmond and N.F. Lepora provided insight into sensor design, assisted with experimental setup and performed critical revisions of the manuscript.

6.1 Motivation & Scope

For autonomous robots to operate effectively in the world they must be able to handle objects safely. When grasping an object, the robot must find the *Goldilocks* zone between gripping too tightly and damaging the object, and too loosely and dropping the object; both of which could result catastrophic damage to the object. The ability of a tactile sensor to detect object slippage can set a lower bound on the safe gripping force, as once slip is detected the grasp can be tightened and the object prevented from falling. One key focus of slip-detection research in robotics is to find when parts of the sensor begin to slip whilst other parts remain in static contact. This phenomenon of slippage of part, but not all, of the contact surface(s) between the sensor and object is termed *incipient* slip [16].

Incipient slip is observed in the skin of the human finger pad. Due to the non-uniform distribution pressure (and hence local normal forces) across the finger pad, some regions may slip before others, where the traction (proportional to normal force) is smaller [51, 52]. On the mechanoreceptor level, this provides significant stimulation of the FA-1 and SA-1 afferents, and has been observed to trigger an increase in grip force [53], although the exact biomechanical and neural mechanisms underpinning this response have yet to be definitively identified.

As stated in the introduction, *incipient* slip is separate to *gross* slip where the entire surface slips – as was the subject of Chapters 2 & 4 – and slip prediction where physical parameters are estimated to establish whether there is a risk of slip. The distinction between these three phases is especially pertinent to this chapter because that there has, historically, been some confusion in the scientific literature between incipient slip and slip prediction. Certain studies claim to present incipient slip but often lack a rigorous validation of its presence.

For example, in a study by Marconi & Melchiorri [251] a 16x16 array of rubber taxels which detect normal force due to its proportionality to electrical resistance measured across the taxel. Using Fast-Fourier-Transforms (FFTs) to compare dominant frequencies when the object is at rest and when slipping they state that "immediately before the first motion of the object the low frequencies components become dominant in the spectrum" and conclude this is incipient slip before saying "It is important to point out again that this effect is present *before* the object starts to slip...". From this, it is reasonable to conclude that they are in fact performing slip prediction or at the very least have performed no direct verification of incipient slip.

This issue persists in more recent studies. Su et al. (2015) observed vibration in BioTac sensors to predict slip was going to occur 30ms before it was detected by an inertial measurement unit atop an object [198]. However, again, as this was not directly observing the slippage of part of the contact area whilst the rest was static this comes under the umbrella of slip prediction. These examples are included to provide clarity for future research into incipient slip but also to motivate the work in this chapter by providing a standard for verifying any incipient slip claimed to be found here.

There are significant barriers that make the elicitation and detection of incipient slip chal-

lenging. Primarily, when a sensor is deformed by a shear force - as is experienced when holding an object - the surface must have sufficient elasticity to allow parts of the sensor to slip while other parts remain stuck, which requires shear deformation between the slipping and stuck parts of the external sensor surface. Additionally, this must be detectable from the sensor output, in this case the camera inside the sensor. Detecting incipient slip is useful because corrective action can be taken before slippage occurs across the entire contact area, hence significantly reducing the likelihood of the object being dropped. It can also form part of a modular system being slotted in alongside gross slip and slip prediction resulting in a robust slip detection system.

The aim of this chapter is to develop a sensor which displays incipient slip by mimicking the biomechanical behaviours of the human finger pad. We modify the existing tactile sensor - the TacTip which has previously been effective at slip detection, yet does not exhibit incipient slip behavior. The TacTip has an internal pins structure which is inspired by intermediate ridges in the human fingertip. In other work, Cramphorn et al. (2017) explored the effect of adding protrusions to the outer TacTip surface; however, the aim of that work was to enhance spatial acuity [107] not induce incipient slip. The protrusions also do not resemble a fingerprint so the focus greatly differs from that of this work.

Here, we extend the TacTip's biomimicry to include ridges on the external surface to facilitate the shear deformation required for incipient slip, as occurs on the human finger pad, facilitated by the fingerprint ridges. This builds upon prior work applying elements of fingerprint mimicry to the TacTip by targeting a specific phenomenon - incipient slip - and designing the sensor such that it provides the necessary physical conditions to induce incipient slip.

This chapter works towards the induction and detection of incipient slip in three phases. The first two phases are different iterations of a novel sensor morphology before the final phase; the introduction of a method to detect incipient slip and react in real time. This chapter's work seeks to answer the final research question: *Does mimicking the human fingerprint result in detectable incipient slip in a tactile sensor?*

6.2 Incipient Slip Sensor: Version 1

6.2.1 Sensor Design

The sensor presented in this work is a modification of the TacTip sensor used in Chapter 3. The key functional requirements for the modification are to introduce a traction differential (i.e. different normal force in different places) and an ability for shear displacement to apply to the parts of the sensor (the ridges) that make contact with the object surface, as occurs in the human finger pad [52] such that some of the contact area slips and some does not. Previously, when an object slipped across the TacTip, there was no discernible incipient slip [243]; the pins all moved together in a linear fashion when gross slip occurred. To solve this, we have added five rings of increasing radius, from a central ring of zero radius (in effect an external pin).

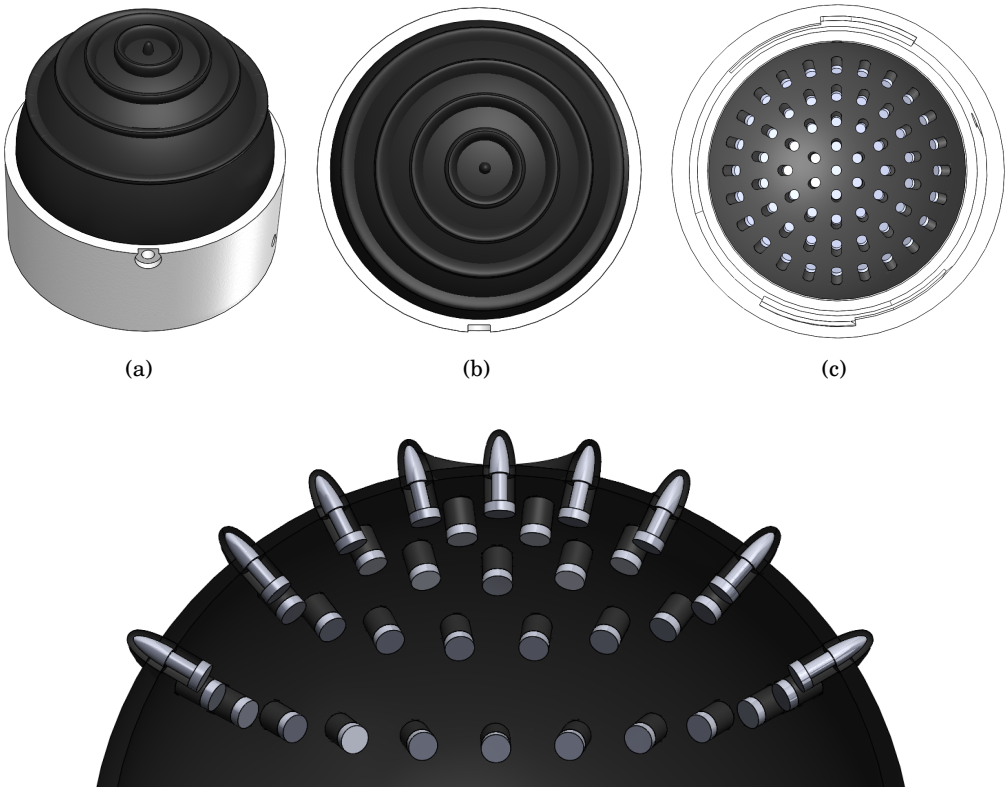

(a) (b) (c)

(d)

Figure 6.1: (a), (b) & (c) CAD renderings of new sensor showing the concentric ring pattern of the fingerprint-inspired ridges to facilitate the shear deformation of incipient slip. The ridges extend 2 mm above the surface of the sensor. (d) Cutaway showing how the pins are embedded in the skin.

In the TacTip, the pins consist of heads of VeroWhitePlus material atop small pillars of TangoBlackPlus. Here, the pin-heads are extended such that they protrude through the pillars and into the ridges (Fig 6.1). The pins act as mechanical transducers so any motion of the ridges results in visible motion of the pins from inside the sensor. As stated in section 6.1 Cramphorn et al. (2017) utilised this transduction principle to improve the spatial acuity of the sensor by adding small (0.5mm) protrusions to the surface of the TacTip, however their focus was purely on perception not slip [107]. Here we modify the TacTip with the express aim of allowing it to experience and subsequently transduce incipient slip (Table 6.1).

Firstly, we have added raised ridges which mimic the friction ridges in the epidermis of the human fingertip. Under the Coulomb model of friction, the maximum frictional force is proportional to the normal force. As stated by Chen et al. (2018) [16], a key requirement for incipient slip is that "the sensor can deform/slip independently of the rest of the sensor due to it having appropriate mechanical compliance". In the hemispherical ‘smooth’ TacTip the neighbouring regions of contact were subject to very similar normal forces. Therefore, the addition

of raised ridges results in the neighbouring contact areas being spaced apart and subject to notably different normal forces, aided by the curvature of the TacTip exterior. This significant difference in normal force - and therefore frictional force - for each ring means that when a shear is applied the TacTip if one ring has sufficient frictional force to remain static the next ring may not. This would facilitate this area of the sensor slipping - as the friction is too low - whilst the inner rings remain static resulting in incipient slip.

Although an precise measure of the smoothness of the previous TacTip was not collected the Stratasys Connex3 Objet260 with which it was printed has a 30 micron resolution which gives an estimate of the surface roughness of the sphere [252]. This indicates that the neighbouring contact regions on the 'smooth' TacTip are extremely close and may explain why incipient slip is not observed.

The structure of the human fingerprint is complex and the width, shape, separation and pattern of ridges is highly variable from person-to-person and changes as we age due to multiple factors such as loss of collagen fibres and rete pegs [253]. This means that the mimicry applied here is centred on there being a pattern of raised ridges on the contact surface of the sensor.

Secondly, we have reduced the thickness of the skin between rings from 1 mm to 0.5 mm, to facilitate shear deformation of the sensor contact surface. Even though the ridges will lead to differing normal forces, the rings are still linked by the interstitial skin. The thicker the skin the higher the coefficient of elasticity, which hinders shear deformation (skin stretch) and hence diminishes the associated incipient slip phenomenon. It should be noted that the added ridges will also bend, which further allows parts of the skin to move independently, and therefore reduces the dependency on the skin stretch for incipient slip to occur.

Finally, as the pins are set in gel, when one pin moves in the TacTip it causes neighbouring pins to move. One consequence of this is that if a single region of the sensor surface was to move it would cause many adjacent pins to move due to this mechanical coupling. To minimise this effect we increase the spacing of the pins such that the projected radius of each ring of pins is 4 mm greater than the ring inside (Fig. 6.2 compares the two designs). Previously the spacing was 3 mm between all adjacent pins laid out in a hexagonal pattern. We also increased the thickness of the pins to reduce the potential for damage when removing support material after 3D printing.

6.2.2 Data Collection Rig

To collect data and perform a reliable comparison to the previous TacTip design we reuse the data collection rig from Chapter 3 (Fig. 6.3). Here, we augment the apparatus by adding an external camera to measure movement of the external surface of the sensor and the acrylic sheet. James et al. (2018) used various shapes made from ABS plastic; however, this is unsuitable here as we need to use a transparent object to make reference recordings of movements on the sensor's surface. We therefore use a sheet of 10 mm thick transparent acrylic. Additionally, we apply markers in a cross pattern to the surface of the sensor so that fixed points on the surface can be

Figure 6.2: Comparison of incipient slip sensor v1 (left column) and previous TacTip design (right column). The added ridges distort the otherwise uniform surface to facilitate incipient slip. The new sensor also has a lower pin density.

easily tracked by the external camera.

Both the external markers and the internal pins are identified and segmented using the Python OpenCV library function *SimpleBlobDetection* which provides a list of blob (x, y) coordinates for each frame. To annotate when gross slip occurs, we attach an ArUco optical marker to the acrylic so its height can be measured by the external camera. When the height of the acrylic sheet changes significantly, we assert that gross slip is occurring. To collect data the sensor is pressed against the acrylic, which is then lifted 50 mm. At this point, the cameras start to record and the arm retracts slowly (moving normal to the acrylic sheet) until the object has completely fallen. Different retraction speeds between 0.1-0.5 mm.s^{-1} at 0.1 mm.s^{-1} intervals are used.

	Modification	Benefit
1	Add raised ridges	Adjacent contact regions have differing normal forces to create traction differential
2	Reduce skin thickness	Skin stretchier to facilitate incipient slip
3	Reduce pin density	Decrease coupling of internal pins to facilitate detection of incipient slip

Table 6.1: The key modifications to TacTip design to facilitate occurrence and detection of incipient slip.

6.2.3 Results

6.2.3.1 External View Analysis

Using the slip detection rig from Sec.6.2.2, we performed 20 repeats at each retraction speed and recorded both the internal and external camera data. Following this, we detected the external markers and internal pins to determine whether incipient slip was present. Despite applying markers to the three innermost ridges, as well as the central pin, the third ring loses contact with the surface before gross slip occurs. Therefore, from here on, we ignored these four markers, leaving nine markers to be tracked, which were in contact for the duration of each trial.

The external camera video showed a clear presence of incipient slip (Fig. 6.4). The markers on the second ring displayed the most obvious movement however the marker atop this ring and the ArUco did not move. This means that parts of the contact surface were slipping when others were not and, crucially, before the object showed any sign of falling. This incipient slip pattern becomes clearer when looking at the data after the markers have been tracked. Again, it is clear that the farthest left and right markers begin to move after ~2.5 s before any others (Fig. 6.5). The markers inside the two markers on each extreme begin to move next. Throughout the experiment, the two topmost markers remain static until gross slip occurs and the object falls after ~6.5 s.

The pattern seen here is broadly in line with predictions made by the Coulomb model of friction, which states that maximum static frictional force is proportional to the normal force on the surface. The domed shape means that the greater the radius of the ring, the lower the normal force, and therefore we would expect the markers further from the centre to slip first. When considering the line of markers placed horizontally across the middle of the sensor this is exactly what we see: the markers on the far left and far right slip first, followed by those markers closer to the centre.

When considering the line of markers placed vertically up the middle of the sensor, the picture becomes more complicated. The top two markers show almost no motion, whereas the bottom

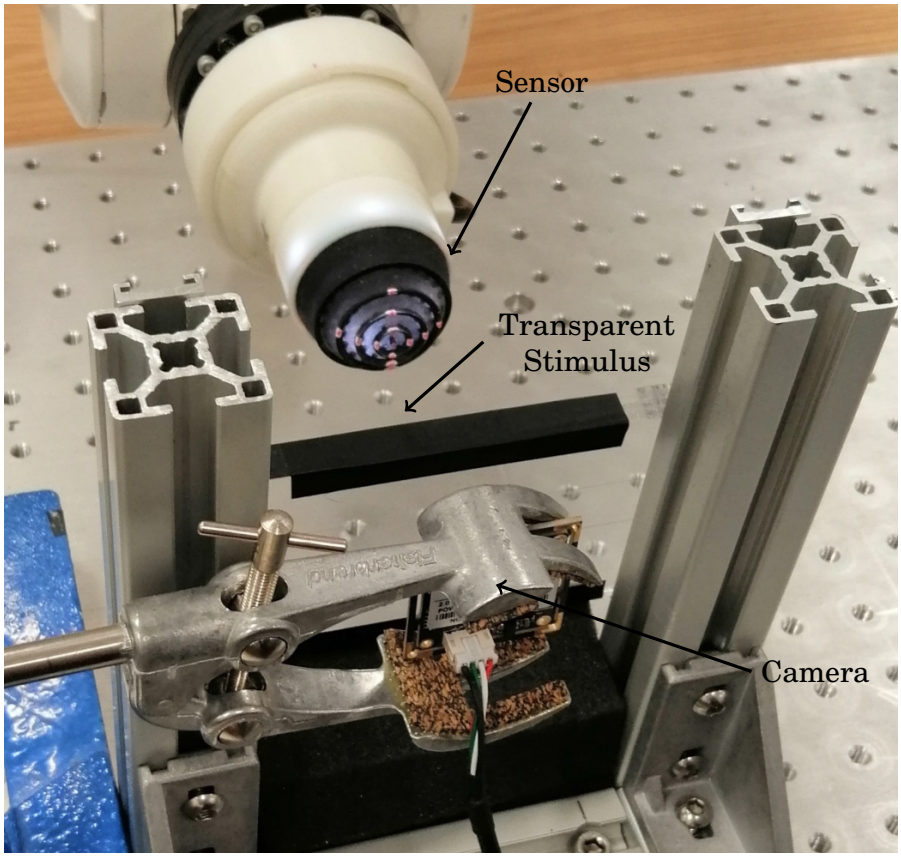

Figure 6.3: Rig for collecting incipient slip data. Modified TacTip attached to an ABB IRB120 six-axis robotic arm; external camera held in a clamp and the transparent acrylic sheet moving in a low friction rail. Black tape has been added to identify the transparent stimulus and to reduce potential effects from strong overhead lighting. The cross pattern of red markers is visible on the sensor surface and is tracked by the external camera.

two markers show noticeable movement. As the sensor is bearing the weight of the acrylic, this causes a large shear force to be applied to the sensor, which most likely causes the normal force distribution across the vertically-aligned markers to become asymmetric.

However, another consideration is the elastic forces between different rings when incipient slip occurs. For relative movement to happen the interstitial skin between rings needs to stretch or compress as their distances necessarily change. Given a situation where horizontal markers begin to slip but the inner ring remains static then, assuming the movement is purely vertical, the distance between markers is given by

$$L = \sqrt{\Delta y^2 + L_0^2} \tag{6.1}$$

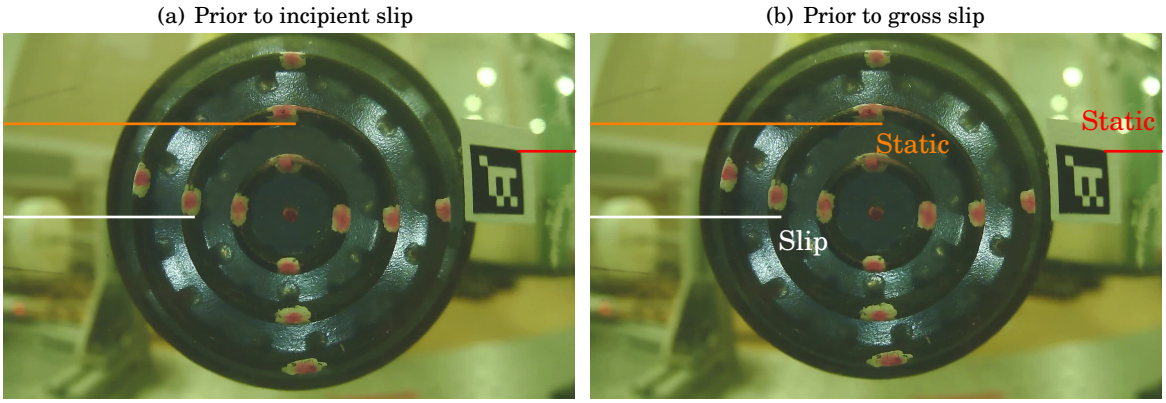

Figure 6.4: External camera view of sensor with markers attached to track fixed points on the surface. (a) Frame from the start of the data collection. (b) Frame taken close to gross slip occurring. For reference, the coloured lines are in the same locations in both images. The marker closest to the white line shows clear movement, however, the marker near the orange line and the ArUco optical marker do not move. Therefore, we see incipient slip: slip of part but not all of the contact surface.

where Δy is vertical slip distance and L_0 is ring separation. This gives the change in length as

$$\Delta L = L - L_0 = L_0 \left(\sqrt{1 + \left(\frac{\Delta y}{L_0} \right)^2} - 1 \right) \tag{6.2}$$

which for small values of Δy can be approximated by Taylor series expansion around $\Delta y = 0$ as

$$\Delta L \approx \frac{\Delta y^2}{2L_0}. \tag{6.3}$$

For the vertical markers in their respective rings a vertical slip means that

$$\Delta L = \Delta y \tag{6.4}$$

and therefore for a given small vertical slip the change in distance between horizontal markers is smaller than vertical markers. Modelling the interstitial skin as a single spring between markers and using Hooke's law we see that less force is required for the horizontal markers to move than the vertical markers. This is a major simplification of the system but does provide some insight into the pattern of marker movement.

6.2.3.2 Internal View Analysis

There are two distinct types of sensor surface movement that cause the majority of the pin movement inside the sensor: translation and pivot. Translation occurs when an external ridge of the TacTip slips and the pin embedded within also translates in the same direction, but perhaps not to the same extent. Pivoting occurs when the ring surface remains static on the object but the

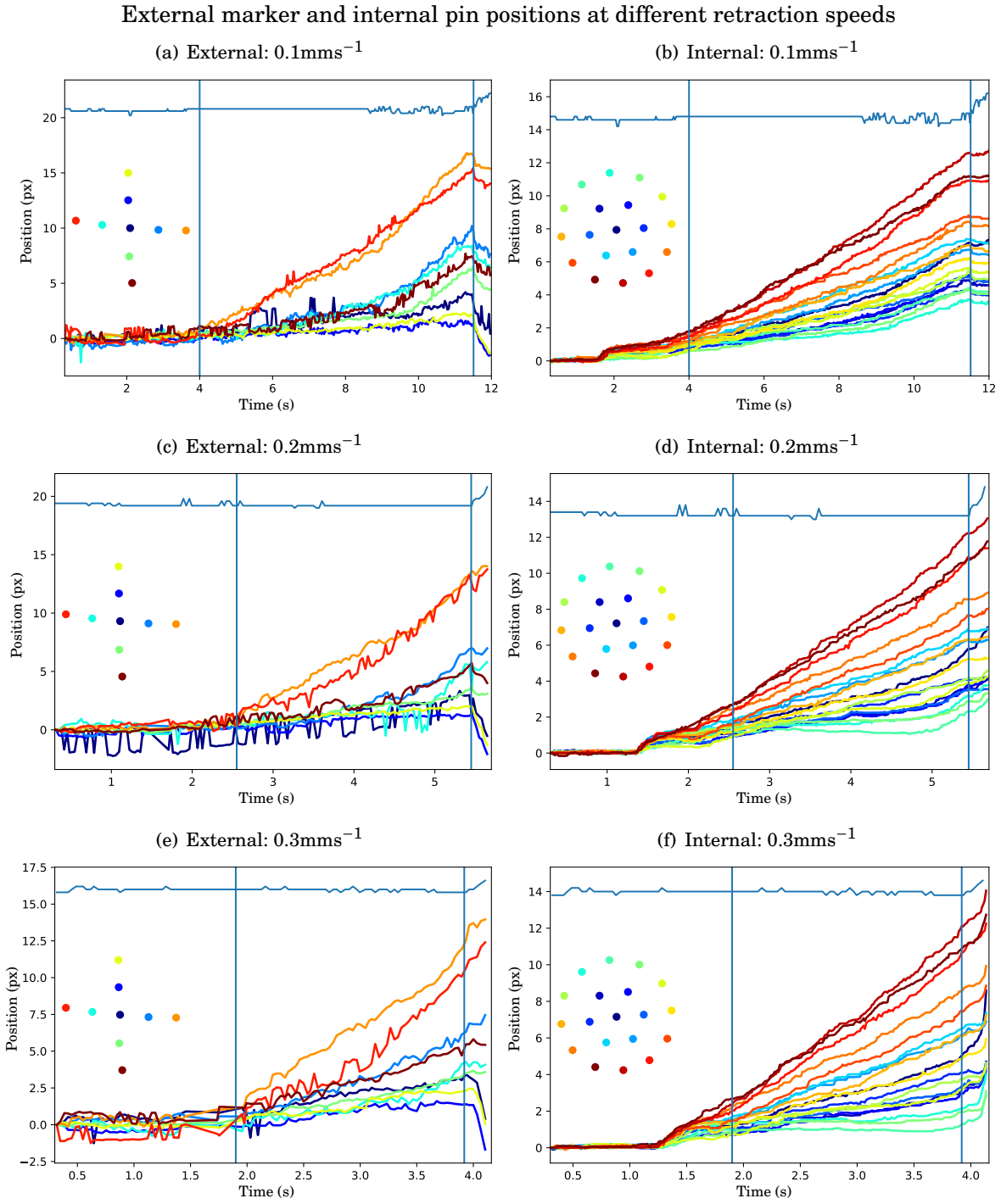

Figure 6.5: Vertical positions of external markers (left col) and internal pins (right col) when allowing an object to slip. Subfigure headings indicate camera position and robot arm retraction speed. Each row is a separate trial. Vertical lines indicate where incipient slip begins (left vertical line) and when the object begins to fall (right vertical line). The blue line at top of each graph is position of ArUco marker on the acrylic object. Note that this is not on the same scale as the y-axis and is included only to provide a ground truth of the time when the object begins to fall. Inset in middle left of each subfigure shows position of markers/pins at t=0 with colours corresponding to line plot.

parts of the skin spanning the ridges moves. As the pins protrude equal distances normal to the skin internally and externally, the effect of pivoting is quite pronounced. This effect somewhat confounds our ability to easily observe movement of the external surface of the ridge against the object (i.e. to detect slip).

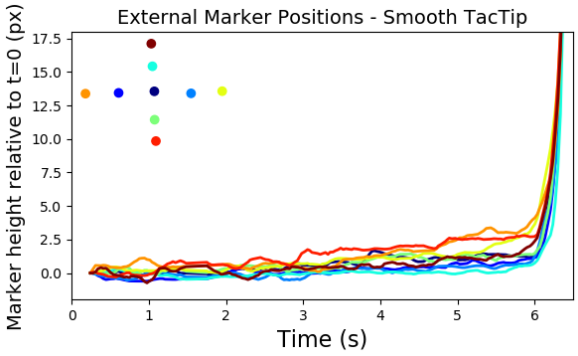

Figure 6.6: No incipient slip signal from external markers attached to smooth TacTip.

To detect incipient slip on the inside we want to see examples of translational pin movement; however, it appears that the pivoting is the dominant effect resulting in pin movement. Thus, it is difficult to determine whether relative translation between pins relates to the occurrence of incipient slip on the external surface (Fig. 6.5), or whether this movement is due to pin pivoting. This does not mean that the effect is not detectable in the pin movement patterns, but rather that it is more challenging to extract. Fundamentally, this is a complex pattern recognition problem which could be approached a number of way including the use of deep learning applied directly on the tactile images [254]. However, as we are interested in the design of a sensor where incipient slip can be directly detected from both internal and external cameras we forgo such analysis here.

6.2.3.3 TacTip Marker Analysis

To confirm that incipient slip is not visible in the previous smooth TacTip design used in previous work [243], we attached markers in the same pattern on the surface of that smooth TacTip and performed the same experiment. As expected, the movement of markers does not display the characteristic incipient slip pattern that is present in the new design (Fig. 6.6). Instead, all markers remain static until gross slip occurs, when they all move in unison. This bulk motion of the surface contributed to making that smooth design of TacTip so effective at detecting gross slip [243].

6.3 Incipient Slip Sensor: Version 2

6.3.1 Sensor Design

The design of the incipient slip sensor version 1 provided one key result; that a concentric ring pattern on the surface of the sensor does induce incipient slip. However, there were several limitations which need to be addressed:

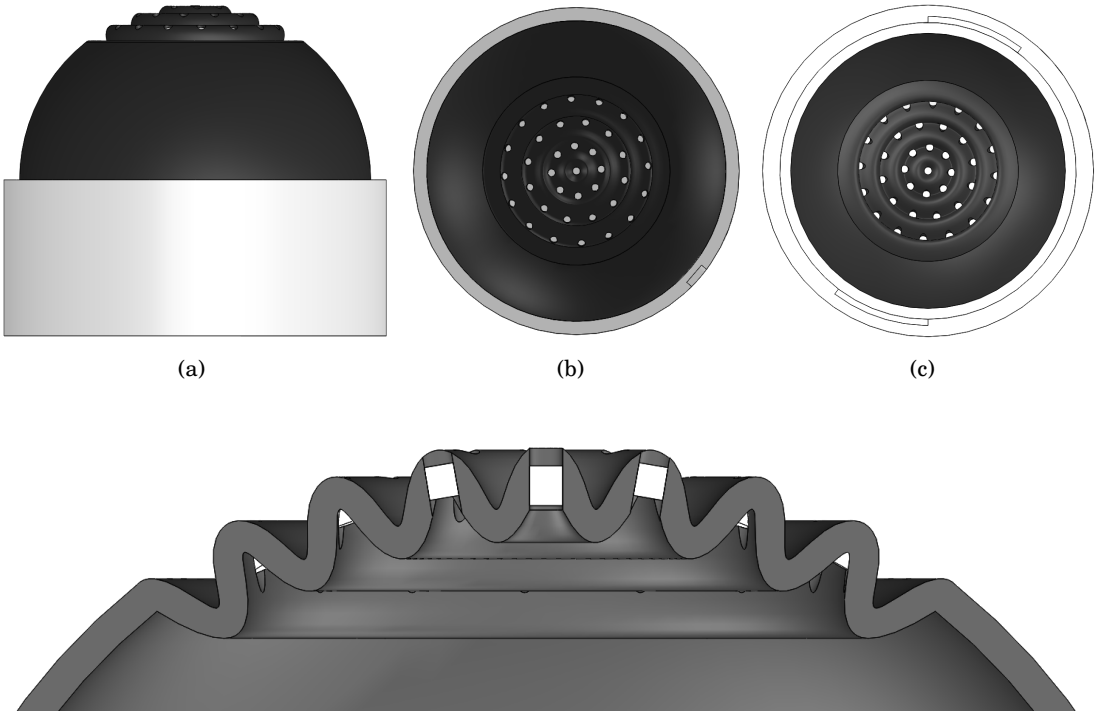

(a) (b) (c)

(d)

Figure 6.7: (a), (b) & (c) CAD renderings of incipient slip sensor v2 showing the updated design. For (b) & (c) note the same pattern of markers on the internal and external surface. (d) Cutaway showing how the oscillating pattern is continued above and below the skin and how the white pins extend throughout the skin. The pins are slightly recessed into the skin to allow for contact to be made with the rubber-like TangoBlackPlus rather than the smooth VeroWhitePlus.

- Incipient slip signal was not clear from internal pins
- External markers do not mirror positions of internal pins
- Pivoting of internal pins is the dominant motion effect.

To combat these issues a new design of sensor is presented (Fig. 6.7). In this version there are several key differences. Firstly, the fingerprint is changed to be a circularly symmetric wave pattern which propagates out from the centre of the sensor. This means that, unlike version 1, both the internal and external surfaces have an undulating pattern. The wave amplitude is 1mm meaning there is a 2mm height difference between peak and trough - as before - but there are no breaks between waves leading to a ring separation of 3mm compared to 4mm for version 1.

Second, the internal pins extend all the way through the skin making them visible from the internal and external camera. This should result in any incipient slip movement on the external surface being reflected in the internal camera image, which is the main goal of this chapter. Additionally, this means that we can easily map from external to internal tracking to help identify

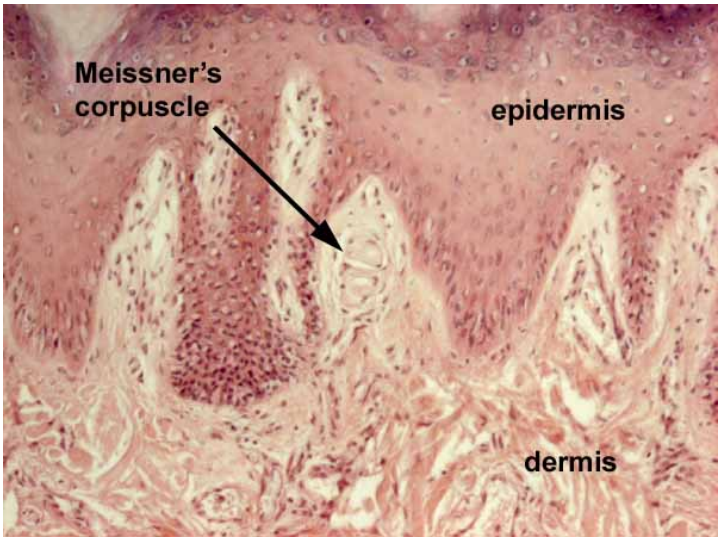

Figure 6.8: Skin histology showing a Meissner's corpuscle within a dermal papilla in the dermis of the human fingertip [255]. The pins at the base of the internal ridges in sensor v2 are therefore analogous to the Meissner's corpuscles.

incipient slip from the inside. As the sensor is 3D-printed as a single unit the pins are printed *in-situ* meaning they are robustly contained within the skin which should not affect structural integrity.

The pins sit on the trough of the wave on the inside and consequently sit on the peak of the wave on the external surface so that they are close to any object being contacted. The pins remain slightly recessed from the external surface to ensure that objects are in contact with the rubber-like TangoBlackPlus which provides higher friction than the VeroWhitePlus pins. A further consequence is that the pins are shorter (1mm) than for version 1 (2mm) which should lead to less pivoting. By having the pins in the trough - as viewed from the internal camera - the pins can be seen as loosely analogous to the Meissner's corpuscle in the human fingertip skin (Fig. 6.8). Although the analogy only extends to *location* of the pins. The Meissner's corpuscles sit within the dermal papillae in the dermis of the human fingertip [255] and are sensitive to local shear [221] whereas the camera in the TacTip calculates the global displacement of the pins.

As before, we utilise the slip data collection rig and track internal and external pins when holding a transparent acrylic object which is allowed to slip.

6.3.2 Results

As before, a flat clear object is held in a low friction rail and the robot arm is retracted at various speeds to allow the object to slip. Figure 6.9 shows the result of tracking all the pins on the internal and external surface and Figure 6.10 shows the same data but focuses on a 0.5s section centred on the spike. Two features of interest are evident from these figures. Firstly, the internal

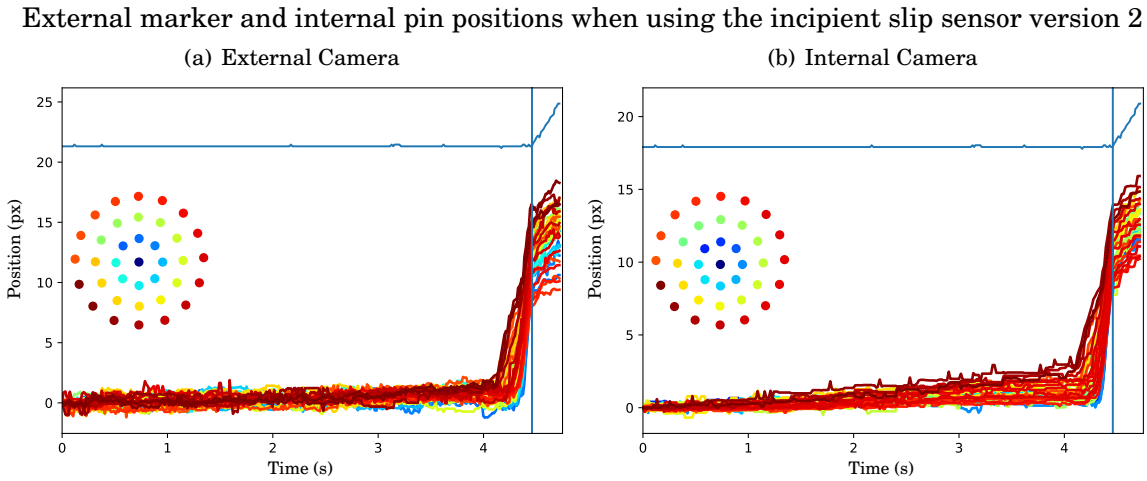

Figure 6.9: Pin positions in two trials with identical conditions when an acrylic object is allowed to slip after being held by the incipient slip sensor. Subfigure headings indicate camera location and robot arm retraction speed. (a) & (c) show the external markers and (b) & (d) the internal pins. The vertical line indicates where when the object begins to fall. The blue line at top of each graph is position of ArUco marker on the acrylic object. The spike which occurs before the object slips indicates incipient slip has occurred. In different experiments the incipient slip signal occurs at different times prior object slippage.

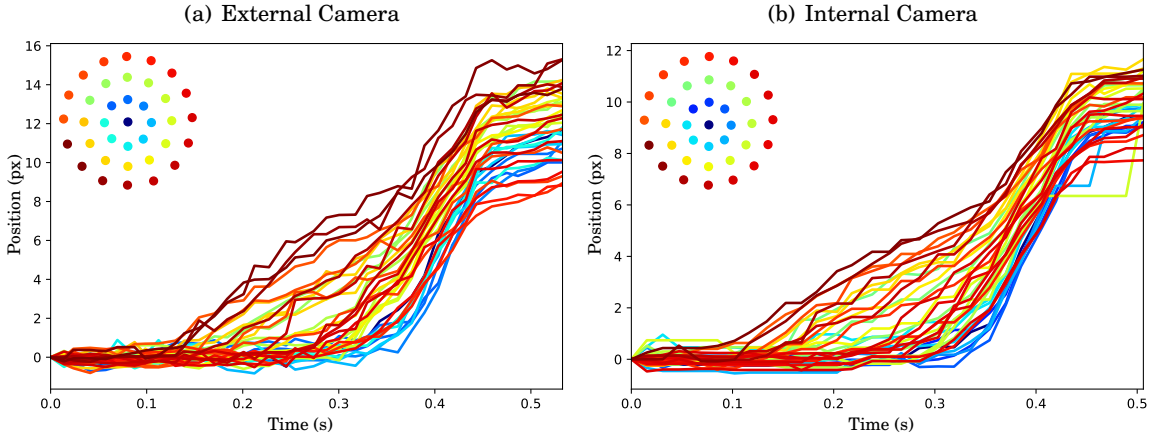

Figure 6.10: Pin positions from (a) the external camera and (b) the internal camera. When looking at a 0.5s section of Figure 6.9 the independent movement - and thus incipient slip - of pins in different rings is clear in both the internal and external plots. From the pin labels (inset top left) the outer pins (red) move before the central pins (blue) consistent with predictions made by the Coulomb friction model.

External marker and internal pin positions showing incipient slip significantly before object slip

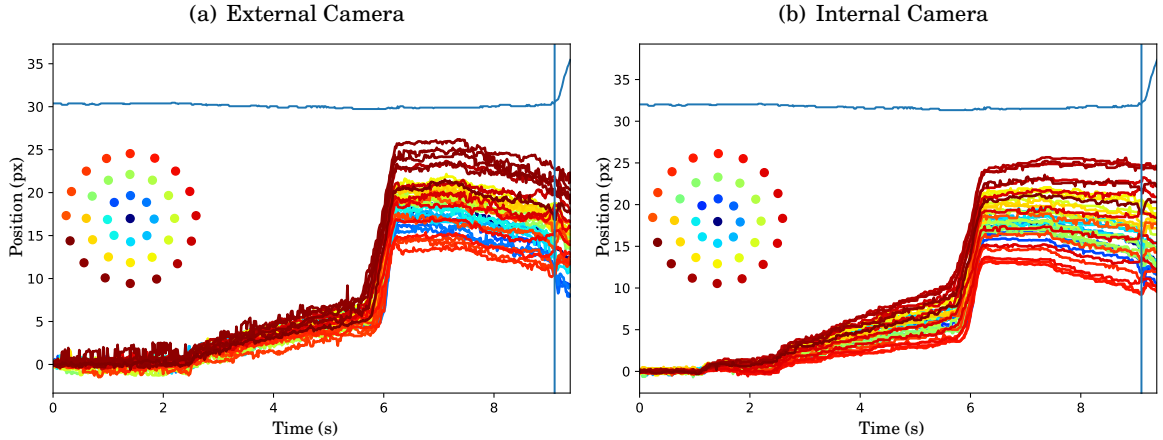

Figure 6.11: Pin positions when an acrylic object is allowed to slip after being held by the incipient slip sensor. (a) show the external markers and (b) the internal pins. The vertical line indicates where when the object begins to fall. The blue line at top of each graph is position of ArUco marker on the acrylic object. The spike which occurs before the object slips shows certain pins move before others thus indicating incipient slip has occurred. In this example incipient slip occurs several seconds prior to object slip.

and external views look very similar with a long flat section preceding a clear movement in pin positions. This is beneficial as the discrepancy in signal between internal and external views present in the previous sensor has been eliminated which should make any incipient slip signal easier to identify from the internal camera.

Secondly, when we zoom in on the spike present in the above data (Fig. 6.10) we can see a independent movement of pins in different rings in both the external and internal cameras. This is a clear benefit of the new design over the old. We can see that the outer pins (red) move before the central pins (blue). Once all pins are moving, by definition, the incipient slip phase ends and we move into the gross slip regime.

At around 4s (Fig. 6.9) when the pins begin to move there is a spike with a width of approximately 0.5s which occurs almost immediately prior to gross slip. However, in other trials (Fig. 6.11) we see this occurs several seconds before object slip. There is the same width of the spike which implies that there is an incipient slip followed by a gross slip and then a sizeable gap before the object slips. It is possible that the slip of one ring causes a knock-on effect for subsequent rings causing a small gross slip independent of when the object falls or this could be a single stick-slip event.

For further analysis we can restrict our view to only the pins placed horizontally and vertically relative to the central pin (Fig. 6.12). Again we can see relative movement of pins across various retraction speeds and pins on the East or West slipping first, followed by the Southern pins and finally the pin in the North. This is consistent with the analysis in Section 6.2.3.1 and the results from the previous sensor. The primary advantage here is that it is visible from the internal

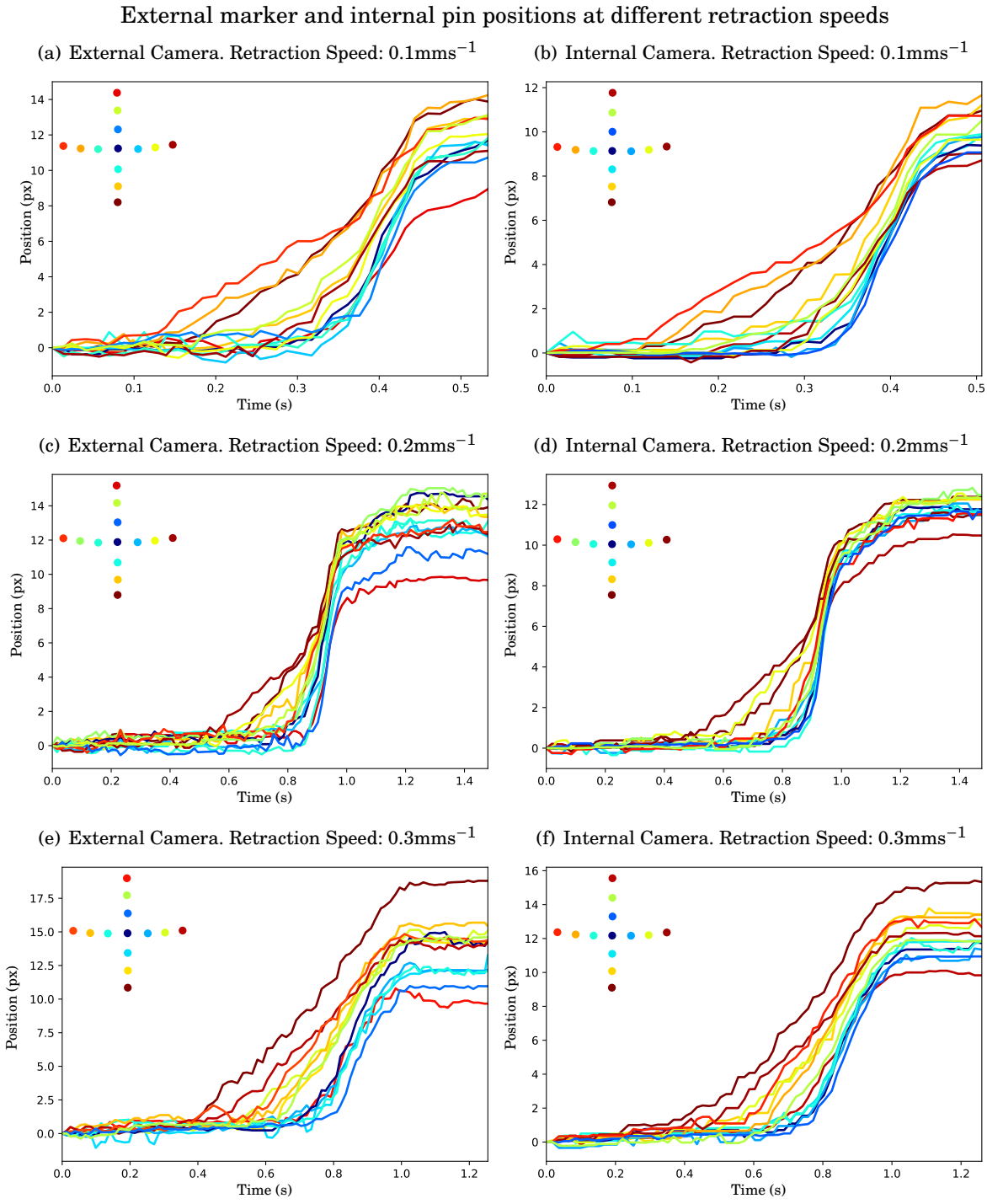

Figure 6.12: Vertical positions of external markers (left col) and internal pins (right col) when allowing an object to slip. Inset in middle left of each subfigure shows position of markers/pins at t=0 with colours corresponding to line plot. In all experiments at different retraction speeds we see the same pattern of pin movement from the internal and external cameras.

camera.

Given that incipient slip is visible from the internal view the next question that must be addressed is can a simple method be used to detect this incipient slip in real time? This is the focus of the next section.

6.4 Real Time Incipient Slip Detection

6.4.1 Experimental Methods

To help determine the usefulness of the second design of incipient slip sensor a short experiment will be conducted to determine whether incipient slip can be detected in real time. The first task is to devise a method of determining which pins are slipping and which are static thereby detecting incipient slip.

Essentially, we want to detect relative movement between some pins and others. This is not as simple as putting a threshold on the speed of pins as there can be a bulk motion of all pins which isn't indicative of slip. Instead, we wish to subtract the bulk velocity of pins from each pin and see if any pins remain with significant movement.

If we consider each pin as belonging either to the set of pins which are undergoing incipient slip I or to the set of static pins $I^{\complement}$. As these are the only two possible sets the static set is the complement as pins cannot belong to both. Therefore we have

$$I \cap I^{\complement} = \emptyset \tag{6.5}$$

$$I \cup I^{\complement} = \mathbb{U} \tag{6.6}$$

where $\emptyset = \{\}$ is the empty set and $\mathbb{U} = \{1, 2, ..., N\}$ is the Universal set containing all N pins.

The output from the sensor is a list of pixel (x, y) coordinates of each pin which are sorted to ensure that the ordering of pins in each frame is identical. From this we can define

$$X(t) = \left[x_{1,t}, x_{2,t}, ..., x_{N,t}\right] \tag{6.7}$$

$$Y(t) = \left[y_{1,t}, y_{2,t}, ..., y_{N,t}\right] \tag{6.8}$$

for the list of x and y positions of pin i at frame t. We can get the frame-to-frame change in position - which is proportional to the velocity - by taking the element-wise subtraction of position at frame $t-1$ from frame t

$$\dot{X}(t) = X(t) - X(t-1) \tag{6.9}$$

$$\dot{Y}(t) = Y(t) - Y(t-1). \tag{6.10}$$

We can then obtain the frame-to-frame displacement of each pin by taking the element-wise Euclidean norm of each pin velocity

$$D(t) = \sqrt{\dot{X}^2(t) + \dot{Y}^2(t)}. \tag{6.11}$$

As the pin detection is subject to some noise it is useful to apply a simple moving average filter on D with a window size W giving

$$\bar{D}_{SM}(t) = \frac{1}{W}\sum_{i=0}^{W-1} D(t-i). = \left[d_{0,t}, d_{1,t}, ..., d_{N,t}\right] \tag{6.12}$$

The average speed of the static pins is given by

$$s(t) = \frac{1}{\left|I^{\complement}\right|}\sum_{p\in I^{\complement}} d_{p,t} \tag{6.13}$$

where $|I^{\complement}|$ is the cardinality of the set of static pins and $d_{p,t}$ is the frame-to-frame displacement of static pin p at frame t. $s(t)$ can be considered to be the bulk motion of the pins. Finally, we need to subtract this value from each pin

$$D_{IS}(t) = D(t) - s(t) \tag{6.14}$$

and if any are above a predefined threshold, s_{thr} they are judged to be undergoing incipient slip and are moved from set $I^{\complement}$ to the set of incipient pins I.

A decision on where incipient slip is judged to be occurring can then be made depending on the cardinality of I - the number of individual pins above the threshold of independent movement. This gives three variables which need to be chosen; the moving average window size, W; the incipient slip speed threshold s_{thr} and the threshold on the number of slipping pins, I_{thr}. These values will be selected by observing the previously collected data at various retraction speeds.

To test whether the above method for detection incipient slip works in real time a modified version of the experiment for data collection is used. The stimulus is once again held but the robot arm is retracted in small increments of 0.2mm and throughout the movement the internal pins are recorded. If, at any point, the number of pins slipping $|I| \geq I_{thr}$ then incipient slip has been detected and the experiment is stopped. The reason for the small increments is that the ABB IRB120 controller cannot perform real-time control and moves sent to the controller cannot be interrupted. Instead, a small move is made and a check for incipient slip is made after each one. $0.2mm$ allows for both a significant change in position and a large enough sequence of frames to be collected.

6.4.2 Results

The purpose of this section is to demonstrate the effectiveness of the incipient slip detection method presented in Section 6.4. The principle of the method is that the bulk motion of the pins is subtracted from all pins which should result in any pins undergoing incipient slip, which will have a significant velocity independent of the bulk motion, being easily identifiable. A threshold is put on this independent motion to decide when a pin is judged to be independently slipping. To reduce the effects of noise a simple moving average window is applied to the pin displacements.

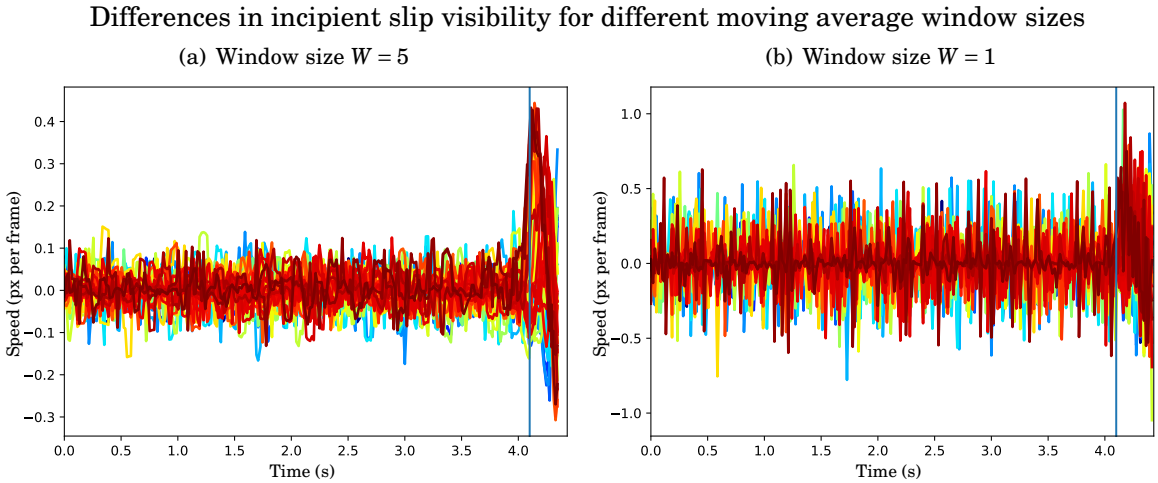

Figure 6.13: The effect of moving average Window size, W, on signal-to-noise ratio of pin speeds in the run up to incipient slip. The vertical blue line indicates the start of incipient slip.

Finally, to reduce false positives a threshold is put on the number of pins slipping before an action is taken. Therefore, prior to performing an experiment where incipient slip is detected in real-time we must determine values for the moving average window size, W; the incipient slip speed threshold s_{thr} and the threshold on the number of slipping pins, I_{thr} using the slipping data previously collected.

Choosing the moving average window size is difficult as it requires a tradeoff between reducing noise and minimising detection delay. A larger window smooths the data but requires more frames and therefore more time when operating online. A window size of $W = 5$ was chosen as it was shown to significantly reduce noise and giving a more noticeable peak associated with incipient slip (Fig. 6.13). This figure is showing the data as a result of applying equation 6.14 and prior to incipient slip we expect no independent movement of pins meaning that the signal is dominated by noise. When incipient slip occurs we expect certain pins to deviate from this flat line in a noticeable spike. With a window size of 1 the peak of pins there is a consistent noise with an amplitude of ~0.5 pixels per frame and a spike with an amplitude of ~1.0; an approximate signal-to-noise ratio (SNR) of 2. At $W = 5$ these values are approximately 0.1 and 0.4 respectively giving an SNR of 4 (Fig. 6.13).

As the window size affects the strength of the incipient slip signal the threshold for individual pin movement, s_{thr}, is dependent on W. A preliminary examination of the data concluded that values of $s_{thr} = 0.2$ and $I_{thr} = 4$ provided reliable detection of incipient slip. Values close to these resulted in similar detection performance and far outside resulted in no detection at all or high levels of false positives. A rigorous optimisation with a larger dataset would likely yield better results but as this is a preliminary investigation into the working principle of the sensor design we are interested to see if incipient slip is detectable online.

When detecting slip in real time the external camera view is recorded but the internal pins are

detected directly from the internal camera stream. This allows for real-time detection of incipient slip by applying the operations given by equation 6.14. Twenty trials were undertaken with retraction speed being randomly selected between 0.1-0.5mms^{-1}. A trial is considered successful if incipient slip is seen to visually occur (by inspecting the external surface) and the object does not fall. In 17 of the 20 trials incipient slip was detected and the retraction of the robot arm halted prior to the object falling.

Once the trial has been halted the external camera feed can be examined to verify that there was movement of the sensor surface but the object did not fall. Figure 6.14 shows two examples of successful detection. In the highlighted trials a small but clear movement of certain pins occurs whereas there is no significant movement of the object or certain areas of the sensor. This demonstrates that it was indeed incipient slip that was being detected prior to gross slip and even more importantly, object slip.

6.5 Tactile Perception Task: Edge Detection

6.5.1 Experiment Description

As discussed in Chapter 4 it is important that any changes made to the sensor for the elicitation and detection of a specific phenomenon should, ideally, not be a significant detriment to other tactile tasks performed. In the case of the reduced sized TacTip for use on the Tactile Model O (T-MO) it was shown in Chapter 4 to have comparable performance on a task where the radial position and angle of the sensor relative to the edge of a 12cm diameter circular disk was detected using a CNN.

Here, as a small extension, the same task is performed to determine whether the incipient slip TacTip presented retains the strong performance of the smooth TacTip at edge perception tasks. As before, the TacTip was placed with the central pin on the edge of the circle and the major axis of the camera aligned tangential to the edge (Fig. 6.15). For each tap radial position and angle relative the the edge were varied randomly. Radial positions were sampled from [-6,9] mm (where negative distances indicate the sensor being closer to the centre of the disc) and angles from [-45,45] degrees. The sensor begins each tap ~1.5mm above the surface and a 5mm tap is made from which seven frames are selected. The architecture of the CNN is the same (Fig. 4.11) and the input is a (128,128) pixel image which has been downsampled from (640,480). 1000 taps are collected for training the CNN split in a ratio of 80:20 for training and validation. A further 500 taps are collected for evaluating the trained network.

6.5.2 Results

To be able to determine the radial position and angle relative to a circular disk a convolutional neural network was trained using the same procedure described by Lepora et al. (2019) [106] and Chapter 4 Section 4.4.2. The CNN is a regressor with two outputs: the radial position relative to

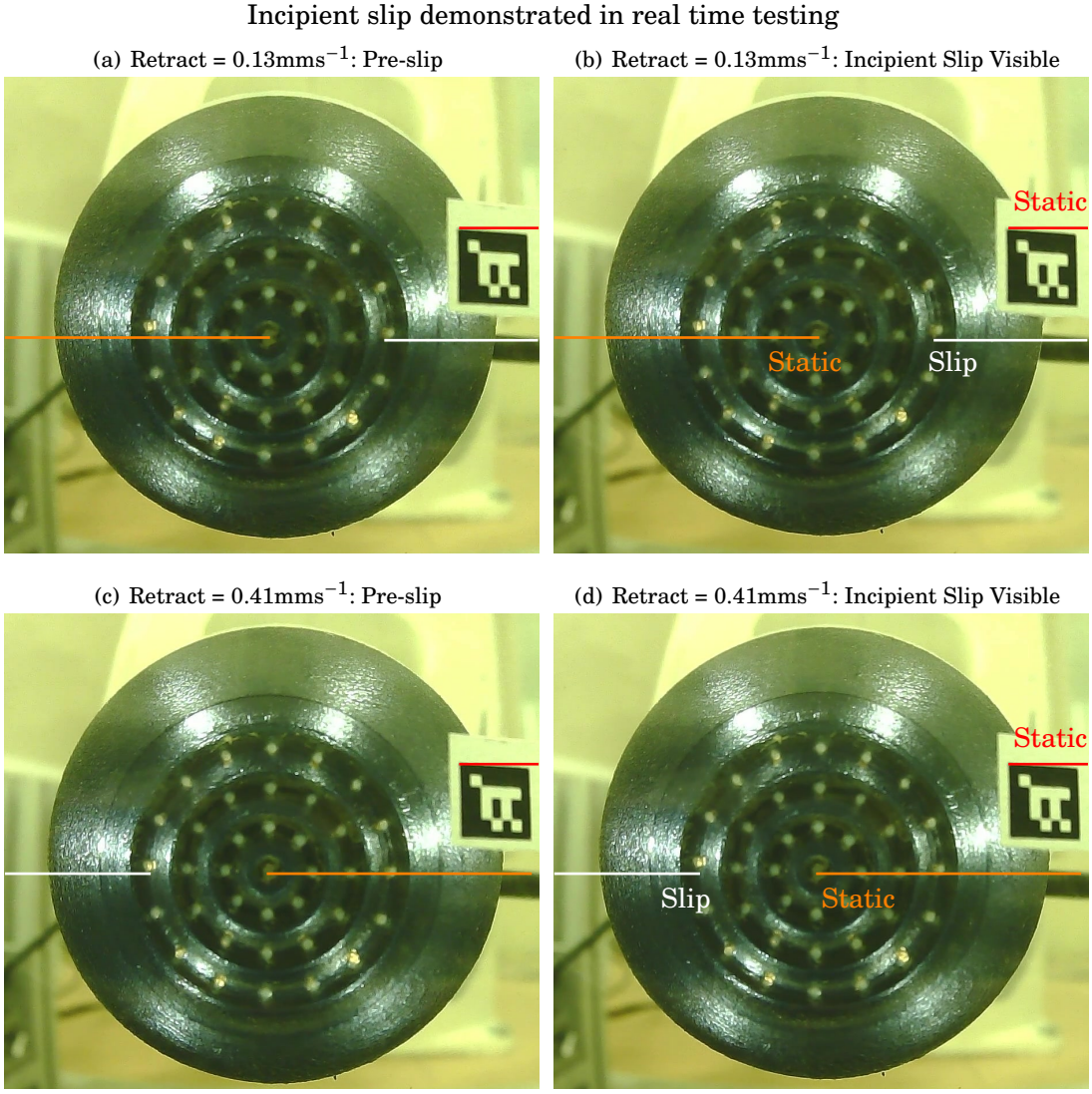

Figure 6.14: Incipient slip occurring in real time testing. Left column shows two different trials pre-slip. The right column, shows after the experiment has concluded. In both trials a small but clear incipient slip of certain pins is seen (white line) whilst the central pin (orange) and object (red) remain still. In both of these trials this was detected and the arm halted prior to the object falling.

the edge and the angle relative to the edge. When testing on 500 taps randomly sampled in the same angle and radius range as the training data the incipient slip sensor was able to resolve radius and angle with mean absolute errors of ~0.3mm and ~2 degrees. This is the same as the smooth TacTip as reported by Lepora et al. (2019) [106].

The similarity in numbers is encouraging as it indicates that the design changes for the incipient slip TacTip does not appear to have hampered the ability to perceive edges. It is not immediately obvious that the new design should perform similarly as the structure of the pins

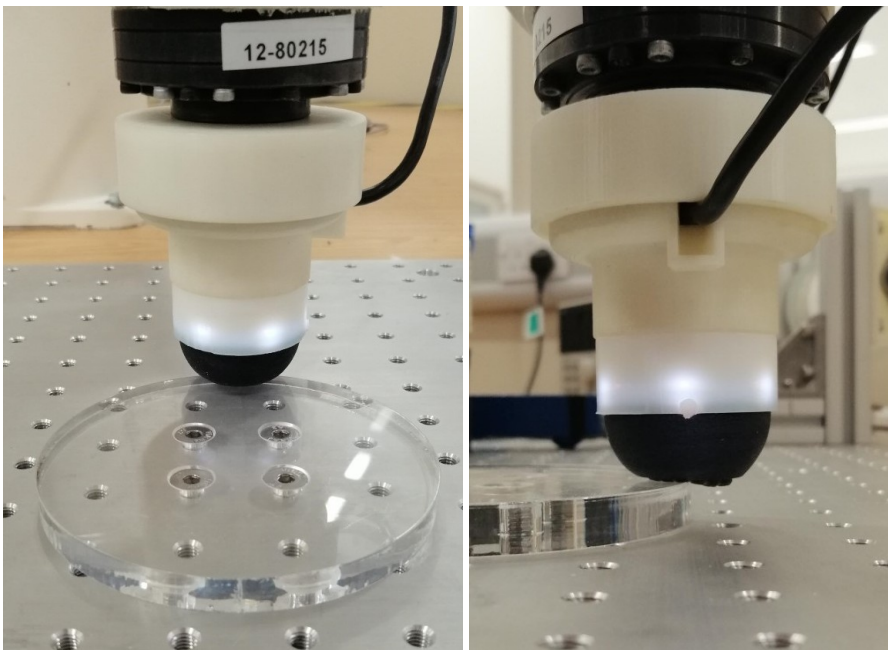

(a) (b)

Figure 6.15: Incipient Slip TacTip sensor attached to ABB IRB120 6 DoF robot arm tapping a circular object. A CNN is used to determine the radial position and angle of the sensor relative to the edge.

has significantly changed. Whilst the pins in the smooth TacTip sit on pillars - similarly to the Merkel cells on the intermediate ridges in the fingertip - here, the pins sit in troughs in the ridges - much like the Meissner's Corpuscles in the human fingertip.

As mentioned in Chapter 4 it is important to note that in Lepora et al. [106] this was tested on a larger test dataset of 2000 taps making it a more reliable test set. Additionally, as this was only a single test we cannot make wider predictions about performance in other tasks. A fair conclusion is that the new design does not appear to have lost the TacTip's strong tactile acuity and the incipient slip sensor design could be used as part of a multi-faceted modular system including incipient slip detection, edge perception, object classification and tactile servo control.

6.6 Discussion & Limitations

I will now discuss several more specific aspects of the work individually with regards to the results presented in this chapter and potential future investigations.

Presence of Incipient Slip: By recording the independent movement of both the internal and external pins it has been shown, without doubt, that a fingerprint inspired TacTip skin does facilitate incipient slip. In the second design this incipient slip was shown to occur at least 0.5s prior to object slip - and often much longer. This is larger than the slip prediction

windows of 30 ms achieved by Su et al. (2015) [198] and 20 ms reported by Veiga et al. [197]. However, here we are using only a single object, so further work is needed for a fair comparison. Having a larger time window for incipient slip onset provides more time - when manipulating an object, for example - to make a decision about whether to grasp tighter or cease movement completely. Additionally, it may not be necessary to react immediately upon incipient slip onset so an interesting study would be to use incipient slip to provide a metric of proximity to gross slip onset.

Friction Estimation: Having the ability to detect physical parameters of the contact between sensor and object could prevent the onset of incipient slip altogether. Having knowledge of the coefficient of friction and the forces applied can be used to determine the stability of contact with an object [207]. A controller can be coupled with this friction estimation to ensure the forces on the grasp remain within a specified margin of safety and reduce the risk of any slip at all. A potential downside of this approach is that estimating coefficients of friction without prior knowledge of an object is difficult [16] but the ability to have some measure of grasp stability without any surface movement would be highly useful and having an ensemble of methods including friction estimation and slip detection would be the best way to maximise grasp stability.

Ridge Morphology: The two sensor designs presented here had the same ridge height however the latter design had each concentric ring much closer together. This was done in an attempt to closer mimic the friction ridges of the human fingertip and provide a more dense contact area. However, the increased interstitial skin and reduced thickness of that skin in the initial design may be responsible for the lengthier incipient slip signal which in some cases occurred for several seconds. Investigation of the relationship between ridge morphology and distribution will be the subject of future research.

Another potential trade-off is between incipient slip signal and gross slip signal. Whilst the first sensor showed a more noticeable external slip signal there was little sign of gross slip (Fig. 6.5) whereas for the second iteration there was a large gross slip spike shortly after incipient slip (Fig. 6.12). Having both incipient slip and gross slip signals strongly present is advantageous because it allows for a modular system which can reliably detect both phenomena for added redundancy. Also, it cannot be guaranteed that incipient slip will always be noticeably present. The effect the ridge morphology and interstitial skin plays in facilitating gross slip will be an important investigation.

For this study the number of pins in the TacTip was reduced from the 127 present in the previous design (Chapter 3). Reducing the number of pins reduces the information density coming from the tactile sensor and therefore may affect the sensor's acuity - although the edge perception task did not suggest a significant loss of acuity here. Including more pins in each ring increases the number of fiducial markers which provide us with the incipient slip signal giving denser coverage of the sensor surface. We are tracking more areas of the sensor - any one of which may slip first - and therefore increase the chance of detecting the initial onset of incipient slip thereby

improving performance. An optimisation of pin density in the design was not performed here but should be considered in future to allow for early detection of incipient slip.

Incipient Slip Detection Method: The presented method was a simple method of extracting independent pin movement which can account for bulk motion of all the pins. Whilst it was successful at detecting incipient slip in real time and preventing the object falling in 17/20 trials there wasn't a rigorous optimisation or investigation of other potential methods. The purpose of this chapter is to demonstrate that a biomimetic fingerprint structure facilitates incipient slip and the real time detection study was intended to show that the incipient slip is detectable. Further investigation of detection methods would be undertaken in tandem with improved sensor design in future.

Part of the difficulty of developing an incipient slip detection method is in getting a ground truth for the precise frame where an individual pin is adjudged to be slipping. Whilst it is clear that pins are moving independently (Fig. 6.12) having a ground truth value for incipient slip on a pin-by-pin basis would allow for better offline testing of a future incipient slip detection method. Additionally, using this data one could display the ratio of stuck to slipping pins which would provide useful information about the timescale over which incipient slip occurs. At the current stage of sensor development a ground truth value would be subject to an error of up to a few frames so this remains a focus of future endeavours. Nevertheless, the primary focus of this chapter where incipient slip is directly verified is a significant result.

Another consideration that must be explored in future is the potential for confusion between slip and the movement of the compliant sensor surface or compliant objects. As the compression of a compliant surface will move the pins it is possible that this movement could be confused for slip. When training a future classifier for incipient slip detection it will be necessary to provide samples which represent pin movement from deformation of the sensor but *do not* relate to slip. However, it should be noted that in Chapter 5 slip was detectable when grasping compliant objects and overall performance using the TacTip has been strong. Regardless, this remains an important consideration which may improve performance.

Materials: In this work incipient slip has only been shown to be present on a single stimulus which moves in a low friction rail system. This is clearly not representative of the real world where a diversity of object shapes, weights and textures exists. The use of the clear stimulus only was to provide a ground truth of the presence of slip rather than relying on asserting that incipient slip occurs. A study of how well the sensor performs in a variety of different scenarios will be conducted with further enhancements to the sensor design.

6.7 Concluding Remarks

In this chapter, two iterations of a biomimetic tactile sensor have been presented which can facilitate and detect incipient slip, as confirmed by recording the movement of markers on the

external surface of the sensor. This is significant as we conclusively show the presence of incipient slip whereas many prior studies assert its existence from data [198, 256, 197]. Several changes to the TacTip design were made based on the physical conditions which facilitate incipient slip. The most significant change involved the addition of ridges - structurally analogous to human the fingerprint - in a concentric ring pattern which allowed for localised shear deformation to occur on the sensor surface for a significant duration prior to the onset of gross slip.

The first version of the sensor showed a clear signal on the external surface but lacked the same clarity from the internal view. To address this the ridged structure was changed to be continuous on both the internal and external surfaces and pins were added to the 'troughs' inside the sensor and extended all the way through the skin. This meant that the internal and external cameras would be recording the same markers which would suffer less from the levering effect which had previously drowned out the incipient slip signal.

If the skin of the TacTip is considered to be analogous to the epidermis of human skin and the gel analogous to the dermis then the ridged structure mimics the ridges of glabrous skin which, on the external surface, results in the fingerprint and on the internal surface results in the intermediate ridges and dermal papillae where the epidermis intersects with the dermis. The pins, in this analogy, work as Meissner's corpuscles sitting at the base of the intermediate ridges, although as previously stated the operating principle is different.. This demonstrates the strong biomimetic origin for the design choices in the new TacTip and may explain the clear incipient slip signal present in both the TacTip's internal and external view as well as in the human fingertip [52].

To summarise, in this chapter it has been shown that a biomimetic fingerprint on the rubber-like surface of an optical tactile sensor can reliably facilitate incipient slip. This is of direct practical utility to robotic hand research on dexterous manipulation of a grasped objects, as when used as part of a modular grasp stability system it would greatly reduces the chance of manipulated objects being dropped. This means that the final research question in this thesis, *does mimicking the human fingerprint result in detectable incipient slip in a tactile sensor*, has been affirmatively answered and the work in this chapter provides a clear direction for future research in the field of incipient slip.

In the subsequent, final, chapter I will summarise the work in this thesis and possible future avenues for exploration which it has facilitated.

CHAPTER 7

DISCUSSION AND FUTURE WORK

In this thesis, several developments in the field of slip detection research have been presented. This final chapter summarises these contributions and indicates further areas of study which could be investigated in the future.

7.1 Discussion and Limitations

Since its conception by Chorley et al. (2009) [2] the fundamental design principle of the sensor has remained unaltered - a camera focuses on a soft silicone mound with a rubber-like skin and information about the contact is inferred from the images. The major change in recent years has been the move to 3D-printing technology [3], exploring different software methods [106, 257, 105] and developing different sensor morphologies for integration onto robot hands [173].

This thesis has made contributions to several areas of slip detection and wider robotic research including robotic hand development, tactile skin morphologies, slip detection using robotic hands and incipient slip detection. I will discuss these contributions and their limitations below:

7.1.1 TacTip Camera Upgrade

The first change made to the TacTip was to upgrade the camera system from a 30FPS Microsoft LifeCam to an ELP camera capable of recording up to 120FPS. The higher frame rate system not only allows for faster reaction times, as the time between frames is smaller, but the camera has the capability to be operated at a choice of resolutions and frame rates. Higher resolution at lower frame rate may be desirable in certain circumstances such as when high acuity is necessary. Whereas higher frame rate is more useful in others, such as when detecting slip. The new system is also much easier to install requiring only four screws to be mounted on pillars in the base of

the TacTip [243]. The previous 3d-printed system required a disassembly to reduce the length of the sensor. The new camera continues to be used as the primary system by the entire Tactile Robotics research group.

Higher frame rate camera modules do exist but their cost can easily run into the thousands of pounds and they can be very large. This contravenes one of the primary design ideals of the TacTip which is to remain low cost. There is also the question of how much more useful higher frame rates would be. Even if you are able to record at many hundreds of frames-per-second it is not assured that this data stream would be usable in real time for decision making related to grasping. In experiments performed in this thesis with the new camera system 100 Hz has been the maximal frame rate achievable. This is still a significant improvement on the 30FPS used previously and is likely to be improved with more streamlined software and more efficient camera data encoders.

7.1.2 Gross Slip Detection

The first contribution of this thesis was the development of a simple method to reliably detect and respond to the onset of gross slip. This is beneficial as it gives a robot the ability to take a corrective action when slip occurs and prevent potentially catastrophic damage to an object hitting the floor. In Chapter 3 a support vector machine (SVM) was used to detect slip on a variety of curved objects which were allowed to fall in a low friction rail with a slipping distance of as little as 14.3mm [243].

An extension to this experiment was to test slip detection on several natural objects. More geometrically simple objects such as a water bottle were regrasped with 90% but a plastic banana was only stopped 30% of the time [258]. The lack of success in this case was due to the irregular shape; slip was detected but the response just pushed the banana off to the side. Each object used was novel to the classifier which shows it does not appear to be restricted to certain geometries. These experiments were conducted under similar conditions and obtained comparable results to Veiga et al. [197] who also performed regrasping with a single BioTac sensor sampling at 100 Hz.

The choice of classification method may be seen by some as 'behind the curve' compared to popular modern methods such as CNNs [13] or LSTMs [206]. However neither method has been shown to significantly outperform SVMs and that is without considering some of the advantages of SVMs. First is training time and dataset size, SVMs do not require large datasets to obtain good performance and can be optimized in only a few minutes. When performing physical tasks collecting large datasets becomes incredibly time-intensive so having a method which performs well on a task after only a few samples is beneficial when using a sensor which goes through many design iterations. Another advantage is the memory requirements to run the model. Unlike deep neural networks which may contain billions of parameters SVMs can be on the order of single megabytes which could be utilised by small computers and microcontrollers without the need for expensive GPUs. These features also make classification time very short. Classification

was clocked at 3 milliseconds in Chapter 3 which is significantly smaller than the time between frames - 10ms at 100Hz.

A limitation of this work is the limited number of testing scenarios. The only considered situation was where an object slips due to gravity. As the SVM learned from the distribution of pin velocities it may be susceptible to false positives when lifting an object and the sensor surface is stretching under a load. Additionally, having a single sensor moving with a single degree of freedom means that the ability to regrasp objects is limited. However, the fact that slip was reliably detected across all objects provides the contribution of Chapter 3. This Chapter also showed that the design and operating principle of the TacTip made further research into slip detection with the TacTip on a more suitable platform - in this case a robotic hand - highly justified.

7.1.3 Tactile Robot Hands

In Chapter 4 the development of the Tactile Model O (T-MO), a three-fingered tactile hand that comprises a GRAB Lab Model O modified to include three TacTip optical tactile sensors in its fingertips, was presented. Small cameras mounted above the 3D-printed fingertips meant that the T-MO retained the TacTip's sensing modality and JeVois vision system modules integrated into the 'palm' performed the image processing. The system is dual-modal, pins in the sensors can be detected onboard the hand or a video stream captured and sent directly to a control PC.

Grasping capability was evaluated using the Gripper Assessment Benchmark and Extended Gripper Assessment Benchmark using the YCB object set [176]. Whilst there was a modest drop in performance compared to the Model O, the Tactile Model O outperformed the iCub and Model T hands highlighting that the addition of tactile sensing did not affect the T-MO's validity as a grasping platform. The primary reason for the loss of grasping performance is the thickness of the fingertip caused by mounting the camera above the sensor surface. The camera needs to be away from the surface so that the field-of-view contains the contact surface. This means that there is no 'fingernail' on the sensor so smaller objects could not be grasped by sliding the fingernail underneath to establish a grasp.

Further work using the T-MO indicated that it had very strong performance at real time slip detection and object regrasping. This meant that in situations where an object was being held and the grasp transitioned from stable to unstable the T-MO was able to detect this and perform an action to recover the stable grasp before the object was dropped. Whilst this was tested on multiple objects, several of which were novel, the grasping mode was always an antipodal pinch and the objects used were large. This was done for two reasons: first, as previously discussed, the T-MO was unable to grasp small objects so the testing was focused on objects the T-MO could comfortably pick up. Secondly, the antipodal pinch was necessary as the sensors are only at the fingertips and that grasping mode therefore maximises sensor contact.

Another success of the T-MO was the ability to apply slip detection to two grasping scenarios

using the same classifier. These scenarios involved grasping an object of unknown weight, first time, without excessive force and being able to react when the weight of an object was changed. Some studies such as Dong et al. [15] use multiple attempts at grasping an object until the desired grasping location and force are determined. Whilst the object set for this task was limited to two objects this shows that slip detection has potential to be used as a metric to not only evaluate the stability of an established grasp but also determine a grasp in the process of being established is sufficiently strong.

Examination of the slip data did not indicate the presence of incipient slip which, given other work on incipient slip in this thesis, can be seen as a limitation. However, the smooth sensor surface indicates that the lack of incipient slip is unsurprising and further work combining the benefits of slip detection on the T-MO with knowledge gained from incipient slip detection on the hemispherical TacTip is required. Ultimately, using gross slip detection, the T-MO demonstrated strong performance at grasping objects, preventing novel objects from being dropped and was useful in real-world grasping scenarios without the need for task-specific classifier training.

7.1.4 Incipient Slip Detection

Following on from gross slip detection the logical next step was the investigation of incipient slip. In Chapter 6, two sensors were presented with a biomimetic fingerprint design which showed a clear incipient slip signal. The principal requirement when it comes to the observation of incipient slip is that independent movement of parts of the sensor surface must be directly observed. Here, this was ensured by extending the internal pins through the skin of the TacTip such that they were visible on the external surface. By testing slip on a transparent object these external markers were tracked and independent movement was confirmed. As discussed in Section 6.1 the confirmation of incipient slip rather than its inference is an issue that persists in studies addressing incipient slip.

Recording both the internal and external markers also allowed for the calculation of a time window, prior to gross slip and object slip, during which incipient slip occurs. Here, incipient slip was shown to occur at least 0.5s prior to object slip - and often much longer. This is an order of magnitude larger than the slip prediction windows of 30 ms achieved by Su et al. (2015) [198] and 20 ms reported by Veiga et al. [197]. However, here we are using only a single object, so further work is needed for a fair comparison.

The two incipient slip sensor designs presented here had small differences in their surface morphology which may have contributed to the differing incipient slip signals. Both had concentric rings of ridges on the external surface with same ridge height however the latter design had each concentric ring much closer together. This was done to mimic human fingertip friction ridges which have little spacing between them and to provide a more dense sensing area. However, the increased interstitial skin and reduced thickness of said skin in the initial design may have contributed to the lengthier incipient slip window; due to outer rings being in a region of lower

normal force. This will be a focus of future research because, as stated, the primary requirement for detecting incipient slip is that the signal is visible on both internal and external surface. Only the second design demonstrated this making it clearly superior.

Another related point to consider is the trade-off between incipient slip signal and gross slip signal. For a given sensor deformation there is only so much the pins can move before returning to their *at rest* positions. Therefore, it makes sense that a larger incipient slip signal would result in a smaller gross slip signal. The first incipient slip sensor presented showed a very strong incipient slip signal but there was little sign of gross slip (Fig. 6.5). Compare this to the tests done with the smooth sensor in Chapter 3 (Fig. 3.7) where the large gross slip signal was what made the sensor so effective at detecting gross slip. The second iteration showed a large gross slip spike shortly after incipient slip (Fig. 6.12). Having both incipient slip and gross slip signals strongly present is advantageous because it allows for a modular system which can reliably detect both phenomena for added redundancy.

Given the TacTip's history as an effective sensor for tactile perception and control it is important to determine whether significantly altering the surface design would affect its other strengths. I demonstrated in Chapter 6 that on an edge perception task following the same data collection and inference procedure as described in Lepora et al. (2019) [106] there was no drop in performance. Whilst this result does not allow for any quantitative discussion of relative performance in perception and control tasks between the two designs, it is fair to conclude that the addition of a fingerprint structure for incipient slip facilitation has not come at the cost of dramatically altered perception capability.

7.2 Future Work

Incipient Slip Sensor Design: The two incipient slip sensors presented in Chapter 6 both showed a clear incipient slip signal. Whilst, ultimately, the second sensor was judged to be more effective as the signal was clear from both cameras, the first sensor showed incipient slip over a longer timescale. There were two primary differences in the sensor design: ring spacing and ridge cross-sectional shape. Increasing the time window during which incipient slip occurs provides more time to change a grasp to prevent failure, giving a large operational benefit. Future work on design will investigate the effect of altering these factors to determine the effect on incipient slip facilitation.

Incipient slip detection method: In Chapter 6 a simple method of extracting independent pin movement was used to detect incipient slip in real-time. The method accounted for bulk motion of all the pins and identified which pins were moving independently. Whilst it was successful at detecting incipient slip in real time and preventing the object falling in 17/20 trials there wasn't a rigorous optimisation or investigation of other potential methods. There are many methods currently used to detect incipient slip [16] and future work performing an analysis of

potential methods would be beneficial for the continued development of incipient slip sensors.

Incipient Slip on Tactile Robot Hands: A logical progression of the work in this thesis would be to combine the results of Chapters 4 and 6 and develop an incipient slip sensor for a multi-fingered tactile hand. This would allow for incipient slip to be tested in real world grasping scenarios with a wide variety of objects. A limitation of the incipient slip work here was that it was tested using a transparent object for verification purposes. Furthermore, it would be of interest to investigate incipient slip correction strategies as was done with gross slip in Chapter 5 with a focus on *when* it is necessary to respond to incipient slip onset. Immediate response to incipient slip may be unnecessary during a grasping task if there is, in fact, no immediate danger of total grasp failure. Instead, the calculation of a metric which determines how close to failure a grasp is would prevent unnecessary grasp planning and allow for the adoption of a risk mitigation policy on a case-by-case basis depending on need.

Tactile Model O Modification: To further increase the utility of the T-MO decreasing the height profile of the distal phalanges and the addition of a fingernail should be investigated. This could be addressed by testing smaller cameras or mirror arrays [129]. These changes should allow for the grasping of small objects as was possible for the GRABLab Model O [159].

7.3 Conclusion

The ultimate goal of this thesis has been to demonstrate the usefulness of slip detection to tactile robotics with a focus on gross and incipient slip detection. The other significant message this thesis sought to present was the benefit of low-cost optical tactile sensing. These aims were broken down in the Introduction into five research questions which will be concluded individually.

The first question raised in the Introduction was: *can a simple method be used with the TacTip biomimetic optical tactile sensor to detect slip and prevent total loss of contact with an object?* It was demonstrated that the TacTip exhibits a strong gross slip signal, an SVM can reliably detect it and a basic response can prevent droppage [243, 258].

Secondly, it was posed: *does the addition of tactile sensing to a robotic manipulator enhance effectiveness of the system?* Through the development and presentation of the T-MO strong performance was demonstrated at grasping and tactile object recognition [239] as well as being highly effective at slip detection [259].

The purpose of creating the T-MO was to answer our third question: *can a low-cost multi-fingered manipulator be used to reliably detect slip?* Using several object to train a support vector machine and then test on both the known objects and novel objects the T-MO was shown to detect slip in real-time. The T-MO also reliably responded to catch these objects to prevent them being dropped.

Having determined that gross slip is reliably detected we next sought to answer: *can slip detection be used as a metric to evaluate the stability of a grasp and improve grasping efficiency?*

This was answered by applying the developed slip classifier to two real world grasping situations: the gradual addition of weight to destabilise an object and first time grasping of objects. With no further training the SVM was successful when applied to both of these tasks indicating that slip detection is useful when establishing grasps and preventing them from failing.

Finally, to progress from gross slip detection it was asked: *does mimicking the human fingerprint result in detectable incipient slip in a tactile sensor?* Adding a concentric ring structure reminiscent of the friction ridges of the human fingerprint and structuring the pins inside the TacTip to resemble the Meissner's corpuscles in the dermal papillae did indeed facilitate detectable incipient slip. Crucially, this was visible when recording both the internal and external markers providing a verifiable incipient slip signal.

To conclude, this thesis has made several contributions to the field of tactile robotics by furthering knowledge relating to gross slip detection, tactile robot grasping and incipient slip. Everything in research has limitations and this work is no exception but this only serves to provide more questions and motivate further research. The avenues of research which this work has opened up shows that slip detection and tactile robot grasping has many decades of research left to be done and many problems still to solve.

When I started out on the journey that was this thesis I wanted determine how useful the ability to reliably detect slip could be. My research has demonstrated that slip detection is highly beneficial in many areas of robot grasping including when lifting objects and using gross and incipient slip detection to reduce the risk of dropping objects, all of which can be achieved using low-cost parts. This highlights how important having slip detection capability is to a robot grasping system and should encourage researchers and manufacturers to consider the inclusion of slip detection as a high priority. Robots endowed with highly sophisticated touch will be better able to interact with the world and more safely engage with humans. When applied carefully and responsibly this has the potential to transform human society for the better. It is, therefore, my hope that this thesis has earned its place as a small part of this ongoing mission to achieve human-level touch capability in robotics.

BIBLIOGRAPHY

[1] R. S. Johansson and J. R. Flanagan, "Coding and use of tactile signals from the fingertips in object manipulation tasks," *Nature Reviews Neuroscience*, vol. 10, no. 5, p. 345, 2009.

[2] C. Chorley, C. Melhuish, T. Pipe, and J. Rossiter, "Development of a tactile sensor based on biologically inspired edge encoding," in *Advanced Robotics, 2009. ICAR 2009. International Conference on*, pp. 1–6, IEEE, 2009.

[3] B. Ward-Cherrier, N. Pestell, L. Cramphorn, B. Winstone, M. E. Giannaccini, J. Rossiter, and N. F. Lepora, "The TacTip Family: Soft Optical Tactile Sensors with 3D-Printed Biomimetic Morphologies," *Soft robotics*, 2018.

[4] A. Bicchi, J. K. Salisbury, and P. Dario, "Augmentation of grasp robustness using intrinsic tactile sensing," in *Robotics and Automation, 1989. Proceedings., 1989 IEEE International Conference on*, pp. 302–307, IEEE, 1989.

[5] S. Luo, W. Mou, K. Althoefer, and H. Liu, "Localizing the object contact through matching tactile features with visual map," in *Robotics and Automation (ICRA), 2015 IEEE International Conference on*, pp. 3903–3908, IEEE, 2015.

[6] R. Bajcsy, S. J. Lederman, and R. L. Klatzky, "Object exploration in one and two fingered robots," in *Proceedings of the 1987 IEEE International Conference on Robotics and Automation, Computer Society Press, New York*, vol. 3, pp. 1806–1810, 1987.

[7] J. C. Rothwell, M. M. Traub, B. L. Day, J. A. Obeso, P. K. Thomas, and C. D. Marsden, "Manual motor performance in a deafferented man," *Brain*, vol. 105, pp. 515–542, 9 1982.

[8] R. Johansson and G. Westling, "Roles of glabrous skin receptors and sensorimotor memory in automatic control of precision grip when lifting rougher or more slippery objects," *Experimental Brain Research*, vol. 56, pp. 550–564, 10 1984.

[9] M. A. Srinivasan, J. M. Whitehouse, and R. H. LaMotte, "Tactile detection of slip: surface microgeometry and peripheral neural codes," *Journal of neurophysiology*, vol. 63, no. 6, pp. 1323–1332, 1990.

[10] A. M. Smith, C. E. Chapman, M. Deslandes, J. S. Langlais, and M. P. Thibodeau, "Role of friction and tangential force variation in the subjective scaling of tactile roughness," *Experimental Brain Research*, vol. 144, no. 2, pp. 211–223, 2002.

[11] M. A. Srinivasan and R. H. LaMotte, "Tactual discrimination of softness," *Journal of Neurophysiology*, vol. 73, no. 1, pp. 88–101, 1995.

[12] R. D. Howe and M. R. Cutkosky, "Sensing skin acceleration for slip and texture perception," in *Robotics and Automation, 1989. Proceedings., 1989 IEEE International Conference on*, pp. 145–150, IEEE, 1989.

[13] M. Meier, F. Patzelt, R. Haschke, and H. J. Ritter, "Tactile Convolutional Networks for Online Slip and Rotation Detection," in *International Conference on Artificial Neural Networks*, pp. 12–19, Springer, Cham, 2016.

[14] Y. Zhang, Z. Kan, Y. A. Tse, Y. Yang, and M. Y. Wang, "FingerVision Tactile Sensor Design and Slip Detection Using Convolutional LSTM Network," *ArXiv preprint*, 10 2018.

[15] S. Dong, W. Yuan, and E. H. Adelson, "Improved GelSight tactile sensor for measuring geometry and slip," in *2017 IEEE/RSJ International Conference on Intelligent Robots and Systems (IROS)*, pp. 137–144, 9 2017.

[16] W. Chen, H. Khamis, I. Birznieks, N. F. Lepora, and S. J. Redmond, "Tactile Sensors for Friction Estimation and Incipient Slip Detection—Toward Dexterous Robotic Manipulation: A Review," *IEEE Sensors Journal*, vol. 18, pp. 9049–9064, 11 2018.

[17] T. J. Prescott, M. J. Pearson, B. Mitchinson, J. C. W. Sullivan, and A. G. Pipe, "Whisking with robots: From rat vibrissae to biomimetic technology for active touch," *IEEE Robotics and Automation Magazine*, vol. 16, no. 3, pp. 42–50, 2009.

[18] P. S. Sreetharan, J. P. Whitney, M. D. Strauss, and R. J. Wood, "Monolithic fabrication of millimeter-scale machines," *Journal of Micromechanics and Microengineering*, vol. 22, p. 055027, 5 2012.

[19] N. F. Lepora, P. Verschure, and T. J. Prescott, "The state of the art in biomimetics," 3 2013.

[20] J. L. Rhudy and C. R. France, "Defining the nociceptive flexion reflex (NFR) threshold in human participants: A comparison of different scoring criteria," *Pain*, vol. 128, pp. 244–253, 4 2007.

[21] N. Wheatland, Y. Wang, H. Song, M. Neff, V. Zordan, and S. Jörg, "State of the art in hand and finger modeling and animation," 2015.

[22] R. Tubiana, J.-M. Thomine, and E. Mackin, "Examination of the Hand and Wrist," Taylor & Francis, 1998.

[23] H.-M. Schmidt and U. Lanz, "Surgical anatomy of the hand," p. 259, Thieme, 2004.

[24] R. S. Johansson and A. B. Vallbo, "Tactile sensory coding in the glabrous skin of the human hand," *Trends in Neurosciences*, vol. 6, pp. 27–32, 1 1983.

[25] R. L. Klatzky and S. J. Lederman, "Touch," in *Handbook of Psychology*, pp. 147–176, Hoboken, NJ, USA: John Wiley & Sons, Inc., 4 2003.

[26] M. J. Hertenstein, D. Keltner, B. App, B. A. Bulleit, and A. R. Jaskolka, "Touch communicates distinct emotions.," *Emotion*, vol. 6, no. 3, pp. 528–533, 2006.

[27] R. Dunbar, "The social role of touch in humans and primates: Behavioural function and neurobiological mechanisms," *Neuroscience & Biobehavioral Reviews*, vol. 34, pp. 260–268, 2 2010.

[28] F. Mancini, A. Bauleo, J. Cole, F. Lui, C. A. Porro, P. Haggard, and G. D. Iannetti, "Whole-body mapping of spatial acuity for pain and touch.," *Annals of neurology*, vol. 75, pp. 917–24, 6 2014.

[29] J. C. Craig, "Grating orientation as a measure of tactile spatial acuity," *Somatosensory & Motor Research*, vol. 16, pp. 197–206, 1 1999.

[30] J. M. Loomis, "On the tangibility of letters and braille," *Perception & Psychophysics*, vol. 29, pp. 37–46, 1 1981.

[31] R. L. Klatzky, S. J. Lederman, and V. A. Metzger, "Identifying objects by touch: An "expert system"," *Perception & Psychophysics*, vol. 37, pp. 299–302, 7 1985.

[32] A. Biswas, M. Manivannan, and M. A. Srinivasan, "Multiscale Layered Biomechanical Model of the Pacinian Corpuscle," *IEEE Transactions on Haptics*, vol. 8, pp. 31–42, 1 2015.

[33] K. S. Severson, D. Xu, M. Van de Loo, L. Bai, D. D. Ginty, and D. H. O'Connor, "Active Touch and Self-Motion Encoding by Merkel Cell-Associated Afferents," *Neuron*, vol. 94, pp. 666–676, 5 2017.

[34] V. B. Mountcastle, "The sensory hand : neural mechanisms of somatic sensation," p. 616, Harvard University Press, 2005.

[35] K. O. Johnson, "The roles and functions of cutaneous mechanoreceptors," *Current Opinion in Neurobiology*, vol. 11, pp. 455–461, 8 2001.

[36] M. Knibestöl, "Stimulus-response functions of slowly adapting mechanoreceptors in the human glabrous skin area.," *The Journal of Physiology*, vol. 245, pp. 63–80, 2 1975.

[37] R. S. Johansson, "Tactile sensibility in the human hand: receptive field characteristics of mechanoreceptive units in the glabrous skin area.," *The Journal of Physiology*, vol. 281, pp. 101–125, 8 1978.

[38] R. Johansson and A. Vallbo, "Spatial properties of the population of mechanoreceptive units in the glabrous skin of the human hand," *Brain Research*, vol. 184, pp. 353–366, 2 1980.

[39] E. R. Kandel, J. H. J. H. Schwartz, and T. M. Jessell, "Principles of neural science," p. 1414, McGraw-Hill, Health Professions Division, 2000.

[40] G. Westling and R. Johansson, "Responses in glabrous skin mechanoreceptors during precision grip in humans," *Experimental Brain Research*, vol. 66, pp. 128–140, 3 1987.

[41] R. Spielman, W. Jenkins, Dumper Kathryn;, A. Lacombe, M. Lovett, and M. Perlmutter, "Psychology," OpenStax, 2014.

[42] J. C. Craig and J. M. Kisner, "Factors affecting tactile spatial acuity," *Somatosensory and Motor Research*, vol. 15, no. 1, pp. 29–45, 1998.

[43] J. M. Wolfe, K. R. Kluender, D. M. Levi, L. Bartoshuk, R. Herz, R. L. Klatzky, and D. M. D. M. Merfeld, "Sensation & perception," p. 15, Sinauer, 2017.

[44] S. Weinstein, "Intensive and extensive aspects of tactile sensitivity as a function of body part, sex and laterality," *The Skin Senses*, 1968.

[45] J. C. Stevens and K. K. Choo, "Temperature sensitivity of the body surface over the life span," *Somatosensory and Motor Research*, vol. 15, no. 1, pp. 13–28, 1998.

[46] R. Johansson and J. Flanagan, "Tactile Sensory Control of Object Manipulation in Humans," in *The Senses: A Comprehensive Reference*, pp. 67–86, Elsevier, 2008.

[47] A. Bodegård, A. Ledberg, S. Geyer, E. Naito, K. Zilles, and P. E. Roland, "Object Shape Differences Reflected by Somatosensory Cortical Activation in Human," *Journal of Neuroscience*, vol. 20, no. 1, 2000.

[48] R. S. Dahiya, G. Metta, M. Valle, and G. Sandini, "Tactile sensing-from humans to humanoids," *IEEE Transactions on Robotics*, vol. 26, pp. 1–20, 2 2010.

[49] J. R. Jenner and J. A. Stephens, "Cutaneous reflex responses and their central nervous pathways studied in man," *The Journal of Physiology*, vol. 333, pp. 405–419, 12 1982.

[50] R. S. Johansson and R. H. Lamotte, "Tactile Detection Thresholds for a Single Asperity on an Otherwise Smooth Surface," *Somatosensory Research*, vol. 1, pp. 21–31, 1 1983.

[51] M. T. Francomano, D. Accoto, and E. Guglielmelli, "Artificial Sense of Slip—A Review," *IEEE Sensors Journal*, vol. 13, pp. 2489–2498, 7 2013.

[52] M. Tada and T. Kanade, "An imaging system of incipient slip for modelling how human perceives slip of a fingertip," in *The 26th Annual International Conference of the IEEE Engineering in Medicine and Biology Society*, vol. 3, pp. 2045–2048, IEEE, 2004.

[53] R. Johansson and G. Westling, "Signals in tactile afferents from the fingers eliciting adaptive motor responses during precision grip," *Experimental Brain Research*, vol. 66, pp. 141–154, 3 1987.

[54] H. R. Nicholls and M. H. Lee, "A Survey of Robot Tactile Sensing Technology," *The International Journal of Robotics Research*, vol. 8, pp. 3–30, 6 1989.

[55] G.-I. Kinoshita, "Classification of Grasped Object's Shape by an Artificial Hand With Multi-element Tactile Sensors," *Information-Control Problems in Manufacturing Technology*, pp. 111–118, 1 1978.

[56] M. Briot and others, "The utilization of an artificial skin sensor for the identification of solid objects," in *9th Int. Symp. on Industrial Robots*, pp. 13–15, 1979.

[57] W. E. Snyder and J. St. Clair, "Conductive Elastomers as Sensor for Industrial Parts Handling Equipment," *IEEE Transactions on Instrumentation and Measurement*, vol. 27, no. 1, pp. 94–99, 1978.

[58] L. D. Harmon, "Automated Tactile Sensing," *The International Journal of Robotics Research*, vol. 1, pp. 3–32, 6 1982.

[59] M. H. Lee, "Tactile sensing: new directions, new challenges," *The International Journal of Robotics Research*, vol. 19, no. 7, pp. 636–643, 2000.

[60] J. P. Christ and A. C. Sanderson, "A Prototype Tactile Sensor Array.," 1982.

[61] P. Dario, D. De Rossi, C. Domenici, and R. Francesconi, "Ferroelectric polymer tactile sensors with anthropomorphic features," in *Proceedings. 1984 IEEE International Conference on Robotics and Automation*, vol. 1, pp. 332–340, 1984.

[62] J. D. Abramowitz, J. W. Goodnow, B. Paul, and others, "Pennsylvania Articulated Mechanical Hand: An End Effector to Determine Shape by Touch," University of Pennsylvania, Department of Computer and Information Science, 1984.

[63] R. A. Boie, "Capacitive impedance readout tactile image sensor," in *Proceedings. 1984 IEEE International Conference on Robotics and Automation*, vol. 1, pp. 370–378, 1984.

[64] R. F. Wolffenbuttel and P. P. L. Regtien, "Integrated capacitive tactile imaging sensor," in *Proc. 16th Int. Symp. Industrial Robots, Brussels*, pp. 633–641, 1986.

[65] G. Kinoshita, T. Hajika, and K. Hattori, "Multifunctional tactile sensors with multielements for fingers," in *Proceedings of the International Conference on Advanced Robotics*, pp. 195–202, 1983.

[66] R.-C. Luo, F. Wang, and Y.-x. Liu, "An imaging tactile sensor with magnetostrictive transduction," in *Intelligent Robots and Computer Vision*, vol. 521, pp. 264–270, 1985.

[67] J. Schoenwald, A. Thiele, and D. Gjellum, "A novel fiber optic tactile array sensor," in *Proceedings. 1987 IEEE International Conference on Robotics and Automation*, vol. 4, pp. 1792–1797, 1987.

[68] N. Ghani, "Esprit 278-a collaborative sensors project," in *CIA4 Europe Conference (4th)*, pp. 59–70, 1988.

[69] Z. Kappassov, J.-A. Corrales, and V. Perdereau, "Tactile sensing in dexterous robot hands — Review," *Robotics and Autonomous Systems*, vol. 74, pp. 195–220, 12 2015.

[70] A. Barlian, W.-T. Park, J. Mallon, A. Rastegar, and B. Pruitt, "Review: Semiconductor Piezoresistance for Microsystems," *Proceedings of the IEEE*, vol. 97, pp. 513–552, 3 2009.

[71] A. Arnau, "Piezoelectric transducers and applications," p. 319, Springer, 2004.

[72] S. Kon, K. Oldham, and R. Horowitz, "Piezoresistive and piezoelectric MEMS strain sensors for vibration detection," in *Sensors and Smart Structures Technologies for Civil, Mechanical, and Aerospace Systems* (M. Tomizuka, C.-B. Yun, and V. Giurgiutiu, eds.), vol. 6529, p. 65292V, International Society for Optics and Photonics, 4 2007.

[73] K. Weiss and H. Worn, "The working principle of resistive tactile sensor cells," in *IEEE International Conference Mechatronics and Automation*, pp. 471–476, IEEE, 2005.

[74] R. Koiva, M. Zenker, C. Schurmann, R. Haschke, and H. J. Ritter, "A highly sensitive 3D-shaped tactile sensor," in *2013 IEEE/ASME International Conference on Advanced Intelligent Mechatronics*, pp. 1084–1089, IEEE, 7 2013.

[75] G. H. Büscher, R. Kõiva, C. Schürmann, R. Haschke, and H. J. Ritter, "Flexible and stretchable fabric-based tactile sensor," *Robotics and Autonomous Systems*, vol. 63, pp. 244–252, 1 2015.

[76] S. Stassi, V. Cauda, G. Canavese, and C. Pirri, "Flexible Tactile Sensing Based on Piezoresistive Composites: A Review," *Sensors*, vol. 14, pp. 5296–5332, 3 2014.

[77] G. G. Gautschi, "Piezoelectric sensorics : force, strain, pressure, acceleration and acoustic emission sensors, materials and amplifiers," p. 264, Springer, 2002.

[78] J. Dargahi, "A piezoelectric tactile sensor with three sensing elements for robotic, endoscopic and prosthetic applications," *Sensors and Actuators A: Physical*, vol. 80, pp. 23–30, 3 2000.

[79] C.-H. Chuang, M.-S. Wang, Y.-C. Yu, C.-L. Mu, K.-F. Lu, and C.-T. Lin, "Flexible tactile sensor for the grasping control of robot fingers," in *2013 International Conference on Advanced Robotics and Intelligent Systems*, pp. 141–146, IEEE, 5 2013.

[80] D. Goger, N. Gorges, and H. Worn, "Tactile sensing for an anthropomorphic robotic hand: Hardware and signal processing," in *2009 IEEE International Conference on Robotics and Automation*, pp. 895–901, IEEE, 5 2009.

[81] M. Zillich and W. Feiten, "A versatile tactile sensor system for covering large and curved surface areas," in *2012 IEEE/RSJ International Conference on Intelligent Robots and Systems*, pp. 20–24, IEEE, 10 2012.

[82] Y. Tenzer, L. P. Jentoft, and R. D. Howe, "The Feel of MEMS Barometers: Inexpensive and Easily Customized Tactile Array Sensors," *IEEE Robotics & Automation Magazine*, vol. 21, pp. 89–95, 9 2014.

[83] P. Piacenza, S. Sherman, and M. Ciocarlie, "Data-Driven Super-Resolution on a Tactile Dome," *IEEE Robotics and Automation Letters*, vol. 3, pp. 1434–1441, 7 2018.

[84] SynTouch, "BioTac Sensor." Available at: https://www.syntouchinc.com/sensor-technology/, 2017.

[85] N. Wettels, V. J. Santos, R. S. Johansson, and G. E. Loeb, "Biomimetic Tactile Sensor Array," *Advanced Robotics*, vol. 22, pp. 829–849, 1 2008.

[86] N. Wettels, A. Parnandi, Ji-Hyun Moon, G. Loeb, and G. Sukhatme, "Grip Control Using Biomimetic Tactile Sensing Systems," *IEEE/ASME Transactions on Mechatronics*, vol. 14, pp. 718–723, 12 2009.

[87] J. A. Fishel and G. E. Loeb, "Bayesian Exploration for Intelligent Identification of Textures," *Frontiers in Neurorobotics*, vol. 6, p. 4, 6 2012.

[88] E. Kerr, S. Coleman, M. McGinnity, and A. Shepherd, "Measurement of Capillary Refill Time (CRT) in Healthy Subjects Using a Robotic Hand," 2018.

[89] Hyung-Kew Lee, Jaehoon Chung, Sun-Il Chang, and Euisik Yoon, "Normal and Shear Force Measurement Using a Flexible Polymer Tactile Sensor With Embedded Multiple Capacitors," *Journal of Microelectromechanical Systems*, vol. 17, pp. 934–942, 8 2008.

[90] A. Schmitz, P. Maiolino, M. Maggiali, L. Natale, G. Cannata, and G. Metta, "Methods and Technologies for the Implementation of Large-Scale Robot Tactile Sensors," *IEEE Transactions on Robotics*, vol. 27, pp. 389–400, 6 2011.

[91] C. A. Jara, J. Pomares, F. A. Candelas, F. Torres, C. A. Jara, J. Pomares, F. A. Candelas, and F. Torres, "Control Framework for Dexterous Manipulation Using Dynamic Visual Servoing and Tactile Sensors' Feedback," *Sensors*, vol. 14, pp. 1787–1804, 1 2014.

[92] J. M. Romano, K. Hsiao, G. Niemeyer, S. Chitta, and K. J. Kuchenbecker, "Human-Inspired Robotic Grasp Control With Tactile Sensing," *IEEE Transactions on Robotics*, vol. 27, pp. 1067–1079, 12 2011.

[93] B. Heyneman and M. R. Cutkosky, "Biologically inspired tactile classification of object-hand and object-world interactions," in *2012 IEEE International Conference on Robotics and Biomimetics (ROBIO)*, pp. 167–173, IEEE, 12 2012.

[94] M. Razavy, "Quantum Theory of Tunneling," World Scientific, 2003.

[95] A. B. Balantekin and N. Takigawa, "Quantum tunneling in nuclear fusion," *Reviews of Modern Physics*, vol. 70, pp. 77–100, 1 1998.

[96] T. Zhang, H. Liu, L. Jiang, S. Fan, and J. Yang, "Development of a Flexible 3-D Tactile Sensor System for Anthropomorphic Artificial Hand," *IEEE Sensors Journal*, vol. 13, pp. 510–518, 2 2013.

[97] T. Martin, R. Ambrose, M. Diftler, R. Platt, and M. Butzer, "Tactile gloves for autonomous grasping with the NASA/DARPA Robonaut," in *IEEE International Conference on Robotics and Automation, 2004. Proceedings. ICRA '04. 2004*, pp. 1713–1718, IEEE, 2004.

[98] T. Zhang, S. Fan, Jingdong Zhao, L. Jiang, and H. Liu, "Multifingered robot hand dynamic grasping control based on fingertip three-axis tactile sensor feedback," in *Proceeding of the 11th World Congress on Intelligent Control and Automation*, pp. 3321–3326, IEEE, 6 2014.

[99] A. Kolker, M. Jokesch, and U. Thomas, "An Optical Tactile Sensor for Measuring Force Values and Directions for Several Soft and Rigid Contacts," in *Proceedings of ISR 2016: 47st International Symposium on Robotics*, pp. 1–6, 6 2016.

[100] K. Shimonomura, "Tactile Image Sensors Employing Camera: A Review," *Sensors*, vol. 19, p. 3933, 9 2019.

[101] A. C. Abad and A. Ranasinghe, "Visuotactile Sensors with Emphasis on GelSight Sensor: A Review," 7 2020.

[102] N. F. Lepora and B. Ward-Cherrier, "Superresolution with an optical tactile sensor," in *Intelligent Robots and Systems (IROS), 2015 IEEE/RSJ International Conference on*, pp. 2686–2691, IEEE, 2015.

[103] N. Pestell, B. Ward-Cherrier, L. Cramphorn, and N. F. Lepora, "Tactile Exploration by Contour Following Using a Biomimetic Fingertip," in *Conference on Biomimetic and Biohybrid Systems*, pp. 485–489, Springer, 2016.

[104] B. Ward-Cherrier, L. Cramphorn, and N. F. Lepora, "Exploiting sensor symmetry for generalized tactile perception in biomimetic touch," *IEEE Robotics and Automation Letters*, vol. 2, no. 2, pp. 1218–1225, 2017.

[105] K. Aquilina, D. A. Barton, and N. F. Lepora, "Principal components of touch," in *Proceedings - IEEE International Conference on Robotics and Automation*, pp. 4071–4078, Institute of Electrical and Electronics Engineers Inc., 9 2018.

[106] N. F. Lepora, A. Church, C. de Kerckhove, R. Hadsell, and J. Lloyd, "From Pixels to Percepts: Highly Robust Edge Perception and Contour Following Using Deep Learning and an Optical Biomimetic Tactile Sensor," *IEEE Robotics and Automation Letters*, vol. 4, pp. 2101–2107, 4 2019.

[107] L. Cramphorn, B. Ward-Cherrier, and N. F. Lepora, "Addition of a biomimetic fingerprint on an artificial fingertip enhances tactile spatial acuity," *IEEE Robotics and Automation Letters*, vol. 2, no. 3, pp. 1336–1343, 2017.

[108] M. E. Giannaccini, S. Whyle, and N. F. Lepora, "Force Sensing with a Biomimetic Fingertip," in *Conference on Biomimetic and Biohybrid Systems*, pp. 436–440, Springer, 2016.

[109] B. Winstone, G. Griffiths, T. Pipe, C. Melhuish, and J. Rossiter, "TACTIP-tactile fingertip device, texture analysis through optical tracking of skin features," in *Conference on Biomimetic and Biohybrid Systems*, pp. 323–334, Springer, 2013.

[110] C. Roke, C. Melhuish, T. Pipe, D. Drury, and C. Chorley, "Lump localisation through a deformation-based tactile feedback system using a biologically inspired finger sensor," *Robotics and Autonomous Systems*, vol. 60, no. 11, pp. 1442–1448, 2012.

[111] N. Pestell, J. Lloyd, J. Rossiter, and N. F. Lepora, "Dual-Modal Tactile Perception and Exploration," *IEEE Robotics and Automation Letters*, vol. 3, pp. 1033–1044, 4 2018.

[112] Broadcom, "AVAGO ADNS-3080." Available at: https://dtsheet.com/doc/729170/avago-adns-3080, 2020.

[113] B. Ward-Cherrier, N. Pestell, and N. F. Lepora, "NeuroTac: A Neuromorphic Optical Tactile Sensor applied to Texture Recognition," in *Accepted for IEEE International Conference on Robotics and Automation*, 3 2020.

[114] S. C. Liu and T. Delbruck, "Neuromorphic sensory systems," 6 2010.

[115] K. Kamiyama, H. Kajimoto, N. Kawakami, and S. Tachi, "Evaluation of a vision-based tactile sensor," in *Robotics and Automation, 2004. Proceedings. ICRA '04. 2004 IEEE International Conference on*, vol. 2, pp. 1542–1547, 4 2004.

[116] K. Sato, K. Kamiyama, N. Kawakami, and S. Tachi, "Finger-shaped gelforce: sensor for measuring surface traction fields for robotic hand," *IEEE Transactions on Haptics*, vol. 3, no. 1, pp. 37–47, 2010.

[117] X. Lin, L. Willemet, A. Bailleul, and M. Wiertlewski, "Curvature sensing with a spherical tactile sensor using the color-interference of a marker array," pp. 603–609, Institute of Electrical and Electronics Engineers (IEEE), 9 2020.

[118] X. Lin and M. Wiertlewski, "Sensing the Frictional State of a Robotic Skin via Subtractive Color Mixing," *IEEE Robotics and Automation Letters*, vol. 4, pp. 2386–2392, 7 2019.

[119] E. Knoop and J. Rossiter, "Dual-mode compliant optical tactile sensor," in *2013 IEEE International Conference on Robotics and Automation*, pp. 1006–1011, 5 2013.

[120] T. Corradi, P. Hall, and P. Iravani, "Bayesian tactile object recognition: learning and recognising objects using a new inexpensive tactile sensor," in *Robotics and Automation (ICRA), 2015 IEEE International Conference on*, pp. 3909–3914, IEEE, 2015.

[121] M. K. Johnson and E. H. Adelson, "Retrographic sensing for the measurement of surface texture and shape," in *2009 IEEE Conference on Computer Vision and Pattern Recognition*, pp. 1070–1077, IEEE, 6 2009.

[122] R. Li, R. Platt, W. Yuan, A. ten Pas, N. Roscup, M. A. Srinivasan, and E. Adelson, "Localization and manipulation of small parts using gelsight tactile sensing," in *Intelligent Robots and Systems (IROS 2014), 2014 IEEE/RSJ International Conference on*, pp. 3988–3993, IEEE, 2014.

[123] X. Jia, R. Li, M. A. Srinivasan, and E. H. Adelson, "Lump detection with a gelsight sensor," in *World Haptics Conference (WHC), 2013*, pp. 175–179, IEEE, 2013.

[124] R. Li and E. H. Adelson, "Sensing and recognizing surface textures using a gelsight sensor," in *Proceedings of the IEEE Conference on Computer Vision and Pattern Recognition*, pp. 1241–1247, 2013.

[125] W. Yuan, R. Li, M. A. Srinivasan, and E. H. Adelson, "Measurement of shear and slip with a GelSight tactile sensor," in *2015 IEEE International Conference on Robotics and Automation (ICRA)*, pp. 304–311, 2015.

[126] D. Baimukashev, Z. Kappassov, and H. A. Varol, "Shear, Torsion and Pressure Tactile Sensor via Plastic Optofiber Guided Imaging," *IEEE Robotics and Automation Letters*, vol. 5, pp. 2618–2625, 4 2020.

[127] J. Chodera, "Examination methods of standing in man," *FU-Czechoslovakian Academy of Sciences*, vol. 1-3, 1957.

[128] S. Saga, R. Taira, and K. Deguchi, "Precise shape reconstruction by activepattern in total-internal-reflection- based tactile sensor," *IEEE Transactions on Haptics*, vol. 7, no. 1, pp. 67–77, 2014.

[129] E. Donlon, S. Dong, M. Liu, J. Li, E. Adelson, and A. Rodriguez, "GelSlim: A High-Resolution, Compact, Robust, and Calibrated Tactile-sensing Finger," in *2018 IEEE/RSJ International Conference on Intelligent Robots and Systems (IROS)*, pp. 1927–1934, IEEE, 10 2018.

[130] Robotiq, "2F-85 and 2F-140 Grippers - Robotiq." Available at: https://robotiq.com/products/2f85-140-adaptive-robot-gripper.

[131] N. Rojas, R. R. Ma, and A. M. Dollar, "The GR2 Gripper: An Underactuated Hand for Open-Loop In-Hand Planar Manipulation.," *IEEE Trans. Robotics*, vol. 32, no. 3, pp. 763–770, 2016.

[132] M. Catalano, G. Grioli, E. Farnioli, A. Serio, C. Piazza, and A. Bicchi, "Adaptive synergies for the design and control of the Pisa/IIT SoftHand," *The International Journal of Robotics Research*, vol. 33, pp. 768–782, 4 2014.

[133] Z. Xu, E. Todorov, Zhe Xu, and E. Todorov, "Design of a highly biomimetic anthropomorphic robotic hand towards artificial limb regeneration," in *2016 IEEE International Conference on Robotics and Automation (ICRA)*, vol. 2016-June, pp. 3485–3492, IEEE, 5 2016.

[134] Shadow Robot Company;, "Dexterous Hand – Shadow Robot Company." Available at: https://www.shadowrobot.com/products/dexterous-hand/, 2019.

[135] IBM, "IBM100 - Deep Blue." Available at: https://www.ibm.com/ibm/history/ibm100/us/en/icons/deepblue/.

[136] O. Vinyals, I. Babuschkin, W. M. Czarnecki, M. Mathieu, A. Dudzik, J. Chung, D. H. Choi, R. Powell, T. Ewalds, P. Georgiev, J. Oh, D. Horgan, M. Kroiss, I. Danihelka, A. Huang, L. Sifre, T. Cai, J. P. Agapiou, M. Jaderberg, A. S. Vezhnevets, R. Leblond, T. Pohlen, V. Dalibard, D. Budden, Y. Sulsky, J. Molloy, T. L. Paine, C. Gulcehre, Z. Wang, T. Pfaff, Y. Wu, R. Ring, D. Yogatama, D. Wünsch, K. McKinney, O. Smith, T. Schaul, T. Lillicrap,

K. Kavukcuoglu, D. Hassabis, C. Apps, and D. Silver, "Grandmaster level in StarCraft II using multi-agent reinforcement learning," *Nature*, vol. 575, pp. 350–354, 11 2019.

[137] DeepMind, "AlphaGo | DeepMind." Available at: https://deepmind.com/research/case-studies/alphago-the-story-so-far.

[138] L. P. Cramphorn, *A touchy subject : development and exploration of tactile sensing for perception and manipulation*.
PhD thesis, University of Bristol, 2019.

[139] C. Piazza, G. Grioli, M. Catalano, and A. Bicchi, "A Century of Robotic Hands," *Annual Review of Control, Robotics, and Autonomous Systems*, vol. 2, pp. 1–32, 5 2019.

[140] L. Jamone, A. Bernardino, and J. Santos-Victor, "Benchmarking the Grasping Capabilities of the iCub Hand With the YCB Object and Model Set," *IEEE Robotics and Automation Letters*, vol. 1, pp. 288–294, 1 2016.

[141] H. Kawasaki, T. Komatsu, and K. Uchiyama, "Dexterous anthropomorphic robot hand with distributed tactile sensor: Gifu hand II," *IEEE/ASME Transactions on Mechatronics*, vol. 7, pp. 296–303, 9 2002.

[142] R. Deimel and O. Brock, "A novel type of compliant and underactuated robotic hand for dexterous grasping," *The International Journal of Robotics Research*, vol. 35, pp. 161–185, 1 2016.

[143] B. Choi, S. Lee, H. R. Choi, and S. Kang, "Development of anthropomorphic robot hand with tactile sensor: SKKU hand II," in *IEEE International Conference on Intelligent Robots and Systems*, pp. 3779–3784, 2006.

[144] J. Butterfaß, M. Grebenstein, H. Liu, and G. Hirzinger, "DLR-Hand II: Next generation of a dextrous robot hand," in *Proceedings - IEEE International Conference on Robotics and Automation*, vol. 1, pp. 109–114, 2001.

[145] E. N. G. Melo, "Anthropomorphic robotic hands: a review," 2014.

[146] J. L. Pons, R. Ceres, and F. Pfeiffer, "Multifingered dextrous robotics hand design and control: A review," *Robotica*, vol. 17, no. 6, pp. 661–674, 1999.

[147] L. Biagiotti, F. Lotti, C. Melchiorri, and G. Vassura, "How Far Is the Human Hand? A Review on Anthropomorphic Robotic End-effectors," 2004.

[148] A. M. Ramos, I. A. Gravagne, and I. D. Walker, "Goldfinger: A non-anthropomorphic, dextrous robot hand," in *Proceedings - IEEE International Conference on Robotics and Automation*, vol. 2, pp. 913–919, Institute of Electrical and Electronics Engineers Inc., 1999.

[149] Robotiq, "3-Finger Adaptive Robot Gripper - Robotiq." Available at: https://robotiq.com/products/3-finger-adaptive-robot-gripper.

[150] B. Technology, "BarrettHand™ — Barrett Technology." Available at: https://advanced.barrett.com/barretthand.

[151] S. M. Heydarabad, F. Milella, S. Davis, and S. Nefiti-Meziani, "High-performing adaptive grasp for a robotic gripper using super twisting sliding mode control," in *Proceedings - IEEE International Conference on Robotics and Automation*, pp. 5852–5857, IEEE, 5 2017.

[152] C. Borst, M. Fischer, S. Haidacher, H. Liu, and G. Hirzinger, "DLR hand II: Experiments and experiences with an anthropomorphic hand," in *Proceedings - IEEE International Conference on Robotics and Automation*, vol. 1, pp. 702–707, 2003.

[153] H. Liu, K. Wu, P. Meusel, N. Seitz, G. Hirzinger, M. H. Jin, Y. W. Liu, S. W. Fan, T. Lan, and Z. P. Chen, "Multisensory five-finger dexterous hand: The DLR/HIT hand II," in *2008 IEEE/RSJ International Conference on Intelligent Robots and Systems, IROS*, pp. 3692–3697, 2008.

[154] X. V. Ha, C. Ha, and D. K. Nguyen, "A General Contact Force Analysis of an Under-Actuated Finger in Robot Hand Grasping," *International Journal of Advanced Robotic Systems*, vol. 13, p. 14, 1 2016.

[155] A. Ajoudani, S. B. Godfrey, M. Bianchi, M. G. Catalano, G. Grioli, N. Tsagarakis, and A. Bicchi, "Exploring Teleimpedance and Tactile Feedback for Intuitive Control of the Pisa/IIT SoftHand," *IEEE Transactions on Haptics*, vol. 7, pp. 203–215, 4 2014.

[156] M. Bianchi, G. Averta, E. Battaglia, C. Rosales, M. Bonilla, A. Tondo, M. Poggiani, G. Santaera, S. Ciotti, M. G. Catalano, and A. Bicchi, "Touch-Based Grasp Primitives for Soft Hands: Applications to Human-to-Robot Handover Tasks and Beyond," in *2018 IEEE International Conference on Robotics and Automation (ICRA)*, pp. 7794–7801, IEEE, 5 2018.

[157] R. Ma and A. Dollar, "Yale OpenHand Project: Optimizing Open-Source Hand Designs for Ease of Fabrication and Adoption," *IEEE Robotics & Automation Magazine*, vol. 24, no. 1, pp. 32–40, 2017.

[158] R. R. Ma, L. U. Odhner, and A. M. Dollar, "A modular, open-source 3D printed underactuated hand," in *Robotics and Automation (ICRA), 2013 IEEE International Conference on*, pp. 2737–2743, IEEE, 2013.

[159] L. U. Odhner, L. P. Jentoft, M. R. Claffee, N. Corson, Y. Tenzer, R. R. Ma, M. Buehler, R. Kohout, R. D. Howe, and A. M. Dollar, "A compliant, underactuated hand for robust manipulation," *The International Journal of Robotics Research*, vol. 33, no. 5, pp. 736–752, 2014.

[160] D. Hackett, J. Pippine, A. Watson, C. Sullivan, and G. Pratt, "An Overview of the DARPA Autonomous Robotic Manipulation (ARM) Program," *Journal of the Robotics Society of Japan*, vol. 31, no. 4, pp. 326–329, 2013.

[161] G. Pratt and J. Manzo, "The DARPA robotics challenge," in *IEEE Robotics and Automation Magazine*, vol. 20, pp. 10–12, 2013.

[162] R. Deimel and O. Brock, "A compliant hand based on a novel pneumatic actuator," in *2013 IEEE International Conference on Robotics and Automation*, pp. 2047–2053, IEEE, 5 2013.

[163] A. Kapandji, "Cotation clinique de l'opposition et de la contre-opposition du pouce," *Annales de Chirurgie de la Main*, vol. 5, pp. 67–73, 1 1986.

[164] S. Levine, P. Pastor, A. Krizhevsky, J. Ibarz, and D. Quillen, "Learning hand-eye coordination for robotic grasping with deep learning and large-scale data collection," *The International Journal of Robotics Research*, vol. 37, pp. 421–436, 4 2018.

[165] I. Lenz, H. Lee, and A. Saxena, "Deep learning for detecting robotic grasps," *The International Journal of Robotics Research*, vol. 34, pp. 705–724, 4 2015.

[166] L. Pinto and A. Gupta, "Supersizing self-supervision: Learning to grasp from 50K tries and 700 robot hours," in *Proceedings - IEEE International Conference on Robotics and Automation*, vol. 2016-June, pp. 3406–3413, Institute of Electrical and Electronics Engineers Inc., 6 2016.

[167] C. Yang, G. Ganesh, S. Haddadin, S. Parusel, A. Albu-Schäeffer, and E. Burdet, "Human-like adaptation of force and impedance in stable and unstable interactions," *IEEE Transactions on Robotics*, vol. 27, pp. 918–930, 10 2011.

[168] A. Yamaguchi and C. G. Atkeson, "Recent progress in tactile sensing and sensors for robotic manipulation: can we turn tactile sensing into vision?1," *Advanced Robotics*, vol. 33, pp. 661–673, 7 2019.

[169] R. Calandra, A. Owens, D. Jayaraman, J. Lin, W. Yuan, J. Malik, E. H. Adelson, and S. Levine, "More Than a Feeling: Learning to Grasp and Regrasp Using Vision and Touch," *IEEE Robotics and Automation Letters*, vol. 3, pp. 3300–3307, 10 2018.

[170] J. Li, S. Dong, and E. Adelson, "Slip Detection with Combined Tactile and Visual Information," in *2018 IEEE International Conference on Robotics and Automation (ICRA)*, 2018.

[171] B. Ward-Cherrier, L. Cramphorn, and N. F. Lepora, "Tactile Manipulation With a TacThumb Integrated on the Open-Hand M2 Gripper," *IEEE Robotics and Automation Letters*, vol. 1, no. 1, pp. 169–175, 2016.

[172] R. R. Ma, A. Spiers, and A. M. Dollar, "M 2 Gripper: Extending the Dexterity of a Simple, Underactuated Gripper," in *Advances in reconfigurable mechanisms and robots II*, pp. 795–805, Springer, 2016.

[173] B. Ward-Cherrier, N. Rojas, and N. F. Lepora, "Model-Free Precise in-Hand Manipulation with a 3D-Printed Tactile Gripper," *IEEE Robotics and Automation Letters*, vol. 2, pp. 2056–2063, 10 2017.

[174] N. Pestell, L. Cramphorn, F. Papadopoulos, and N. F. Lepora, "A Sense of Touch for the Shadow Modular Grasper," *IEEE Robotics and Automation Letters*, vol. 4, pp. 2220–2226, 4 2019.

[175] Shadow Robot Company;, "Modular Grasper – Shadow Robot Company." Available at: https://www.shadowrobot.com/products/modular-grasper/, 2020.

[176] B. Calli, A. Walsman, A. Singh, S. Srinivasa, P. Abbeel, and A. M. Dollar, "Benchmarking in Manipulation Research: Using the Yale-CMU-Berkeley Object and Model Set," *IEEE Robotics & Automation Magazine*, vol. 22, pp. 36–52, 9 2015.

[177] J. Lin, R. Calandra, and S. Levine, "Learning to identify object instances by touch: Tactile recognition via multimodal matching," in *Proceedings - IEEE International Conference on Robotics and Automation*, vol. 2019-May, pp. 3644–3650, Institute of Electrical and Electronics Engineers Inc., 2019.

[178] J. Li, S. Dong, and E. H. Adelson, "End-to-end pixelwise surface normal estimation with convolutional neural networks and shape reconstruction using GelSight sensor," in *2018 IEEE International Conference on Robotics and Biomimetics (ROBIO)*, pp. 1292–1297, IEEE, 12 2018.

[179] A. Yamaguchi and C. G. Atkeson, "Combining finger vision and optical tactile sensing: Reducing and handling errors while cutting vegetables," in *2016 IEEE-RAS 16th International Conference on Humanoid Robots (Humanoids)*, pp. 1045–1051, IEEE, 11 2016.

[180] A. Yamaguchi and C. G. Atkeson, "Implementing tactile behaviors using FingerVision," in *IEEE-RAS International Conference on Humanoid Robots*, pp. 241–248, IEEE Computer Society, 12 2017.

[181] A. Schmitz, M. Maggiali, L. Natale, B. Bonino, and G. Metta, "A tactile sensor for the fingertips of the humanoid robot iCub," in *2010 IEEE/RSJ International Conference on Intelligent Robots and Systems*, pp. 2212–2217, IEEE, 10 2010.

[182] M. A. Abd, I. J. Gonzalez, T. C. Colestock, B. A. Kent, and E. D. Engeberg, "Direction of Slip Detection for Adaptive Grasp Force Control with a Dexterous Robotic Hand," in *2018 IEEE/ASME International Conference on Advanced Intelligent Mechatronics (AIM)*, pp. 21–27, IEEE, 7 2018.

[183] F. Veiga, B. B. Edin, and J. Peters, "Grip Stabilization through Independent Finger Tactile Feedback Control," *Sensors*, vol. 20, no. 6, 2018.

[184] A. Schmitz, Y. Bansho, K. Noda, H. Iwata, T. Ogata, and S. Sugano, "Tactile object recognition using deep learning and dropout," in *2014 IEEE-RAS International Conference on Humanoid Robots*, pp. 1044–1050, IEEE, 11 2014.

[185] A. J. Spiers, M. V. Liarokapis, B. Calli, and A. M. Dollar, "Single-Grasp Object Classification and Feature Extraction with Simple Robot Hands and Tactile Sensors," *IEEE Transactions on Haptics*, vol. 9, pp. 207–220, 4 2016.

[186] Google, "Soli: Home." Available at: https://atap.google.com/soli/.

[187] Z. Flintoff, B. Johnston, and M. Liarokapis, "Single-Grasp, Model-Free Object Classification using a Hyper-Adaptive Hand, Google Soli, and Tactile Sensors," in *2018 IEEE/RSJ International Conference on Intelligent Robots and Systems (IROS)*, pp. 1943–1950, IEEE, 10 2018.

[188] H. Iwata and S. Sugano, "Design of human symbiotic robot TWENDY-ONE," in *2009 IEEE International Conference on Robotics and Automation*, pp. 580–586, IEEE, 5 2009.

[189] D. Watkins-Valls, J. Varley, and P. Allen, "Multi-modal geometric learning for grasping and manipulation," in *Proceedings - IEEE International Conference on Robotics and Automation*, vol. 2019-May, pp. 7339–7345, Institute of Electrical and Electronics Engineers Inc., 5 2019.

[190] Simlab, "Allegro Hand." Available at: http://www.simlab.co.kr/Allegro-Hand.htm.

[191] M. Li, Y. Bekiroglu, D. Kragic, and A. Billard, "Learning of grasp adaptation through experience and tactile sensing," in *2014 IEEE/RSJ International Conference on Intelligent Robots and Systems*, pp. 3339–3346, IEEE, 9 2014.

[192] D. Cockbum, J. P. Roberge, T. H. L. Le, A. Maslyczyk, and V. Duchaine, "Grasp stability assessment through unsupervised feature learning of tactile images," in *Proceedings - IEEE International Conference on Robotics and Automation*, pp. 2238–2244, Institute of Electrical and Electronics Engineers Inc., 7 2017.

[193] A. M. Okamura, M. L. Turner, and M. R. Cutkosky, "Haptic exploration of objects with rolling and sliding," in *Proceedings - IEEE International Conference on Robotics and Automation*, vol. 3, pp. 2485–2490, IEEE, 1997.

[194] C. Yang, Z. Li, and E. Burdet, "Human like learning algorithm for simultaneous force control and haptic identification," in *IEEE International Conference on Intelligent Robots and Systems*, pp. 710–715, 2013.

[195] P. Falco, S. Lu, C. Natale, S. Pirozzi, and D. Lee, "A Transfer Learning Approach to Cross-Modal Object Recognition: From Visual Observation to Robotic Haptic Exploration," *IEEE Transactions on Robotics*, vol. 35, pp. 987–998, 8 2019.

[196] X. Song, H. Liu, J. Bimbo, K. Althoefer, and L. D. Seneviratne, "A novel dynamic slip prediction and compensation approach based on haptic surface exploration," in *IEEE International Conference on Intelligent Robots and Systems*, pp. 4511–4516, 2012.

[197] F. Veiga, H. Van Hoof, J. Peters, and T. Hermans, "Stabilizing novel objects by learning to predict tactile slip," in *Intelligent Robots and Systems (IROS), 2015 IEEE/RSJ International Conference on*, pp. 5065–5072, IEEE, 2015.

[198] Z. Su, K. Hausman, Y. Chebotar, A. Molchanov, G. E. Loeb, G. S. Sukhatme, and S. Schaal, "Force estimation and slip detection/classification for grip control using a biomimetic tactile sensor," in *Humanoid Robots (Humanoids), 2015 IEEE-RAS 15th International Conference on*, pp. 297–303, IEEE, 2015.

[199] B. Sundaralingam, A. S. Lambert, A. Handa, B. Boots, T. Hermans, S. Birchfield, N. Ratliff, and D. Fox, "Robust learning of tactile force estimation through robot interaction," in *Proceedings - IEEE International Conference on Robotics and Automation*, vol. 2019-May, pp. 9035–9042, Institute of Electrical and Electronics Engineers Inc., 5 2019.

[200] R. A. Romeo and L. Zollo, "Methods and Sensors for Slip Detection in Robotics: A Survey," 2020.

[201] M. R. Tremblay and M. R. Cutkosky, "Estimating friction using incipient slip sensing during a manipulation task," in *Robotics and Automation, 1993. Proceedings., 1993 IEEE International Conference on*, pp. 429–434, IEEE, 1993.

[202] S. Hirai and others, "Two-dimensional dynamic modeling of a sliding motion of a soft fingertip focusing on stick-to-slip transition," in *Robotics and Automation (ICRA), 2010 IEEE International Conference on*, pp. 4315–4321, IEEE, 2010.

[203] D. Kondo, S. Okada, T. Araki, E. Fujita, M. Makikawa, S. Hirai, and others, "Development of a low-profile sensor using electro-conductive yarns in recognition of slippage," in *2011 IEEE/RSJ International Conference on Intelligent Robots and Systems*, pp. 1946–1953, IEEE, 2011.

[204] C. Schurmann, R. Haschke, H. Ritter, and A. CITEC, "Modular high speed tactile sensor system with video interface," in *Tactile sensing in Humanoids–Tactile Sensors and beyond@ IEEE-RAS Conference on Humanoid Robots (Humanoids), Paris, France*, 2009.

[205] Y. Massalim, Z. Kappassov, and H. A. Varol, "Deep Vibro-Tactile Perception for Simultaneous Texture Identification, Slip Detection, and Speed Estimation," *Sensors*, vol. 20, p. 4121, 7 2020.

[206] B. Zapata-Impata, P. Gil, F. Torres, B. S. Zapata-Impata, P. Gil, and F. Torres, "Learning Spatio Temporal Tactile Features with a ConvLSTM for the Direction Of Slip Detection," *Sensors*, vol. 19, p. 523, 1 2019.

[207] J. Reinecke, A. Dietrich, F. Schmidt, and M. Chalon, "Experimental comparison of slip detection strategies by tactile sensing with the BioTac® on the DLR hand arm system," pp. 2742–2748, Institute of Electrical and Electronics Engineers Inc., 9 2014.

[208] Y. Shtessel, C. Edwards, L. Fridman, and A. Levant, "Sliding mode control and observation," vol. 10, Springer, 2014.

[209] A. Cirillo, P. Cirillo, G. De Maria, C. Natale, and S. Pirozzi, "Control of linear and rotational slippage based on six-axis force/tactile sensor," in *Robotics and Automation (ICRA), 2017 IEEE International Conference on*, pp. 1587–1594, IEEE, 2017.

[210] F. E. Viña, Y. Bekiroglu, C. Smith, Y. Karayiannidis, and D. Kragic, "Predicting slippage and learning manipulation affordances through Gaussian Process regression," in *IEEE-RAS International Conference on Humanoid Robots*, vol. 2015-Febru, pp. 462–468, IEEE Computer Society, 2015.

[211] Y. Wang, X. Wu, D. Mei, L. Zhu, and J. Chen, "Flexible tactile sensor array for distributed tactile sensing and slip detection in robotic hand grasping," *Sensors and Actuators, A: Physical*, vol. 297, p. 111512, 10 2019.

[212] M. Stachowsky, T. Hummel, M. Moussa, and H. A. Abdullah, "A slip detection and correction strategy for precision robot grasping," *IEEE/ASME Transactions on Mechatronics*, vol. 21, no. 5, pp. 2214–2226, 2016.

[213] L. Li, F. Sun, B. Fang, Z. Huang, C. Yang, and M. Jing, "Learning to detect slip for stable grasping," in *Robotics and Biomimetics (ROBIO), 2017 IEEE International Conference on*, pp. 430–435, IEEE, 2017.

[214] G. Canepa, R. Petrigliano, M. Campanella, and D. De Rossi, "Detection of incipient object slippage by skin-like sensing and neural network processing," vol. 28, pp. 348–356, 6 1998.

[215] S. Dong, D. Ma, E. Donlon, and A. Rodriguez, "Maintaining grasps within slipping bounds by monitoring incipient slip," in *Proceedings - IEEE International Conference on Robotics and Automation*, vol. 2019-May, pp. 3818–3824, Institute of Electrical and Electronics Engineers Inc., 5 2019.

[216] A. Rigi, F. Baghaei Naeini, D. Makris, and Y. Zweiri, "A Novel Event-Based Incipient Slip Detection Using Dynamic Active-Pixel Vision Sensor (DAVIS)," *Sensors*, vol. 18, no. 2, p. 333, 2018.

[217] J. Feng and Q. Jiang, "Slip and roughness detection of robotic fingertip based on FBG," *Sensors and Actuators, A: Physical*, vol. 287, pp. 143–149, 3 2019.

[218] H. Khamis, R. Izquierdo Albero, M. Salerno, A. Shah Idil, A. Loizou, and S. J. Redmond, "PapillArray: An incipient slip sensor for dexterous robotic or prosthetic manipulation – design and prototype validation," *Sensors and Actuators A: Physical*, vol. 270, pp. 195–204, 2 2018.

[219] H. Khamis, B. Xia, and S. J. Redmond, "A novel optical 3D force and displacement sensor – Towards instrumenting the PapillArray tactile sensor," *Sensors and Actuators A: Physical*, vol. 291, pp. 174–187, 6 2019.

[220] T. Narita, S. Nagakari, W. Conus, T. Tsuboi, and K. Nagasaka, "Theoretical Derivation and Realization of Adaptive Grasping Based on Rotational Incipient Slip Detection," pp. 531–537, Institute of Electrical and Electronics Engineers (IEEE), 9 2020.

[221] Y. Roudaut, A. Lonigro, B. Coste, J. Hao, P. Delmas, and M. Crest, "Touch sense: functional organization and molecular determinants of mechanosensitive receptors," *Channels*, vol. 6, no. 4, pp. 234–245, 2012.

[222] H. Yousef, M. Boukallel, and K. Althoefer, "Tactile sensing for dexterous in-hand manipulation in robotics - A review," *Sensors and Actuators, A: Physical*, vol. 167, no. 2, pp. 171–187, 2011.

[223] Stratasy, "Tango: A Soft Flexible 3D Printing Material | Stratasys." Available at: https://www.stratasys.com/materials/search/tango.

[224] N. F. Lepora, "Biomimetic Active Touch with Fingertips and Whiskers," *IEEE Transactions on Haptics*, vol. 9, no. 2, pp. 170–183, 2016.

[225] C. Cortes and V. Vapnik, "Support-vector networks," *Machine Learning*, vol. 20, no. 3, pp. 273–297, 1995.

[226] M. Aizerman, "Theoretical foundations of the potential function method in pattern recognition learning," *Automation and remote control*, vol. 25, pp. 821–837, 1964.

[227] S. S. Keerthi and C. J. Lin, "Asymptotic behaviors of support vector machines with gaussian kernel," *Neural Computation*, vol. 15, pp. 1667–1689, 7 2003.

[228] J. James, A. Church, L. Cramphorn, and N. Lepora, "Tactile Model O: Fabrication and testing of a 3d-printed, three-fingered tactile robot hand," *arXiv preprint arXiv:1907.07535*, 7 2019.

[229] R. R. Selvaraju, M. Cogswell, A. Das, R. Vedantam, D. Parikh, and D. Batra, "Grad-cam: Visual explanations from deep networks via gradient-based localization," in *Proceedings of the IEEE international conference on computer vision*, pp. 618–626, 2017.

[230] L. H. Gilpin, D. Bau, B. Z. Yuan, A. Bajwa, M. Specter, and L. Kagal, "Explaining explanations: An overview of interpretability of machine learning," in *2018 IEEE 5th International Conference on data science and advanced analytics (DSAA)*, pp. 80–89, IEEE, 2018.

[231] S. S. Sheppard, B. H. Tongue, and T. Anagnos, "Statics : analysis and design of systems in equilibrium," p. 636, Wiley, 2007.

[232] S. Garrido-Jurado, R. Muñoz-Salinas, F. J. Madrid-Cuevas, and M. J. Mar\'\in-Jiménez, "Automatic generation and detection of highly reliable fiducial markers under occlusion," *Pattern Recognition*, vol. 47, no. 6, pp. 2280–2292, 2014.

[233] C. P. Diehl and G. Cauwenberghs, "SVM Incremental Learning, Adaptation and Optimization," in *Proceedings of the International Joint Conference on Neural Networks*, vol. 4, pp. 2685–2690, 2003.

[234] I. Goodfellow, Y. Bengio, and A. Courville, "Deep Learning," MIT Press, 2016.

[235] L. Itti, "JeVois Smart Machine Vision Camera." Available at: www.jevois.org, 2019.

[236] R. Shirato, A. Abe, H. Tsuchiya, and M. Honda, "Effect of fingernail length on the hand dexterity," *Journal of Physical Therapy Science*, vol. 29, no. 11, pp. 1914–1919, 2017.

[237] D. P. Kingma and J. Ba, "Adam: A Method for Stochastic Optimization," 12 2014.

[238] A. Dollar, "YCB Gripper Assessment Benchmark Results." Available at: http://www.ycbbenchmarks.com/world-records/, 2019.

[239] J. W. James, A. Church, L. Cramphorn, and N. F. Lepora, "Tactile Model O: Fabrication and Testing of a 3D-Printed, Three-Fingered Tactile Robot Hand," *Soft Robotics*, p. soro.2020.0019, 12 2020.

[240] H. Dang and P. K. Allen, "Stable grasping under pose uncertainty using tactile feedback," *Autonomous Robots*, vol. 36, pp. 309–330, 4 2014.

[241] H. Liu, D. Guo, and F. Sun, "Object Recognition Using Tactile Measurements: Kernel Sparse Coding Methods," *IEEE Transactions on Instrumentation and Measurement*, vol. 65, pp. 656–665, 3 2016.

[242] M. Regoli, N. Jamali, G. Metta, and L. Natale, "Controlled tactile exploration and haptic object recognition," in *2017 18th International Conference on Advanced Robotics (ICAR)*, pp. 47–54, 7 2017.

[243] J. W. James, N. Pestell, and N. F. Lepora, "Slip Detection With a Biomimetic Tactile Sensor," *IEEE Robotics and Automation Letters*, vol. 3, pp. 3340–3346, 10 2018.

[244] M. Hays, L. Osborn, R. Ghosh, M. Iskarous, C. Hunt, and N. V. Thakor, "Neuromorphic vision and tactile fusion for upper limb prosthesis control," in *2019 9th International IEEE/EMBS Conference on Neural Engineering (NER)*, pp. 981–984, IEEE, 3 2019.

[245] Van Anh Ho, Zhongkui Wang, and S. Hirai, "Beam bundle model of human-like fingertip for investigation of tactile mechanism," in *2013 IEEE/RSJ International Conference on Intelligent Robots and Systems*, pp. 4491–4498, IEEE, 11 2013.

[246] L. M. Rosset, M. Florek-Jasinska, M. Suppa, and M. A. Roa-Garzón, "Experimental study on model- vs. learning-based slip detection," in *2019 19th International Conference on Advanced Robotics (ICAR)*, pp. 493–500, 2019.

[247] D. Jurafsky and J. H. Martin, "Speech and language processing : an introduction to natural language processing, computational linguistics, and speech recognition," p. 988, Pearson Prentice Hall, 2009.

[248] S. Wang, Z. Li, C. Liu, X. Zhang, and H. Zhang, "Training data reduction to speed up SVM training," *Applied Intelligence*, vol. 41, pp. 405–420, 9 2014.

[249] Haibo He and E. Garcia, "Learning from Imbalanced Data," *IEEE Transactions on Knowledge and Data Engineering*, vol. 21, pp. 1263–1284, 9 2009.

[250] G. F. Hughes, "On the Mean Accuracy of Statistical Pattern Recognizers," *IEEE Transactions on Information Theory*, vol. 14, no. 1, pp. 55–63, 1968.

[251] L. Marconi and C. Melchiorri, "Incipient Slip Detection and Control Using a Rubber-Based Tactile Sensor," *IFAC Proceedings Volumes*, vol. 29, pp. 475–480, 6 1996.

[252] "Connex3 objet260 3d printer for multi-color multi-material models." Available at: https://www.stratasys.com/3d-printers/objet260-connex3.

[253] K. L. Monson, M. A. Roberts, K. B. Knorr, S. Ali, S. B. Meagher, K. Biggs, P. Blume, D. Brandelli, A. Marzioli, R. Reneau, and F. Tarasi, "The permanence of friction ridge skin and persistence of friction ridge skin and impressions: A comprehensive review and new results," *Forensic Science International*, vol. 297, pp. 111–131, 4 2019.

[254] J. W. James, S. J. Redmond, and N. F. Lepora, "A Biomimetic Tactile Fingerprint Induces Incipient Slip," in *IEEE/RSJ International Conference on Intelligent Robots and Systems(IROS)*, (Las Vegas), 10 2020.

[255] J. N. Hoffmann, A. G. Montag, and N. J. Dominy, "Meissner corpuscles and somatosensory acuity: The prehensile appendages of primates and elephants," in *Anatomical Record - Part A Discoveries in Molecular, Cellular, and Evolutionary Biology*, vol. 281, pp. 1138–1147, John Wiley & Sons, Ltd, 11 2004.

[256] I. Fujimoto, Y. Yamada, T. Morizono, Y. Umetani, and T. Maeno, "Development of artificial finger skin to detect incipient slip for realization of static friction sensation," in *Proceedings of IEEE International Conference on Multisensor Fusion and Integration for Intelligent Systems, MFI2003.*, pp. 15–20, IEEE, 2003.

[257] N. F. Lepora and J. Lloyd, "Optimal deep learning for robot touch: Training accurate pose models of 3D surfaces and edges," *IEEE Robotics and Automation Magazine*, vol. 27, pp. 66–77, 6 2020.

[258] J. W. James and N. F. Lepora, "Slip Detection on Natural Objects with a Biomimetic Tactile Sensor," in *Conference on Biomimetic and Biohybrid Systems*, pp. 232–235, Springer, 2018.

[259] J. W. James and N. F. Lepora, "Slip Detection for Grasp Stabilization With a Multifingered Tactile Robot Hand," *IEEE Transactions on Robotics*, pp. 1–14, 2020.